Aalborg Universitet

Interference-robust Air Interface for 5G Small Cells

Managing inter-cell interference with advanced receivers and rank adaption

Tavares, Fernando Menezes Leitão

[Link to publication from Aalborg University](#)

Interference-robust Air Interface for 5G Small Cells

Managing inter-cell interference with advanced receivers and rank adaptation

Ph.D. Dissertation
Fernando Menezes Leitão Tavares

Abstract

Since the release of the first High Speed Packet Access (HSPA) networks in 2005, the demand for mobile broadband services has increased continuously at staggering rates, fuelled by the mass adoption of smartphones. It is forecast that this trend will continue for at least the next decade, pushing the existing wireless network infrastructure to the limit. Mobile network operators must invest in network expansion to deal with this problem, but the predicted network requirements show that a new Radio Access Technology (RAT) standard will be fundamental to reach the future target performance. This new 5th Generation (5G) RAT standard is expected to support data rates greater than 10 Gbps with very low latency, very low energy consumption and provide the required scalability that will allow the network to transport a 1000 to 10000 times more mobile data traffic in 2020 than a similar network would do in 2010.

To meet these challenging network capacity expansion requirements, the design of the new 5G RAT standard will make use of three main strategies: more antennas, more spectrum and more cells. All these strategies will have important roles in the new system, but the deployment of a massive number of small cells, especially indoors, is expected to provide the largest improvement in network capacity. However, the benefits of this type of ultra-dense deployment do not come for free; strong inter-cell interference, an inherent problem of dense networks, has the potential to limit the expected gains. Due to the fundamental role of inter-cell interference in this type of networks, the inter-cell interference problem must be addressed since the beginning of the design of the new standard.

This Ph.D. thesis deals with the design of an interference-robust air interface for 5G small cell networks. The interference robustness is achieved by the clever design of the radio frame structure in such a way that interference suppression receivers can efficiently and effectively mitigate the effects of inter-cell interference. A detailed receiver model is derived (including also receiver imperfections, such as estimation errors and receiver front-end limitations) and applied in extensive system-level simulation campaigns. These simulations show that, when the interference-robust air interface design is

used, interference suppression receivers are indeed a valid alternative to traditional Inter-cell Interference Coordination (ICIC) techniques that are commonly applied to improve the outage performance of these networks.

Moreover, a novel inter-cell interference management concept is proposed. This concept is based on the effect that the rank adaptation decisions in one cell cause on the neighbouring cells when interference suppression receivers are used. The concept, known as victim-aware rank adaptation, may be used to improve the outage data rates of the network. In particular, the Maximum Rank Planning (MRP) technique is shown to outperform traditional frequency reuse planning, with the advantage of lower implementation complexity due to the simplified planning process.

Resumé

Mobil bredbåndskommunikation har været i en konstant og voldsom vækst siden introduktionen af High Speed Packet Access (HSPA) i 2005, primært næret af den brede accept af smartphones. Det forventes at tendensen vil fortsætte minimum det kommende tiår og dermed strække den eksisterende trådløse netværksinfrastruktur til sit yderste. For at imødegå begrænsningerne er det nødvendigt at mobiloperatørerne investerer i udvidelser af deres netværk. Det er dog klart fra netværkskravene at en ny teknologistandard for radiotilgang vil være påkrævet for at kunne opfylde målkravene. En sådan ny 5. generations (5G) radioteknologi forventes at supportere datarater der overstiger 10 Gbps med meget lav tidsforsinkelse, meget lavt strømforbrug, og en skalerbarhed der tillader netværket at transportere 1.000 til 10.000 gange mere mobildatatrafik i 2020 end et tilsvarende netværk tillader i 2010.

For at imødekomme disse udfordrende krav til ekspansion af netværkskapacitet vil designet af en ny 5G radioteknologi gøre brug af tre hovedstrategier: Flere antenner, udvidet frekvensspektrum, og flere radioceller. Disse strategier vil hver især have en afgørende rolle i 5G, men den massive udrulning af små radioceller, specielt indendørs, forventes at bidrage med den største forbedring af netværkskapaciteten. Kapacitetsforbedringen kommer dog ikke uden omkostninger; den kraftige inter-celle interferens, der er resultat af netværksfortætningen, kan potentielt begrænse de forventede forbedringer. I betragtning af den centrale rolle som inter-celle interferens udgør i denne type netværk, er det oplagt at adressere inter-celle interferensproblematikken allerede i designet af en ny 5G standard.

Denne ph.d. afhandling omhandler designet af en interferensrobust radiogrænseflade for et 5G netværk med små radioceller. Robustheden overfor interferens er opnået ved et intelligent design af radio rammestrukturen, således at interferensundertrykkende modtagere effektivt kan undertrykke effekten af inter-celle interferens. Der er udviklet en detaljeret modtagermodel, inkluderende ikke-idealiteter såsom estimeringsfejl og signalbegrænsninger i modtagerdelen, og denne model er anvendt i et omfattende sæt af systemsimuleringer. Resultaterne fra simuleringerne viser at interferensundertrykkende modtagere, i samspil med den interferensrobuste radiogrænse-

flade, udgør et essentielt alternativ til traditionelle inter-celle interferensko-ordinations teknikker (ICIC) der typisk anvendes til at forbedre dækningen for de mest (interferens) udsatte brugere.

Afhandlingen foreslår også et nyskabende koncept for interferenshånd-tering. Konceptet er baseret på den effekt som rank-opdateringer i een celle bevirker på naboceller når interferens-undertrykkende modtagere benyttes. Konceptet, benævnt "victim-aware" rank-opdatering, kan benyttes til at for-bedre dækningen for interferens- udsatte brugere; det vises i afhandlingen, at specielt teknikken med Maximum Rank Planning (MRP) giver bedre dækn-ing end traditionel frekvensplanlægning, og tilmed med fordel af en lavere implementeringskompleksitet grundet en simplere planlægningsproces.

Contents

Thesis Details

Thesis Title: Interference-robust Air Interface for 5G Small Cells: Managing inter-cell interference with advanced receivers and rank adaptation

Ph.D. Student: Fernando Menezes Leitão Tavares

Supervisors: Assoc. Prof. Troels B. Sørensen, Aalborg University

                Prof. Preben Mogensen, Aalborg University

                Assoc. Prof. Gilberto Berardinelli, Aalborg University

The main body of this thesis consist of the following papers.

[A] Fernando Menezes Leitão Tavares, Gilberto Berardinelli, Nurul Huda Mahmood, Troels Bundgaard Sørensen and Preben Mogensen, "On the Potential of Interference Rejection Combining in B4G Networks", IEEE 78th Vehicular Technology Conference (VTC Fall), September 2013.

[B] Fernando Menezes Leitão Tavares, Gilberto Berardinelli, Nurul Huda Mahmood, Troels Bundgaard Sørensen and Preben Mogensen, "On the impact of receiver imperfections on the MMSE-IRC receiver performance in 5G networks", IEEE 79th Vehicular Technology Conference (VTC Spring), May 2014.

[C] Fernando Menezes Leitão Tavares, Gilberto Berardinelli, Nurul Huda Mahmood, Troels Bundgaard Sørensen and Preben Mogensen, "Inter-cell interference management using maximum rank planning in 5G small cell networks", IEEE 11th International Symposium on Wireless Communications Systems (ISWCS), August 2014.

[D] Fernando Menezes Leitão Tavares, Gilberto Berardinelli, Davide Catania, Troels Bundgaard Sørensen and Preben Mogensen, "Managing inter-cell interference with advanced receivers and rank adaptation in 5G small cells", *submitted to* IEEE 21st European Wireless (EW) Conference, May 2015.

This thesis has been submitted for assessment in partial fulfilment of the Ph.D. degree. The thesis is based on the submitted or published scientific papers which are listed above. Parts of the papers are used directly or indirectly in the extended summary of the thesis. As part of the assessment, co-author statements have been made available to the assessment committee and are also available at the Faculty. The thesis is not in its present form acceptable for open publication but only in limited and closed circulation as copyright may not be ensured.

Preface

This thesis is the result of a research project carried out at the Wireless Communication Networks (WCN) section, Institute of Electronic Systems, Aalborg University, Denmark. The work was carried out in parallel with the mandatory courses and teaching/working obligations required to obtain the Ph.D. degree.

The thesis investigates concepts related to the design of an interference-robust air interface for 5th Generation (5G) ultra-dense small cell networks; in particular, the investigation is focused on concepts related to the use of advanced receivers and rank adaptation techniques as tools for managing inter-cell interference.

To my beloved wife, Ana Paulla.

Words will never be enough to express how thankful I am for each and every moment we have been together. Life at your side has been happier than I could ever expect, especially now that we were blessed with the birth of our beloved son, Daniel. I will always be truly thankful for your love and dedication.

Fernando Menezes Leitão Tavares
February 17th, 2015

List of Abbreviations

256-QAM 256-ary Quadrature Amplitude Modulation

3GPP 3rd Generation Partnership Program

4G 4th Generation

5G 5th Generation

ABS Almost Blank Subframe

ADC Analog-to-Digital Converter

AF Activity Factor

AGC Automatic Gain Control

AMC Adaptive Modulation and Coding

AP Access Point

AWGN Additive White Gaussian Noise

BLER Block Error Rate

CDF Cumulative Distribution Function

CoMP Coordinated Multi-Point

CP Cyclic Prefix

CSG Closed Subscriber Group

DCCH Downlink Control Channel

DFT-s-OFDM DFT-spread OFDM

DL Downlink

DMRS Demodulation Reference Signal

DR Deployment Ratio

DRX Discontinuous Reception

DSB Data-Symbol Based

EDGE Enhanced Data Rates for GSM Evolution

EVM Error Vector Magnitude

FBMC Filter Bank Multicarrier

FDD Frequency Division Duplex

FD-ICIC Frequency-domain ICIC

FFR Fractional Frequency Reuse

FR1 Frequency Reuse 1

FR2 Frequency Reuse 2

FR4 Frequency Reuse 4

FRP Frequency Reuse Planning

GNSS Global Navigation Satellite System

GP Guard Period

GPS Global Positioning System

GSM Global System for Mobile Communications

HSPA High Speed Packet Access

ICIC Inter-cell Interference Coordination

IMT International Mobile Telecommunications

IRC Interference Rejection Combining

ITU International Telecommunication Union

LNA Low-Noise Amplifier

LTE Long Term Evolution

LTE-A Long Term Evolution - Advanced

MA Multiple Access

MCL Minimum Coupling Loss

MCS Modulation and Coding Scheme

MIMO Multiple-Input Multiple-Output

ML Maximum Likelihood

MMSE Minimum Mean Square Error

MRC Maximal Ratio Combining

MRP Maximum Rank Planning

MTC Machine Type Communications

OFDM Orthogonal Frequency Division Multiplexing

OOBE Out-of-Band Emission

OSG Open Subscriber Group

PAPR Peak-to-Average Power Ratio

PMI Precoding Matrix Index

PTP Precision Time Protocol

QPSK Quadrature Phase Shift Keying

RAT Radio Access Technology

RI Rank Indicator

RSB Reference-Symbol Based

SC-FDM Single-Carrier FDM

SDCH Shared Data Channel

SDR Software-Defined Radio

SIC Successive Interference Cancellation

SINR Signal-to-Interference-plus-Noise Ratio

SNR Signal-to-Noise Ratio

SRA Selfish Rank Adaptation

SU-MIMO Single-User Multiple-Input Multiple-Output

TB Transport Block

TDD Time Division Duplex

TD-ICIC Time-domain ICIC

TRA Taxation-based Rank Adaptation

UCCH Uplink Control Channel

UE User Equipment

UFMC Universal-Filtered Multi-Carrier

UL Uplink

UMTS Universal Mobile Telecommunications System

URC Ultra Reliable Communication

WRC World Radiocommunication Conference

ZT-DFT-s-OFDM Zero-Tail DFT-s-OFDM

Part I

Extended Summary

Chapter 1

Introduction

Our society continues to demand more and better mobile broadband services with every passing day. Since the release of the first High Speed Packet Access (HSPA) networks in 2005 [1], the demand for mobile broadband services has increased continuously at staggering rates, fuelled by the mass adoption of smartphones. It is forecast that this trend will continue for at least the next decade, pushing the existing wireless network infrastructure to the limit. Mobile network operators must keep up with this demand, preparing their networks for the future capacity and performance requirements. While operators all around the world are busy deploying their 4th Generation (4G) networks, the mobile industry and the academia are already starting to investigate the 5th Generation (5G) of mobile networks.

There is consensus in the mobile industry that 5G will not consist in a single new Radio Access Technology (RAT) like its predecessor. It will consist in a framework in which different RATs will coexist, each of them operating with a different goal. Given the important role that dense small cell networks are expected to play in future heterogeneous deployments, a RAT optimized for this type of networks fits perfectly in the 5G framework.

This research work is part of a larger research and development project to design a novel 5G RAT concept optimized for dense small cell networks. One of the project's main challenges is how to cope with the severe inter-cell interference conditions that limit the performance of this type of deployment. This Ph.D. thesis deals with this problem and proposes the use of advanced receivers capable of suppressing interference as the main tool to mitigate and manage the negative effect caused by inter-cell interference on the performance of small cell networks.

1.1 5G mobile networks

According to a study on the long-term historical progress of information technologies [2], the performance of essential information technology components (data storage, communication and computation) improves between 25% and 40% per year. At these rates, approximately 10 to 30 times better performance is expected every decade and 100 to 1000 times better every two decades. These multiplicative factors seem to match well with the evolution of cellular networks from the 1st to the 4th generation [3].

This historical trend is however not continuous [2]. When new technology is developed, its performance improves exponentially until it reaches its natural physical limits. At this point, it is surpassed by new revolutionary technology which is just starting its development history. Again, the evolution of cellular networks RAT seems to follow this trend, with a new RAT standard been specified approximately 10 years after its predecessor, creating the opportunity to relieve the burden of backward compatibility and to take advantage of the evolution of technological components, such as better digital signal processing and radio frequency circuitry. This is the main reason why the mobile industry believes a new generation of RAT standards should be specified until 2020 (roughly 10 years after the specification of Long Term Evolution - Advanced (LTE-A), agreed to be the 4th generation of mobile communication technology) [3].

1.1.1 General 5G mobile network requirements

With the 2020 horizon in mind, industry and academia have started the exploratory research phase that precedes the standardization process (expected to begin around 2016). Although consensus has not been reached yet, a set of high-level requirements for the 5G networks has already been defined. Using the technological progress growth rate, 5G is expected to outperform at least 10 times 4G in all performance aspects [4, 5, 6], such as:

- 10 Gbps peak data rate (both downlink and uplink);
- 100 Mbps cell edge data rate;
- Less than 1 ms latency;
- Wake-up time from "inactive" to "active" mode in the order of 10 ms;
- 10 to 100 times more connected devices per area;

Other requirements are also under discussion as, for example, better support for Machine Type Communications (MTC) by improving significantly the energy efficiency (10 year-long battery life for sensor-like MTC devices) [7], and support for Ultra Reliable Communication (URC) links [8], that will be important to enable mission critical services.

However, the most challenging requirement for 5G seems to be the required network capacity. Demand for mobile broadband services continue to increase at staggering rates. Forecasts such as Cisco's Global Mobile Data Traffic Forecast Update predict that global mobile data traffic will continue to increase at a annual growth rate of 61% from 2013 to 2018. At this pace, network capacity should increase approximately 117 times in the next decade.
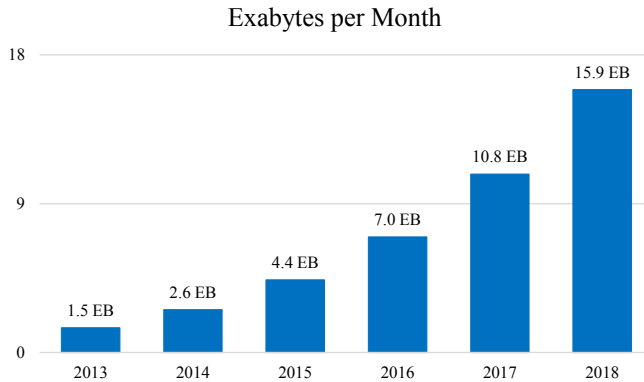
Exabytes per Month

Fig. 1.1: Cisco forecasts 15.9 Exabytes per month of mobile data traffic by 2018

If other factors, such as the increasing number of cellular network subscribers, are included in the forecast, data traffic volume is expected to increase between approximately 160 to 500 times from 2010 to 2020 [4]. Extrapolating this numbers to 2030, data traffic volume will increase from approximately 2300 or 14000 times as compared to 2010 [9]. Considering that 5G networks will carry most of this data until they are replaced by new networks, it is clear that providing sufficient network capacity will indeed be a challenging task.

To fulfil the challenging capacity expansion requirement, new solutions will be required. There are three basic strategies to expand network capacity [10]:

- improve spectral efficiency per link;
- increase the amount of used spectrum;
- increase the number of cells per area;

The first option has limited impact. To increase spectral efficiency per link, systems must rely on Multiple-Input Multiple-Output (MIMO) technol-

5

ogy and increase considerably the number of transmit and receive antennas per device to reach higher spatial multiplexing factors. However, given the complexity and costs of multi-antenna devices, it is unlikely that the number of antennas used by most of the devices will increase by a factor larger than two or four.

The use of large portions of millimetre-wave (mm-wave) spectrum range (from 30 to 300 GHz) has been considered as an option to increase the capacity of the network [11]. However, for systems operating at lower carrier frequencies, in the so called centimetre-wave (cm-wave) range (from 3 to 30 GHz), there is some consensus that the biggest contributor to capacity expansion will be the increase in the total number of cells [6]. For this reason, it is expected that ultra-dense small cell deployments will become a key feature of 5G networks.

1.1.2 Ultra-dense small cell deployments

Higher network capacity may be achieved by increasing network density (deploying more infrastructure nodes to increase the reuse of spectrum resources). Ideally, network planners would continue to reduce the inter-site distance of a homogeneous hexagonal cell deployment. However, this strategy is not economically feasible (due to high cost of site acquisition) nor technically efficient (due to uneven geographical traffic distribution) [10].

Instead, heterogeneous networks have become the industry trend [12]. These networks are composed of tightly integrated layers of macro cells (high-power base stations) and small cells (low-power base stations). In this setup, the macro cells ensure basic service coverage, while small cells provide high capacity in high traffic density areas.

A recent study on LTE-A heterogeneous networks concluded that a three layer network composed of macro cells, outdoor small cells and indoor small cells will be necessary to guarantee high quality service as data traffic demand increases a thousand times [13]. Different network configurations were tested with the target of at least 10 Mbps to more than 90% of all users, and according to the study, the outdoor and the indoor small cell layers should be roughly ten times and a hundred times denser than the macro cell layer, respectively. Moreover, the indoor small cell layer was found to be fundamental for the network due to the high outdoor-to-indoor penetration losses and the fact that about 70% of all traffic is generated indoors. In fact, it was not possible to find a network configuration without indoor small cells that reached the target performance.

Another important conclusion of this study [13] was the need for more spectrum. Even if the three layer heterogeneous LTE-A network uses the entire existing International Mobile Telecommunications (IMT) spectrum (including 2nd and 3nd generation re-farmed spectrum), the network would not

be able to reach the capacity target as the user throughput requirement increases from 1 to 10 Mbps. The study suggests the use of an extra 200 MHz band at 3.5 GHz carrier frequency to reach the target. The International Telecommunication Union (ITU) has signalled that a new globally harmonized spectrum band from 3.4 to 4.9 GHz may indeed be allocated for mobile broadband services at the World Radiocommunication Conference (WRC) that will occur in 2015. Also according to the same study [13], this new spectrum should ideally be used only by small cell layers, to avoid complex cross-layer inter-cell interference problems, with relatively aggressive traffic steering applied to move traffic towards the small cell layers.

Using this LTE-A network expansion study as a guideline for the future, it has become clear that ultra-dense small cell layers will play a major role in future mobile networks. However, LTE-A is only a barely adequate RAT for ultra-dense small cells, especially for indoor small cells. For this reason, the research and development of a more adequate small cells RAT that takes into account characteristics of this type of networks is so important.

1.1.3 5G small cell RAT concept

Motivated by the need for a new RAT, a new project was started with the goal of designing a new 5G RAT concept optimized for small cells operating on the new 3.4 to 4.9 GHz spectrum range. This project was born from the cooperation between Nokia Networks and the Wireless Communication Networks research group at Aalborg University, Denmark.

One of the main goals of this research project is to find adequate solutions to reduce the impact of inter-cell interference on the performance of ultra-dense small cell networks. A small cell network operating on dedicated spectrum is free of cross-layer inter-cell interference problems. This is a great advantage, because this type of interference is difficult to manage and degrades considerably the performance of the network. However, small cells still interfere with each other, and the same-layer inter-cell interference increases as the cells become smaller.

In LTE-A networks, multiple different Inter-cell Interference Coordination (ICIC) solutions have been proposed for mitigating the inter-cell interference problem, e.g. static and adaptive Fractional Frequency Reuse (FFR) [14]. LTE-A Release 10 and 11 focused on co-channel interference coordination solutions for heterogeneous networks scenarios [12]. In 2013, the 3rd Generation Partnership Program (3GPP) started to investigate solutions specifically designed for dense small cell networks operating on dedicated spectrum, but still the emphasis was on interference coordination techniques [15, 16, 17].

A different approach for coping with severe inter-cell interference is to rely on the use of interference suppression receivers. The theory behind these receivers is already well known [18, 19, 20] and attempts to use them

in cellular networks have occurred in the past. In fact, interference suppression concepts have been used in Global System for Mobile Communications (GSM) [21, 22, 23] and Universal Mobile Telecommunications System (UMTS) [24, 25, 26] cellular networks, as an attempt to deal with increased levels of interference. However, until recently, their practical implementation was considered too complex and costly (especially for the user equipment side). This situation is changing quickly. The technological evolution of electronic components, especially the digital components that continue to follow Moore's law [27], enable the use of complex advanced receiver methods at economically feasible costs even in lower end devices.

Recently, the use of this type of receivers has been considered by 3GPP for LTE-A networks [28, 29, 30, 31, 32, 33]. The conclusions of these studies show that, under specific conditions, interference suppression receivers can indeed reduce the negative effects of inter-cell interference in LTE-A networks. However, there are also many situations, including important use cases, in which interference suppression receivers barely improve the performance of the network.

The main reason for these low performance gains is the fact that LTE-A networks were not designed to rely on interference suppression receivers as a tool to manage inter-cell interference and the standard cannot be updated to include the necessary features to support the required suppression performance due to backward compatibility problems. In LTE-A networks, the role of interference suppression receivers is limited only to an extra "best-effort" layer of protection. In the case of the new 5G RAT, the opportunity to design a system in which interference suppression receivers play a major role in mitigating inter-cell interference is still open.

1.2 Objectives and scientific methodology

The main objective of this research work is to test the hypothesis that practical interference suppression receivers may be used as the main tool to manage inter-cell interference in ultra-dense small cell networks. This hypothesis leads to a number of research questions to be answered:

- If ideal conditions are assumed, what are the effective inter-cell interference suppression capabilities of these receivers?
- How does the system design influence the receiver's interference suppression capability?
- If conditions are not ideal (e.g. receiver imperfections), do advanced receivers still guarantee satisfactory performance?
- Is it possible to use interference rejection receivers as an alternative to traditional ICIC techniques? How?

Since this project is not based on an existing system, the following general steps were used to test the hypothesis and answer the research questions:

1. Survey and literature review about advanced multi-antenna receiver, focusing on their interference suppression capabilities;

2. Design of the necessary system features to provide support for high-performance inter-cell interference suppression;

3. Development of an interference suppression receiver model, that takes into account the proposed RAT concept design and the effects of receiver imperfections;

4. Performance evaluation comparing the proposed solution to traditional inter-cell interference management techniques.

This project requires the development of a receiver model for the evaluation of the performance of the proposed solutions. Ideally, the performance would be evaluated analytically, but considering the need to evaluate the performance of a large network involving multiple cells and devices, an analytical evaluation would be unfeasible given the complexity of the system. For this reason, system-level simulations are used for assessing the network performance.

Typically, system-level simulation models do not capture adequately the operational details of the physical layer, especially details regarding interference suppression capabilities (as it is, for example, the case of link-to-system interfaces in the form of look-up tables). Therefore, the development of a new system-level simulation receiver model that captures these details was a fundamental part of this research work.

1.3 Contributions and publications

This section presents the list of publications that have been authored or co-authored during this Ph.D. project. The papers are grouped according to their relevance to this thesis. The main content of this thesis is based on the following four conference papers, which have been reprinted at the end of this document.

- Fernando Menezes Leitão Tavares, Gilberto Berardinelli, Nurul Huda Mahmood, Troels Bundgaard Sørensen and Preben Mogensen, "On the Potential of Interference Rejection Combining in B4G Networks", IEEE 78th Vehicular Technology Conference (VTC Fall), September 2013.

  Contribution: This paper presents the first results regarding the potential benefits of interference suppression in 5G small cell networks,

presenting the system-level simulation receiver model and a comparison between the interference-aware Interference Rejection Combining (IRC) receiver and the interference-unaware Maximal Ratio Combining (MRC) receiver. The performance of both receivers is compared in two different indoor small cell scenarios with different static frequency reuse plans.

- Fernando Menezes Leitão Tavares, Gilberto Berardinelli, Nurul Huda Mahmood, Troels Bundgaard Sørensen and Preben Mogensen, "On the impact of receiver imperfections on the MMSE-IRC receiver performance in 5G networks", IEEE 79th Vehicular Technology Conference (VTC Spring), May 2014.

   Contribution: This paper extends the system-level simulation receiver model presented in the first paper by including the effects of receiver imperfections (channel response and received signal covariance matrix estimation errors, and receiver front-end imperfections related to dynamic range problems). The receivers are tested considering different estimation methods and receiver front-end configurations to evaluate the level of performance degradation and whether the gains due to the use of interference suppression were maintained.

- Fernando Menezes Leitão Tavares, Gilberto Berardinelli, Nurul Huda Mahmood, Troels Bundgaard Sørensen and Preben Mogensen, "Inter-cell interference management using Maximum Rank Planning in 5G small cell networks", IEEE 11th International Symposium on Wireless Communications Systems (ISWCS), August 2014.

   Contribution: This paper presents the Maximum Rank Planning (MRP) technique, a novel method to manage inter-cell interference using the victim-aware rank adaptation concept. This simple technique is compared to Frequency Reuse Planning (FRP) and it is shown that MRP is a valid alternative to traditional inter-cell interference management techniques. The proposed technique offers the advantage of simpler network management since resource allocation plans are not necessary.

- Fernando Menezes Leitão Tavares, Gilberto Berardinelli, Davide Catania, Troels Bundgaard Sørensen and Preben Mogensen, "Managing inter-cell interference with advanced receivers and rank adaptation in 5G small cells", *submitted to* IEEE 21st European Wireless (EW) Conference, May 2015.

   Contribution: In this paper, the possibility of using interference suppression receivers as an alternative to traditional inter-cell interference

management techniques is verified in three different indoor small cell scenarios. The paper present performance evaluation results including the use of victim-aware rank adaptation techniques and the extended receiver model that includes the use of Successive Interference Cancellation (SIC) receivers to further improve network performance.

A journal paper presenting a comprehensive evaluation of interference suppression receivers in 5G small cell networks is planned for submission in a forthcoming special issue of the Journal of Signal Processing Systems (JSPS).

Besides the aforementioned publications, this project contributed to the following two conference papers regarding the proposed 5G RAT concept.

- Preben Mogensen, Kari Pajukoski, Esa Tiirola, Eeva Lähetkangas, Jaakko Vihriälä, Seppo Vesterinen, Matti Laitila, Gilberto Berardinelli, Gustavo Wagner Oliveira da Costa, Luis Guilherme Uzeda Garcia, Fernando Menezes Leitão Tavares and Andrea Fabio Cattoni, "5G small cell optimized radio design", IEEE 2013 Global Communications Conference (GLOBECOM), December 2013.

- Preben Mogensen, Kari Pajukoski, Esa Tiirola, Jaakko Vihriälä, Eeva Lähetkangas, Gilberto Berardinelli, Fernando Menezes Leitão Tavares, Nurul Huda Mahmood, Mads Lauridsen, Davide Catania and Andrea Fabio Cattoni, "Centimeter-Wave Concept for 5G Ultra-Dense Small Cells", IEEE 79th Vehicular Technology Conference (VTC Spring), May 2014.

Moreover, the following conference papers regarding different concepts that are related to the 5G RAT concept were also co-authored.

- Eeva Lähetkangas, Kari Pajukoski, Gilberto Berardinelli, Fernando Menezes Leitão Tavares, Esa Tiirola, Ilkka Harjula, Preben Mogensen and Bernhard Raaf, "On the Selection of Guard Period and Cyclic Prefix for Beyond 4G TDD Radio Access Network", IEEE 19th European Wireless (EW) Conference, April 2013.

- Oscar Tonelli, Gilberto Berardinelli, Fernando Menezes Leitão Tavares, Andrea Fabio Cattoni, Istvan Kovacs, Troels Bundgaard Sørensen, Petar Popovski and Preben Mogensen, "Experimental validation of a distributed algorithm for dynamic spectrum access in local area networks", IEEE 77th Vehicular Technology Conference (VTC Spring), May 2013.

- Gilberto Berardinelli, Fernando Menezes Leitão Tavares, Nurul Huda Mahmood, Oscar Tonelli, Andrea Fabio Cattoni, Troels Bundgaard Sørensen and Preben Mogensen, "Distributed synchronization for Beyond

4G Indoor Femtocells", IEEE 20th International Conference on Telecommunications (ICT), May 2013.

- Gilberto Berardinelli, Fernando Menezes Leitão Tavares, Troels Bundgaard Sørensen, Preben Mogensen and Kari Pajukoski, "Zero-tail DFT-spread-OFDM signals", IEEE 2013 Global Communications Conference (GLOBECOM) Workshop, December 2013.

- Gilberto Berardinelli, Fernando Menezes Leitão Tavares, Olav Tirkkonen, Troels Bundgaard Sørensen and Preben Mogensen, "Distributed Initial Synchronization for 5G small cells", IEEE 79th Vehicular Technology Conference (VTC Spring), May 2014.

- Nurul Huda Mahmood, Gilberto Berardinelli, Fernando Menezes Leitão Tavares, Mads Lauridsen, Preben Mogensen and Kari Pajukoski, "An Efficient Rank Adaptation Algorithm for Cellular MIMO Systems with IRC Receivers", IEEE 79th Vehicular Technology Conference (VTC Spring), May 2014.

- Nurul Huda Mahmood, Gilberto Berardinelli, Fernando Menezes Leitão Tavares and Preben Mogensen, "A distributed interference-aware rank adaptation algorithm for local area MIMO systems with MMSE receivers", IEEE 11th International Symposium on Wireless Communications Systems (ISWCS), August 2014.

- Gilberto Berardinelli, Fernando Menezes Leitão Tavares, Troels Bundgaard Sørensen, Preben Mogensen and Kari Pajukoski, "On the potential of zero-tail DFT-spread-OFDM in 5G networks", IEEE 80th Vehicular Technology Conference (VTC Fall), September 2014.

- Gilberto Berardinelli, Jakob Lindbjerg Buthler, Fernando Menezes Leitão Tavares, Oscar Tonelli, Dereje Assefa, Farhood Hakhamaneshi, Troels Bundgaard Sørensen and Preben Mogensen, "Distributed Synchronization of a testbed network with USRP N200 radio boards", Asilomar Conference on Signals, Systems and Computers (ASILOMAR), November 2014.

- Dereje Assefa Wassie, Gilberto Berardinelli, Fernando Menezes Leitão Tavares, Oscar Tonelli, Troels Bundgaard Sørensen and Preben Mogensen, "Experimental Evaluation of Interference Rejection Combining for 5G Small Cells", *accepted to* IEEE Wireless Communications and Networking Conference (WCNC2015), March 2015.

- Dereje Assefa Wassie, Gilberto Berardinelli, Fernando Menezes Leitão Tavares, Troels Bundgaard Sørensen and Preben Mogensen, "Experimental Verification of Interference Mitigation techniques for 5G Small

Cells", *accepted to* IEEE 81st Vehicular Technology Conference (VTC Spring), May 2015.

1.4 Thesis outline

This dissertation consists of 5 chapters and 2 appendices, which are organized as follows:

- *Chapter 2: Inter-cell interference mitigation using interference suppression receivers* is dedicated to the analysis of the fundamental concepts behind the use of interference suppression receivers as a tool to manage inter-cell interference, including a brief discussion using information theory concepts. The chapter also presents the analysis of the aspects required for supporting high-performance interference suppression using advanced multi-antenna receivers, which was a key input for the design of the RAT concept.

- *Chapter 3: Interference Robust Air Interface for 5G Small Cells* describes 5G RAT concept for ultra-dense small cell networks, which was proposed in [6]. The first part of the chapter provides an overall description of the concept, whereas the remainder of the chapter presents the design solutions and features used to provide the support for interference suppression receiver.

- *Chapter 4: Performance Evaluation* presents an extensive set of performance evaluation results used to test the main hypothesis of this investigation.

- *Chapter 5: Conclusions and Future Work* concludes the thesis and presents recommendations for the next steps that will bring the new 5G concept closer to reality, including interesting and important topics for future investigations.

- *Appendix A: Receiver Model* presents the details of the receiver model developed for the performance evaluation study.

- *Appendix B: Detailed Simulation Assumptions* describes in details the simulation assumptions and the simulation tool developed for and used in this project.

Chapter 2

Inter-cell interference mitigation using interference suppression receivers

2.1 Introduction

The performance of modern wireless networks is often limited by the interference between multiple communication links. Interference distorts the desired signal and reduces the probability of successful reception. If strong enough, interference may even hinder the possibilities of communication. This is the reason why techniques for reducing the negative effect caused by interference in the performance of wireless communication links, collectively known as interference mitigation techniques, are so important.

Interference is a problem that comes in many forms: inter-symbol interference caused by multiple propagation paths, adjacent-channel interference caused by out-of-band emissions, inter-carrier interference caused by frequency offset in Orthogonal Frequency Division Multiplexing (OFDM) symbols, etc. As the wireless communication technology evolves, interference mitigation techniques have become more effective, to the point that some types of interference do not pose much of a challenge any more. For example, the use of OFDM has reduced considerably the negative effects of inter-symbol interference and adjacent-channel interference, which are problems that still limit the performance of Global System for Mobile Communications (GSM)/Enhanced Data Rates for GSM Evolution (EDGE) networks [34, 35, 36, 37].

Co-channel interference generated by the simultaneous use of frequency resources by multiple cells is a complex problem that still poses significant

challenges for cellular network designers. This chapter presents a discussion about the use of interference suppression receivers as a tool to manage and mitigate the effects of inter-cell interference.

2.2   Understanding inter-cell interference mitigation

Information theory provides a good framework to study the case of neighbour cells that interfere with each other. Figure 2.1 shows a schematic of the two-user Gaussian Interference Channel [38], as it is called in information theory. In this figure, $h_{jk}, j, k = 1, 2$ represent the channel gain between transmitter j and receiver k.
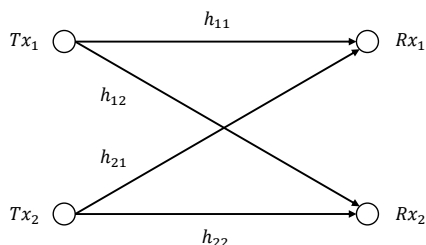
Fig. 2.1: Two-user Gaussian Interference Channel.

Although deceptively simple, the general capacity region for this channel is still unknown, i.e. tight performance bounds are only known for some particular cases [38]. The simplest of the solutions is to treat interference as noise, which is the best strategy when interference is low ($|h_{11}| > |h_{21}|$ and $|h_{22}| > |h_{12}|$). When interference is strong ($|h_{21}| > |h_{11}|$ and $|h_{12}| > |h_{22}|$), joint decoding is the solution. Other more complex solutions also exist, such as the Han-Kobayashi Inner Bound [39, 38]. The combination of treating interference as noise and joint decoding is known to be capacity achieving if both the transmitters use Gaussian point-to-point codes (codes that maximize the utility of the Gaussian point-to-point channel) [40].

Given the complexity of the other solutions, interference is usually treated as noise, but this solution is only useful when interference is weak. Intuitively, the solution for the strong interference problem comes from the split of the interference channel into Multiple Access (MA) channels. The split into two MA channels allows the use of solutions that are known to maximize the performance of this type of channel, such as time-division multiple access and successive cancellation decoding [38]. The difference in this case

as compared to the real MA channel is that each receiver will discard the signal sent by the interfering transmitter. The complete solution is then obtained by coordinating the allocation of resources in the different MA channels such that the allocations are orthogonal.

This is the basis for the use of inter-cell interference mitigation techniques based on resource orthogonalization. The use of these techniques started early in the history of cellular networks. As networks became larger and more complex, the techniques evolved to fulfil new requirements. Intelligence was included to automate the process of deciding the best strategy for each pair of interfering links (treat interference as noise or use orthogonal resource) and to decide the best resource allocation.

Another way to deal with the interference channel problem is to add communication links connecting the transmitters or the receivers to each other. The two options are depicted in Figure 2.2.
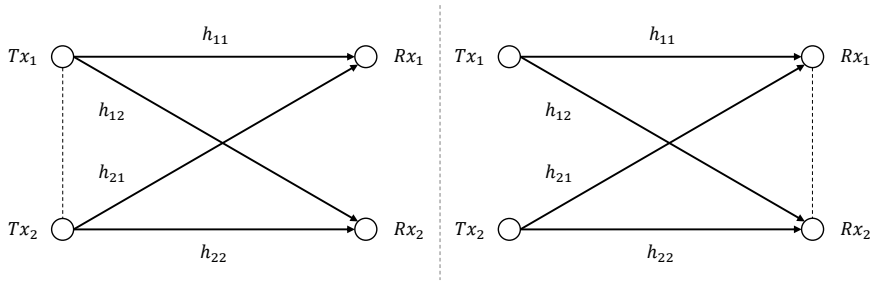
Fig. 2.2: MIMO Broadcast Channel (left) and MIMO Multiple Access Channel (right) formed by connecting two transmitters and two receivers, respectively.

According to information theory, solutions for both cases are known if the extra communication links are perfect [38]. When transmitters are connected, the interference channel becomes a Multiple-Input Multiple-Output (MIMO) Broadcast Channel. When the receivers are connected, it becomes a MIMO Multiple Access Channel. Both options may be used in cellular networks, by connecting base stations using high speed, low latency links, thus forming a MIMO Broadcast Channel in downlink and a MIMO Multiple Access Channel in uplink. This is the main idea of Coordinated Multi-Point (CoMP) or Network MIMO techniques [41, 42]. These techniques mitigate the effects of inter-cell interference by effectively turning multiple cells into a single one.

In scenarios in which the use of high speed, low latency communication links between the base stations is not an option (due to high deployment costs, for example), these methods cannot be applied. However, if devices are equipped with multiple antennas, MIMO technology offers other options

for dealing with the inter-cell interference problem.

The study of the MIMO interference channel is a hot topic in the information theory field, but similarly to the single antenna device case, the bounds of the capacity region are still unknown [38]. Generally, the same solutions for the scalar Gaussian interference channel may be applied to the vector channel. Complex techniques for achieving high network capacity have also been proposed, including for example the use of interference alignment methods [43, 44]. The main limitation of these techniques is the need for multi-cell coordination, a feature that limits the use of interference alignment in large networks.

An alternative solution for the MIMO interference channel with independent cells is to use the same intuitive idea of splitting the interference channel into MA channels. Figure 2.3 exemplifies the split of an Gaussian Vector Interference Channel in which the receivers use two antennas each into two Gaussian Vector Multiple Access Channels [38]. In this figure, $h_{jk}, j, k = 1, 2$ represents the channel gain vector between transmitter j and receiver k.
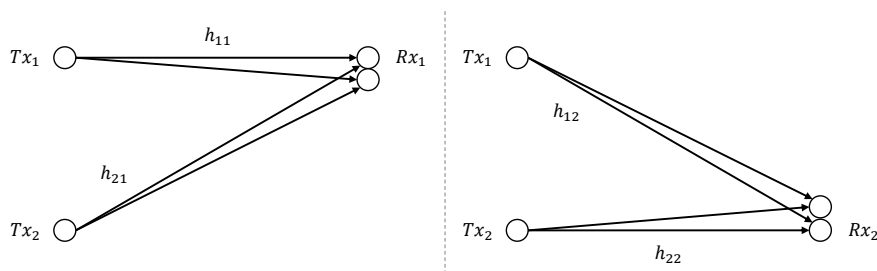
Fig. 2.3: MIMO Interference Channel split into two MIMO MA channels.

Besides the solutions for the single antenna MA channels, the capacity of this MA channel may also be maximized using the spatial domain. The optimal solution (sum-capacity) of the Gaussian Vector Multiple Access Channel is obtained with a water-filling solution that aligns the signal direction and the amount of power at the transmitter side based on channel conditions [45].

The water-filling solution is not suitable for the channel in Figure 2.3, because transmitters are independent, and therefore the transmitted signal are individually generated and encoded. In this case, the spatial domain may be used to deal with inter-cell interference by applying the same receiver techniques applied to separate multiple simultaneous MIMO spatial multiplexing signals. This is the basis for the use of interference suppression receivers to mitigate the effects of inter-cell interference in cellular networks.

The inter-cell interference mitigation techniques that operate in the spatial

domain follows the same general principles of techniques operating in the other domains, e.g. time, frequency and code domains. However, the number of degrees of freedom that are available to separate the signals is limited by the number of receive antennas, whereas in the other domains, the system may be designed with arbitrarily large number of orthogonal resources. This limitation leads to situations in which there are more signals than receive antennas to separate them.

In the case of a point-to-point MIMO channel, it is well accepted that the number of simultaneous transmitted signals should be smaller than or equal to the number of antennas of the device with the smallest number of antennas. However, in the case of the MIMO MA channel (and by extension the MIMO interference channel), the number of transmitted signals may be higher than the number of receive antennas, as it is exemplified in Figure 2.4.
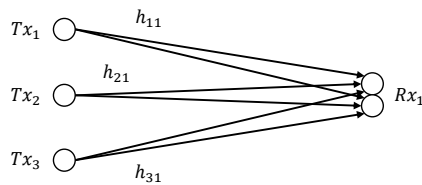
Fig. 2.4: MIMO MA channel with more transmitters than receive antennas.

Fortunately, the interference suppression receivers can deal with this situation. The signal separation will not be ideal and some interference contribution from interference sources will still distort the useful signal, but it is expected that the use of interference suppression receivers can reduce the impact of inter-cell interference. However, the performance of interference suppression receivers in 5th Generation (5G) dense small cells is still unknown. This information is particularly important to help decide which inter-cell interference management mechanisms should the new 5G Radio Access Technology (RAT) concept [6] rely on.

Another complicating factor regarding the use of interference suppression receivers to mitigate inter-cell interference is the use of spatial multiplexing. If devices are equipped with multiple antennas for both transmission and reception, spatial multiplexing may be used to boost the maximum rates that the MIMO point-to-point link can reach. This is another situation, depicted in Figure 2.5, in which the number of simultaneous signals can become larger than the number of receive antennas.

In MIMO point-to-point links, rank adaptation algorithms are used to
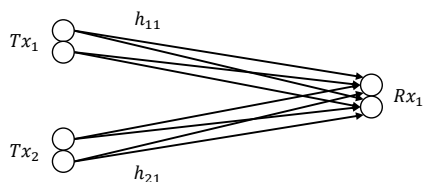
Fig. 2.5: MIMO MA channel with more transmitted signals than receive antennas.

adjust the ideal number of simultaneous signals, according to channel conditions. In the MIMO MA channel case, interference-aware rank adaptation algorithms may be used to adjust the number of streams also according to the interference conditions. In this case, the rank adaptation algorithm should balance the trade-off between the spatial multiplexing and inter-cell interference suppression.

If the number of streams in all the cells is selected in a cooperative manner, it may be possible to adjust the network conditions to match the number of signals with the number of receive antennas available. The study of techniques that adjust the parameters of rank adaptation to optimize the performance of the network instead of the performance of single links independently is also a topic that deserves attention.

2.3 Using MIMO receivers for inter-cell interference suppression

To suppress interference, MIMO receivers that are able to deal with multiple signals at the same time must be used. The optimal MIMO receiver in which the signal sources are individually generated and encoded is the Maximum Likelihood (ML) receiver [19]. This receiver jointly processes the multiple received signals, performing an exhaustive search over the space formed by the combination of all possible transmitted signals. Unfortunately, the search space increases exponentially with the number of signals, and the complexity of the ML receiver becomes prohibitively high. The complexity is further exacerbated in the case of coded transmissions. For this reason, the use of suboptimal low complexity receivers that closely approximate the performance of the ML receiver is preferred.

The complexity of the joint processing receiver may be reduced by split-

ting the receiver into two stages: a signal combining stage and a signal decoding stage [19]. Multiple receiver types can be obtained by combining different signal combining and signal decoding stages, including interference suppression receiver types.

The signal combining stage performs linear operations with the multiple signals received by the multiple antennas and generates estimates of the signals to be decoded. The optimal combination is the use of the Minimum Mean Square Error (MMSE) combining rule [20]; using this rule, the combiner stage outputs signal estimates with the highest possible Signal-to-Interference-plus-Noise Ratio (SINR). It has been proved that the MMSE combiner preserves the mutual information of all received signals and that there is no performance loss (same performance of ML receiver), if the two-stage receiver uses a MMSE combiner and a joint signal decoding stage [19]. Using the MMSE combiner stage, the receiver can effectively mitigate the mutual interference caused by multiple received signals. Due to this capability, a receiver that uses a MMSE combiner stage to suppress interference is usually referred to as an Interference Rejection Combining (IRC) receiver or a MMSE-IRC receiver.

Unfortunately, the complexity of the joint signal decoding stage also increases exponentially. The simplest alternative to this problem is to decode each signal individually, treating post-combining residual interference as noise. This simple alternative is currently used by the majority of MIMO receivers.

Another suboptimal alternative is to apply the Successive Interference Cancellation (SIC) principle [38, 18, 46], which consists in the iterative process of removing the interference contribution of each decoded signal from the signals that have not been decoded yet. The SIC principle can be applied to any received signal (including inter-cell interfering signals) as far as the side information necessary to decode the signal is available at the receiver.

By combining the MMSE combining stage with the decoding stage options at hand, the receiver designer obtains two MIMO receivers that may be used to suppress interference: the IRC receiver, composed by a MMSE combining stage and a individual decoding stage, and the IRC-SIC receiver, composed by a MMSE combining stage and a SIC decoding stage. These options are presented in Figure 2.6.

In the following subsections, each of these receivers will be described. The subsections will also include a discussion on what affects the receiver's ability to suppress interference and how the system should be designed to support their operation.
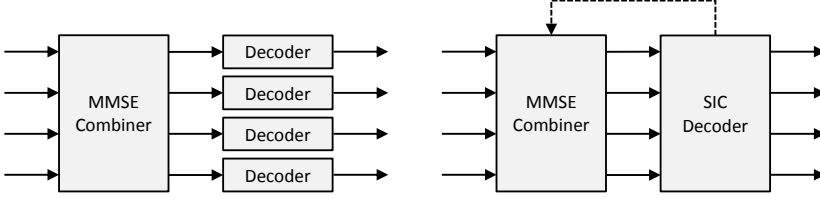
Fig. 2.6: IRC receiver (left) and IRC-SIC receiver (right).

2.3.1 IRC receiver

The interference suppression capability of the IRC receiver lies only in the MMSE combiner stage. To better explain this capability, a receiver model is used throughout this subsection. This receiver model is explained in detail in Appendix A.

The model assumes a wireless network system based on OFDM in which all network nodes transmit time-aligned frames. The network is composed of multiple devices, each of them with N_{tx} transmit and N_{rx} receive antennas. The OFDM baseband received signal vector $\mathbf{r}\,[N_{rx} \times 1]$ at one of these devices is given in the frequency domain by

$$\mathbf{r} = \sum_{k=1}^{N_T} \sum_{l=1}^{N_S^k} \mathbf{h}_{k,l} s_{k,l} + \mathbf{n} \tag{2.1}$$

where N_T is the number of transmitting devices, N_S^k is the number of data streams transmitted by the k-th device, $\mathbf{h}_{k,l}\,[N_{rx} \times 1]$ is the equivalent channel response vector through which $s_{k,l}$, the l-th data signal transmitted by the k-th transmitter, reaches the receiver. Vector $\mathbf{n}\,[N_{rx} \times 1]$ is the additive noise vector. This equation is valid for a generic subcarrier of a generic OFDM symbol. The subcarrier and symbol indexes are not displayed for the sake of notation simplicity.

Estimates of data symbols are obtained by combining the received signals using a weighting vector and are used by the decoding stage to obtain the transmitted bits. The estimate of the i-th data symbol transmitted by the j-th transmitter is given by

$$\hat{s}_{i,j} = \mathbf{w}_{i,j}^H \mathbf{r} \tag{2.2}$$

where $(\cdot)^H$ is the Hermitian conjugate operator and $\mathbf{w}_{i,j}\,[N_{rx} \times 1]$ is the combining vector for the data signal $s_{i,j}$. Using the MMSE combining rule, the

combining vector $\mathbf{w}_{i,j}$ is calculated according to

$$\mathbf{w}_{i,j} = \mathbf{R}_r^{-1}\mathbf{h}_{i,j} \tag{2.3}$$

where $\mathbf{R}_r\ [N_{rx} \times N_{rx}]$ is the covariance matrix of the received signal $\mathbf{r}$, defined as

$$\mathbf{R}_r = \mathbb{E}\{\mathbf{r}\mathbf{r}^H\} \tag{2.4}$$

where $\mathbb{E}\{\cdot\}$ is the expectation operator. Figure 2.7 shows the schematic for the IRC receiver model.
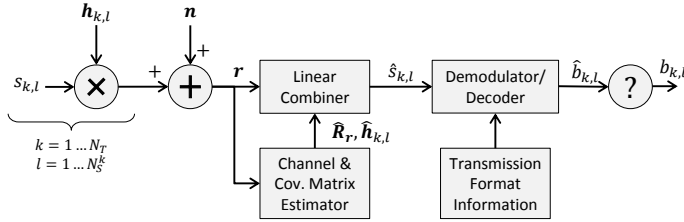
Fig. 2.7: IRC receiver schematic.

In practical receivers, the values of $\mathbf{h}_{i,j}$ and $\mathbf{R}_r$ must be estimated to calculate the combining vector $\mathbf{w}_{i,j}$, as given by

$$\mathbf{w}_{i,j} = \hat{\mathbf{R}}_r^{-1}\hat{\mathbf{h}}_{i,j} \tag{2.5}$$

where $\hat{\mathbf{h}}_{i,j}$ and $\hat{\mathbf{R}}_r$ are the estimates of $\mathbf{h}_{i,j}$ and $\mathbf{R}_r$, respectively. The quality of the estimation is a key element that affects the operation of the MMSE combining stage. In modern wireless systems, the estimation process of the channel response vectors is aided by pilot or reference signals [47, 48, 49, 50]. These signals are designed in such a way that the channel coefficients may be estimated with sufficient accuracy, and adequate time, frequency and sampling resolution.

Conversely, contemporary systems do not provide aids for the estimation of the received signal covariance matrix. In systems in which interference is negligible or the sum of the multiple interference signals may be modelled as a single uncorrelated signal at the different receive antennas, the lack of estimation aids is not critical. By treating interference as spatially uncorrelated noise, wideband long-term estimates of the interference-plus-noise power at each receive antenna may be used to generate an estimate of the covariance matrix. This is assumption is reasonable for scenarios in which the overall interference statistics do not change quickly over time.

Unfortunately, this is not the case of all scenarios. It is expected that inter-cell interference will have different characteristics in small cell networks due to many factors, e.g. the number of users per cell and the proximity of transmitters. In this case, it is common to find a single or few interfering sources that are responsible for most of the interfering power. As these interference sources change, the overall interference statistics change abruptly, affecting considerably the accuracy of the received signal covariance matrix. Besides, without the averaging effect due to the sum of multiple sources, it is not reasonable to assume that the interference signals at the receive antennas will be uncorrelated. Therefore, the full covariance matrix must be estimated, not only the diagonal elements.

Therefore, to guarantee that the IRC receiver will be able to reject inter-cell interference, the system must be designed to aid the covariance matrix estimation process, providing the means for the receiver to use accurate and timely estimates. The following list summarizes the key aspects that must be considered to meet this design requirement.

Inter-cell Synchronization

The first aspect that must be considered in the design of a system in which the IRC receiver will be used to reject inter-cell interference is inter-cell synchronization. The presence of signals that are not time aligned complicates the estimation process. In this case, the receiver must rely on long-term estimation to account for the uncertainties, reducing the time/frequency/spatial resolution of the estimation.

The design of contemporary cellular systems only provides the means for the synchronization necessary for the coherent detection, i.e. the synchronization mechanism is designed to align the receiver with the transmitter that sends the desired signals. Receivers may synchronize reception with more than one transmitter, but RAT standards do not provide native mechanisms for the synchronization of transmitters in different cells (they must rely on other standards).

Other mechanisms may be used for synchronizing cells when necessary. Good examples are the synchronization of base stations using Global Navigation Satellite Systems (GNSSs) [51], such as the Global Positioning System (GPS) system, or methods to provide carrier-grade synchronization signals, such as the Synchronous Ethernet (ITU-T G.8261, G.8262 and G.8264) and the IEEE 1588 Precision Time Protocol (PTP) standards [52, 53, 54]. These are viable options in many situations in which synchronization is necessary, but not all of them. For example, GPS synchronization does not work well in indoor scenarios, where the GPS signal is often attenuated to undetectable levels, and the PTP standard requires the installation of special transparent network equipment or the use of direct dedicated links between base stations,

a requirement that is not economically feasible in many scenarios.

Therefore, a system that expects to use IRC receivers to effectively reject inter-cell interference cannot rely on the existing options. The system must provide a novel native mechanism for the inter-cell synchronization.

Frame format design

The accuracy of the covariance matrix estimation also depends on the frame format design. One of the key aspects of the design is interference stabilization. First, the period of application of the covariance matrix estimate is defined by the period in which the interference sources do not change. Whenever the interference sources change, a new estimate is necessary to accurately represent the new interference conditions. Second, if interference sources do not change during the estimation period, it is possible to use longer estimation periods (with more samples) that yield higher interference estimation accuracy. Conversely, if interference change during this period, the estimate is affected by systemic errors; the estimate will represent a combination of the interference conditions, before and after the change.

Ideally, the frame should be designed to guarantee long periods in which interference sources do not change, providing high accuracy estimation with low estimation overhead. However, shorter periods are necessary to support low latency and to provide more flexibility for radio resource management. Therefore, to balance flexibility and estimation accuracy, the frame design should use an interference stabilization period that is just long enough to provide sufficient estimation accuracy.

The required amount of samples, and consequently the length of the estimation period, depends on the covariance matrix estimation method applied. The methods may be classified in Data-Symbol Based (DSB) and Reference-Symbol Based (RSB) methods [30, 29, 55]. The former type of method uses the received data symbols to perform a direct estimation of the covariance matrix. The estimator for the DSB method is given by

$$\hat{\mathbf{R}}_r = \frac{1}{Q_{DS}} \sum_{\substack{<f,t> \\ \in \mathcal{P}_{DS}}} \mathbf{r}(f,t)\mathbf{r}(f,t)^H \tag{2.6}$$

where $\mathcal{P}_{DS}$ is the set of indexing pairs for the subcarriers of the OFDM symbols in which data symbols are transmitted and Q_{DS} is the cardinality of $\mathcal{P}_{DS}$.

The RSB methods perform indirect estimation of the covariance matrix, using channel response estimates to aid the estimation process. The use of channel response estimates helps to reduce the uncertainty about the received signals, reducing the number of samples needed for accurate estimation. The

estimator for the RSB mehod is given by

$$\hat{\mathbf{R}}_r = \sum_{k=1}^{N_T} \sum_{l=1}^{N_S^k} \hat{\mathbf{h}}_{k,l} \hat{\mathbf{h}}_{k,l}^H + \hat{\mathbf{R}}_n \qquad (2.7)$$

where $\hat{\mathbf{R}}_n$ is the estimate of $\mathbf{R}_n$, which is given by

$$\hat{\mathbf{R}}_n = \frac{1}{Q_{RS}} \sum_{\substack{<f,t> \\ \in \mathcal{P}_{RS}}} (\mathbf{r}(f,t) - \sum_{k=1}^{N_T} \sum_{l=1}^{N_S^k} \hat{\mathbf{h}}_{k,l} p_{k,l}(f,t))(\mathbf{r}(f,t) - \sum_{k=1}^{N_T} \sum_{l=1}^{N_S^k} \hat{\mathbf{h}}_{k,l} p_{k,l}(f,t))^H$$

$$(2.8)$$

where $p_{k,l}$ represents the l-th reference symbols transmitted by the k-th transmitter, $\mathcal{P}_{RS}$ is the set of indexing pairs for the subcarriers of the OFDM symbols in which reference symbols (used for covariance matrix estimation) are transmitted and Q_{RS} is the cardinality of $\mathcal{P}_{RS}$.

The use of RSB methods is a clear advantage for systems that require agility and flexibility, because the smaller number of required samples (as compared to the DSB methods), reduces the need for long estimation periods and therefore allows for shorter frame formats. However, the use of RSB methods implies the frame format must be designed taking into account the need for accurate estimation of the channel response vectors (ideally also including the estimation of vectors regarding inter-cell interferers).

The frame design should also include mechanisms to guarantee orthogonality between reference symbols used by transmitters in different cells. This requirement is commonly disregarded when interference is treated as noise, but in strong inter-cell interference scenarios, such design choice leads to low-accuracy channel response vectors due to interference between reference symbols transmitted at the same frame positions (in the case of separation of reference symbols in time and frequency domains) or using the same codes or sequences (in the code domain case).

To further facilitate the estimation process, the frame format design must ensure data symbols and reference symbols transmitted by different devices (either in the same cell or in neighbour cells) do not interfere with each other. Reference symbols and data symbols have different characteristics that make their estimation processes different. Therefore, it must be enforced that the separation of data and reference symbols is consistent among all transmitted signals (both intra-cell and inter-cell).

As an example, in Long Term Evolution (LTE) Release 8, pilot symbols were intended only for intra-cell interference estimation [48], with orthogonal reference sequences designed to allow the separate estimation of the channels relative to the different sectors of the same base station [56]. In Long Term Evolution - Advanced (LTE-A), new methods to improve the channel estimation were included, but the focus was still intra-cell estimation [57, 58].

The lack of consistency in the position of reference symbols make it very difficult for receivers to perform inter-cell channel estimation, as it is the case with LTE Frequency Division Duplex (FDD) when different MIMO transmission modes are used by devices transmitting over the same resource block. In Time Division Duplex (TDD) systems, such as LTE TDD, there is the possibility of Uplink (UL) to Downlink (DL) or DL to UL interference. In this case, consistent reference symbol positions is required between both link directions [48].

For these reasons, it is fundamental that the design of the frame format for the new 5G RAT takes into account these guidelines if the IRC receiver is expected to be used as an effective tool to suppress inter-cell interference.

Rank and Precoding Matrix Adaptation

Rank and precoding matrix adaptation is a key feature of MIMO systems. Precoding matrix adaptation algorithms are used to improve the robustness of the link by choosing the precoding weights for each transmitted spatial streams, whereas rank adaptation chooses the ideal number of transmitted data stream, balancing the trade-off between transmit diversity and spatial multiplexing gains.

When the IRC receiver is used to reject inter-cell interference, the rank adaptation algorithms must be modified to consider this characteristic of the receiver, because the trade-off is not only between transmit diversity and spatial multiplexing any longer; inter-cell interference rejection must be included among the trade-off factors.

The capability to reject interference that is inherent to the IRC receiver is limited by the number of receive antennas. As a rule of thumb, the IRC receiver can reject up to $N_{rx} - 1$ interference signals at a time, where N_{rx} is the number of receive antennas, as mentioned before. The receiver does not differentiate interference signals based on whether they come from the transmitter that sends the desired signal (inter-stream interference) or another transmitter (inter-cell interference). Therefore, if there is the need to reject more inter-cell interference streams, the transmitter must use less spatial streams. The responsible for making this decision is the rank adaptation algorithm.

Rank adaptation algorithms that are aware of inter-cell interference rejection (hereby referred to as IRC-aware algorithms) may be selfish or victim-aware [59, 60, 61]. Since the number of interfering streams that may be rejected by the IRC receiver is limited by the total number of receive antennas, the decision of one transmitter regarding the number of data streams to send impacts the performance of a receiver in another cell. A selfish rank adaptation algorithm ignores this effect and attempts to maximize the performance of the link. A victim-aware algorithm considers this effect and focus on the

overall network performance.

Overall network performance can vary considerably based on the type of rank adaptation algorithm used. It is therefore necessary to investigate which types of rank adaptation algorithms are recommended for 5G small cell network scenarios, so that RAT design guidelines regarding their use can be defined.

2.3.2 IRC-SIC receiver

The IRC-SIC receiver is the combination of the MMSE combiner stage with a decoding stage that uses the SIC technique. Figure 2.8 shows the schematic for the IRC-SIC receiver model.
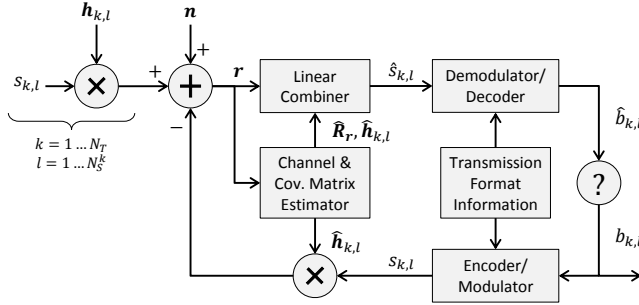
Fig. 2.8: IRC-SIC receiver schematic.

The interference cancellation part of the IRC-SIC receiver lies in the loop that is used to rebuild the interference signals using the decoded signals. Every signal that is successfully decoded is encoded and multiplied by the channel response estimates and then subtracted from the total received signal vector. After this step is completed, the receiver attempts to decode another signal and the cycle continues either until all desired signals are decoded or no more signals can be decoded.

The following equation shows the interference cancellation step. The received signal vector **r** after each iteration is given by

$$\mathbf{r} = \sum_{k=1}^{N_T} \sum_{l=1}^{N_S^k} \mathbf{h}_{k,l} s_{k,l} + \mathbf{n} - \sum_{k,l \in \mathcal{D}} \hat{\mathbf{h}}_{k,l} s_{k,l} \tag{2.9}$$

where $\mathcal{D}$ is the set of signals that are already decoded.

The performance of the IRC-SIC receiver depends largely on the number of signals that it is able to decode. Ideally, the system design should maximize the probability that the receiver will have all the required information

for decoding as many signals as possible. The following list summarizes the key aspects (besides the aspects already described concerning the IRC receiver) that must be considered to reach this goal.

Decoding information signalling

The decoding stage can only decode a signal if the required side information is available. Side information describes the transmitted signal characteristics. For example, in the case of LTE networks, the decoding process requires transmission information parameters, such as Modulation and Coding Scheme (MCS), Precoding Matrix Index (PMI), Rank Indicator (RI), Transport Block (TB) size, just to mention a few [48, 62].

Receivers may attempt to blindly decode the side information required for decoding, but this approach is inefficient and reduces the probability of successful data decoding. For this reason, the side information is transmitted using control channels that are dimensioned to carry the required information to decode the desired signals with the smallest possible overhead.

Using this information, the receiver can apply the interference cancellation principle to the inter-stream interference. Since all signals are desired (although they assume the role of interferers when another desired signal is being decoded), all the required information to decode them must be available at the receiver even if interference cancellation is not to be applied.

Conversely, there are no mechanisms designed to transmit the side information regarding inter-cell interference to the interfered receivers in neighbour cells. This condition limits the applicability of SIC to inter-cell interference. Therefore, if SIC is expected to be used for this purpose, the system should assist the receivers to obtain the information about inter-cell interference. One possibility is to include control channels that carry this information to other cells. However, there must be a balance between the performance gains due to inter-cell interference cancellation and the performance losses due to increased control channel overhead.

Spatial stream to codeword mapping

When multiple signals are transmitted using spatial streams, these signals may be combined in a single codeword that aggregates the symbols from all streams or in multiple codewords. In LTE, for example, the spatial stream to codeword mapping defines that transmissions with more than 2 spatial streams, i.e transmissions with two, four or eight spatial streams, are mapped to two codewords only [48]. This decision was made to reduce the control channel overhead since transmission format information must be transmitted for each codeword. However, it may limit the interference cancellation gains, because the maximum theoretical SIC gain can only be achieved if one spatial

data stream corresponds to one codeword. Nevertheless, the ideal number from the system-level point of view may be lower depending on the balance between control channel overhead and performance gains.

Link adaptation

Link adaptation algorithms are fundamental to match the ideal MCS to the channel conditions. The algorithm controls the Block Error Rate (BLER) by selecting the ideal MCS, aiming at maximizing the transmission data rates, considering the required retransmissions in case a transmission fails.

When SIC receivers are used, it is important to consider the impact of the choice of the MCS on the BLER of all spatial streams at once. Take as an example the case of a system in which a IRC-SIC receiver is used and the transmitter sends two spatial streams mapped onto two codewords. For the first codeword, the probability of successful reception is a function of the MCS selected by the link adaptation algorithm and the SINR at reception time. For the second codeword, the same is valid, but the SINR depends on whether the first codeword was decoded or not. This situation complicates the selection of the MCS for the second codeword, because the SINR can be very different in each case.

If the algorithm chooses to be conservative, assuming that the first codeword will probably not be decoded, the benefits of interference cancellation disappear. If it is aggressive and assumes the first codeword will be decoded, it may lead to excessively high retransmission rates. Therefore, smart link adaptation algorithms specifically designed for systems in which IRC-SIC receivers are used are required.

The situation gets even more complicated when the IRC-SIC receiver is expected to cancel inter-cell interference, because even if the side information required for decoding the inter-cell interference signal is available, the SINR of the interference signals may not be sufficient to decode them. The required SINR depends on the MCS used for transmission, but the selection of MCS does not take into account the fact that some receivers may benefit from decoding and cancelling them.

The receivers may attempt to decode the signals opportunistically, but the benefits of this strategy are expected to be low (interference links tend to have lower capacity than the main links) [63, 64]. The use of victim-aware link adaptation algorithms, following the same idea of victim-aware rank adaptation algorithms, is a possibility that still needs to be investigated. These algorithms may attempt to choose the MCS to increase the probability that the interfered receivers will be able to decode and cancel them. However, its feasibility and potential benefits are still unknown.

2.3.3 Receiver front-end imperfections

In theory, very strong interference signals can lead to saturated signals at the receiver input, making it impracticable to separate desired and interfering signals using interference suppression techniques. The impact caused by these interference signals depends on receiver characteristics, such as the receiver's dynamic range.

Ideally, an Automatic Gain Control (AGC) mechanism adjusts the gain of the receiver's amplifiers, such as the Low-Noise Amplifier (LNA), in such a way that the dynamic range of the Analog-to-Digital Converter (ADC) module is best utilized [65, 66, 55]. However, if interference signals are much stronger than the desired signals, the ADC's dynamic range may not be sufficient for correctly converting the signals from the analog to the digital domain, leading to signals with amplitude larger than the ADC's full range (which causes signal clipping) or signals with too low amplitude (which leads to poor Signal-to-Noise Ratio (SNR) due to quantization noise). This problem is further exacerbated due to AGC estimation delays.

These effects may affect the performance of the receiver directly or indirectly: directly, by reducing the signal's SINR, and indirectly, by reducing the quality of the channel response and received signal covariance matrix estimates. Moreover, since these effects occur at the receiver front-end, the interference suppression techniques cannot be applied to alleviate the problem. These techniques may only be applied after analog-to-digital conversion. Therefore, it is important to measure the impact of receiver imperfections on the receiver's interference suppression capabilities.

2.4 Summary

The use of advanced MIMO receivers to suppress inter-cell interference has the potential to largely improve the performance of wireless networks, but this potential will only be reached if the system is carefully designed to provide the support for the receiver's operation. The system design must address multiple aspects, such as inter-cell synchronization, channel estimation support and side information availability. These aspects must be evaluated alongside the multiple other aspects that define the design requirements for the 5G RAT concept. For this reason, it is important to consider the support for interference suppression receivers right at the beginning of the concept design process.

Chapter 3

Interference-robust air interface for 5G small cells

3.1 Introduction

In this chapter, the design of the proposed interference-robust air interface concept for 5G small cells is presented. The design process that led to this concept included multiple design targets based on the system performance required to meet the future customers expectations. The first part of the chapter describes the general design targets and solutions for the 5G RAT concept proposed in [6]. This overall description is used to explain the basic system characteristics that were taken into account during the design of inter-cell interference mitigation solutions. In the remainder of the chapter, the support to traditional inter-cell interference mitigation solutions is briefly described, followed by a detailed description of the solutions used to provide the required support for the use of interference suppression receivers as the main tool to manage inter-cell interference in the target scenarios.

It is important to mention that the 5G RAT concept is the result of a co-operation project between Nokia Networks and the Wireless Communication Networks research group at Aalborg University, Denmark. This thesis discusses the contributions made to the project regarding the use of advanced receivers to suppress and manage inter-cell interference.

3.2 General design targets and solutions

A careful design of the RAT concept must aim at fulfilling the performance requirements using solutions that are both simple and cost-effective. Figure 3.1 presents the general design targets for the RAT concept together with

the key technologies that may be used to reach them [4, 6, 67]. The mapping between the technologies and the targets they address is also shown in the figure.
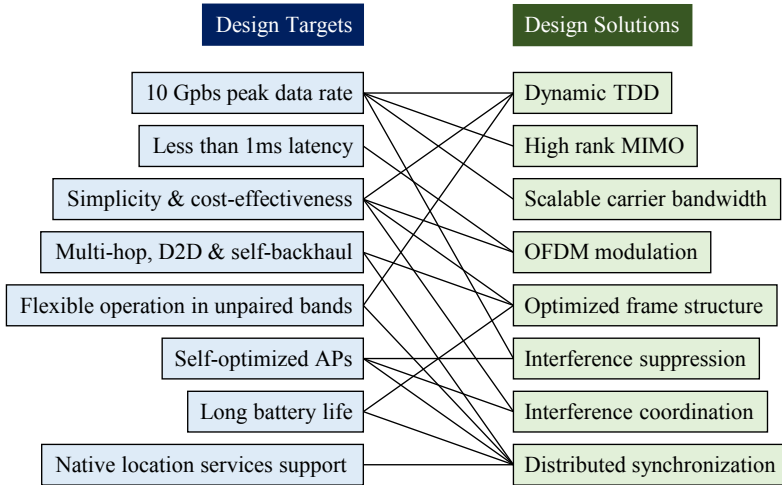
Fig. 3.1: 5G small cell RAT concept design targets and solutions.

As the figure shows, multiple solutions will be used to address each of the design requirements. In the following subsections, selected system features relevant to the design of the inter-cell interference suppression support features are discussed.

3.2.1 Reaching the peak data rate target

The 10 Gbps peak data rate target is the starting point to the definition of basic characteristics of the RAT. The bandwidth and spectral efficiency required to reach the target data rate at the physical layer are given by:

$$R = BS \tag{3.1}$$

where R is the data rate in bits/s, B is the bandwidth in Hz and S is the spectral efficiency in bits/s/Hz.

The peak data rate will only be reached at favourable conditions. Therefore, the maximum spectral efficiency of the system will be given by the spectral efficiency of the highest modulation and coding scheme multiplied by the maximum number of simultaneous spatial data streams used for transmission. Ideally, spectral efficiency much higher than that of LTE-A would be desired, but a more reasonable assumptions is that this number will not

increase much. It is expected that better transceivers will be able to use 256-ary Quadrature Amplitude Modulation (256-QAM) (due to the use of higher quality electronic components), whereas four transmit and receive antennas will become the standard for devices operating in the cm-wave spectrum. Using these numbers, the required bandwidth to reach the 10 Gbps target is 312.5 MHz.

However, this analysis assumes an overhead-free system. Assuming 20% overhead, which is close to the overhead in LTE, the required bandwidth becomes 390.625 MHz. For this reason, it is assumed that 400 MHz will be required, leaving 21.875% of margin to be used as overhead, if necessary. Note that, even in the 3.4 to 4.9 GHz spectrum region, it may be difficult to allocate contiguous 400 MHz bands. Thus, the RAT concept must support the use of carrier aggregation.

3.2.2 Dynamic TDD

The system is designed according to a cell-based architecture, with the Access Point (AP) clearly defined as the controller of the cell, i.e. the AP is responsible for scheduling when each User Equipment (UE) associated to the cell should access the radio resources.

A cell-based architecture requires a duplexing scheme to separate UL and DL transmission. Considering the target deployment conditions, TDD was considered a better option than FDD for multiple reasons:

- possibility to use unpaired bands;
- lower device cost due to the use of duplexing switches instead of duplexing filters;
- possibility to exploit channel reciprocity;
- possibility to adjust UL/DL resource allocation depending on traffic dynamics;

The last item of the list is a key aspect of the concept design. Macro cells and small cells have different data traffic demand dynamics. The demand for the traffic generated by a single user changes very quickly over time. The same is also valid for the ratio between DL and UL traffic. However, the total demand and the average UL/DL ratio change slowly in macro cells, due to the large number of users served per cell, as it is exemplified by Figure 3.2. The split of resources allocated for DL and UL transmissions also changes slowly, without big impact in the performance of the network.

Small cells will serve a much smaller number of users at the same time. Therefore, demand and ratio are expected to change much faster. If the split of resources is not adapted at the same rate, performance will be degraded. As an example, the ideal UL/DL resource ratio can change instantaneously,

in a small cell with only one connected user, when this user begins to upload something to the cloud right after downloading something from a remote server.
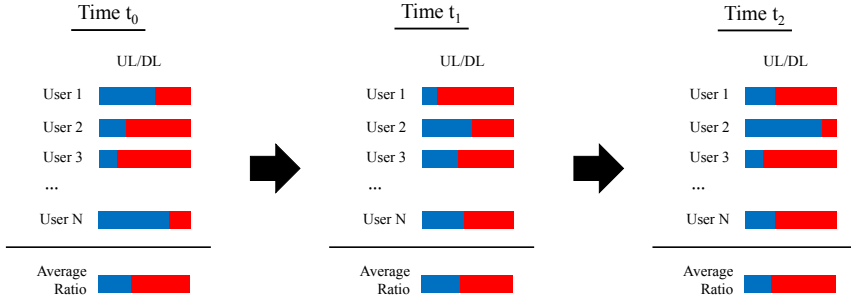
Fig. 3.2: Example of variation of UL/DL traffic demand over time, showing the demand for different users and the resulting average UL/DL traffic ratio.

A solution for this problem is the use of flexible UL/DL resource allocation, also known as Dynamic TDD [68, 69]. When Dynamic TDD is used, each cell can decide the link direction (DL or UL) independently at each frame, enabling the possibility of adjusting instantaneously to variations in traffic demand.

Ideally, it must be possible to allocate 100% of the resources for a single direction if necessary. However, even if the traffic is completely unidirectional, the transmission of data still requires the use of control channel in both directions, due to the need to exchange of important control messages, such as acknowledgements and channel quality measurements. Figure 3.3 shows the schematic of the Dynamic TDD frame structure designed for the 5G cm-wave RAT concept [67, 70, 71].
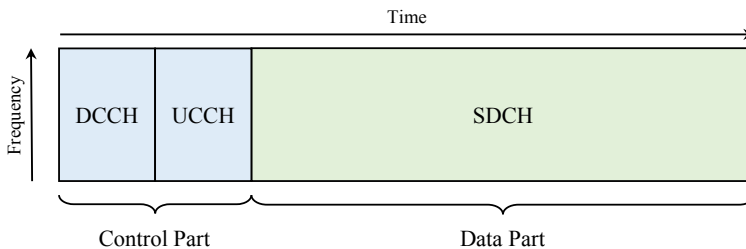
Fig. 3.3: Proposed 5G RAT frame format [67].

This frame is composed of a control part that includes both a Downlink Control Channel (DCCH) and a Uplink Control Channel (UCCH), and a data part that includes a Shared Data Channel (SDCH) that may be used for DL or UL transmissions. Since the control and data part are independent, there is no limitation to the allocation of resources for any direction, i.e. every frame may be selected for DL or UL transmissions irrespective of selection in previous frames.

The use of the SDCH is limited to one direction at a time, i.e. in each cell, the AP may not schedule DL and UL transmissions in the same frame. Besides, every device is expected to transmit for the whole duration of the SDCH. The reasons for these restrictions will be explained in Section 3.4.

3.2.3 Meeting the low latency target

To meet the 1 ms latency target, the full transmission procedure in both UL and DL directions must be completed in 1 ms or less. The full procedure includes the exchange of request and grant messages before data transmissions, the data transmissions itself and the exchange of acknowledgement messages after data transmission. This process requires the use of multiple frames. Figures 3.4 and 3.5 explains how the full transmission procedure can be completed in four frames in DL and UL directions, respectively [70].
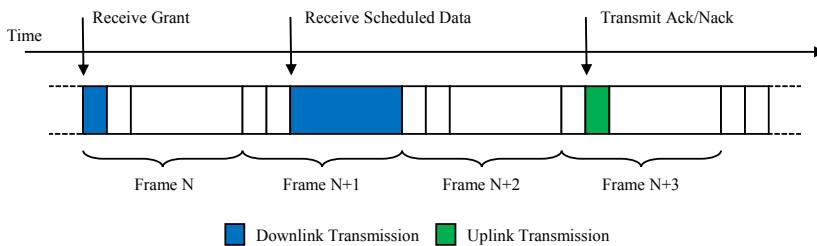
Fig. 3.4: Downlink transmission procedure.

In DL, the AP transmits a scheduling grant message over the DCCH at frame N, followed by the transmission of data over the SDCH at frame N+1. Due to the time needed to process the data at the receiver, it is assumed that the acknowledgement message (Ack/Nack) is transmitted by the UE over the UCCH at frame N+3.

In UL, the UE first transmits a scheduling request message over the UCCH at frame N+1, followed by the transmission of the scheduling grant message by the AP over the DCCH at frame N+1. The UE transmits the data over the SDCH at frame N+2 and the procedure ends with the transmission of the
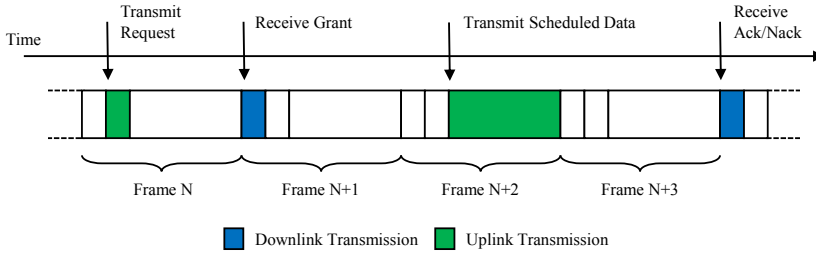
Fig. 3.5: Uplink transmission procedure.

acknowledgement message over DCCH at frame N+4.

Both transmission procedures require a minimum of 4 frames to complete. Therefore, to meet the 1 ms latency target, the frame length must be 0.25 ms or less, and the format must include opportunities to transmit control messages in both link directions at each frame.

3.2.4   Waveform

Even though novel waveforms have been proposed for 5G networks, OFDM is still considered a reasonable solution, balancing well simplicity and capability [67, 6]. OFDM has indeed many disadvantages including high Peak-to-Average Power Ratio (PAPR), high Out-of-Band Emission (OOBE) and the mandatory use of Cyclic Prefixs (CPs) to cope with the time dispersion of the multipath channel. Nevertheless, OFDM is much simpler than other proposed waveforms, such as Filter Bank Multicarrier (FBMC) [72, 73] and Universal-Filtered Multi-Carrier (UFMC) [74] and provides simple support for MIMO techniques [75].

A variant of OFDM that is only marginally more complex and still supports MIMO techniques very well are the DFT-spread OFDM (DFT-s-OFDM) waveforms. DFT-s-OFDM, also known as Single-Carrier FDM (SC-FDM), is the waveform used in UL transmissions in LTE/LTE-A [48]. This waveform has lower PAPR than OFDM, a feature that can reduce the transmitter's energy consumption (due to higher power amplifier efficiency). This advantage comes at the cost of higher BLER when compared to OFDM at the same SNR level.

The novel Zero-Tail DFT-s-OFDM (ZT-DFT-s-OFDM) [76, 77, 75] is almost as simple as the traditional DFT-s-OFDM and has the advantage of better OOBE than OFDM and the possibility to dynamically adjust the length of the cyclic prefix, without impacting the system numerology. The main benefit of this feature is to extend the range of the small cell without the need for time

advance procedure, a procedure used to compensate the propagation delays in large cells. The main disadvantage of the time advance procedure is the longer time required to setup a new link, which increases latency and energy consumption due to longer "wake up" periods.

The possibility of applying the ZT-DFT-s-OFDM waveform to the proposed 5G RAT concept is still under investigation. Therefore, OFDM waveform is assumed in this thesis.

3.2.5 System numerology

The proposed 5G RAT concept uses 0.25 ms long frames, composed of 14 OFDM symbols and three Guard Periods (GPs) for transitions from UL to DL and vice-versa [67, 6]. The guard periods are positioned such that the shared data part may be used for UL or DL transmissions regardless of the transmission direction in previous frames or in the control part. The Figure 3.6 presents a detailed schematic of the frame, whereas Table 3.1 summarizes the frame structure numerology. The table also shows the numerology of other relevant systems for comparison.
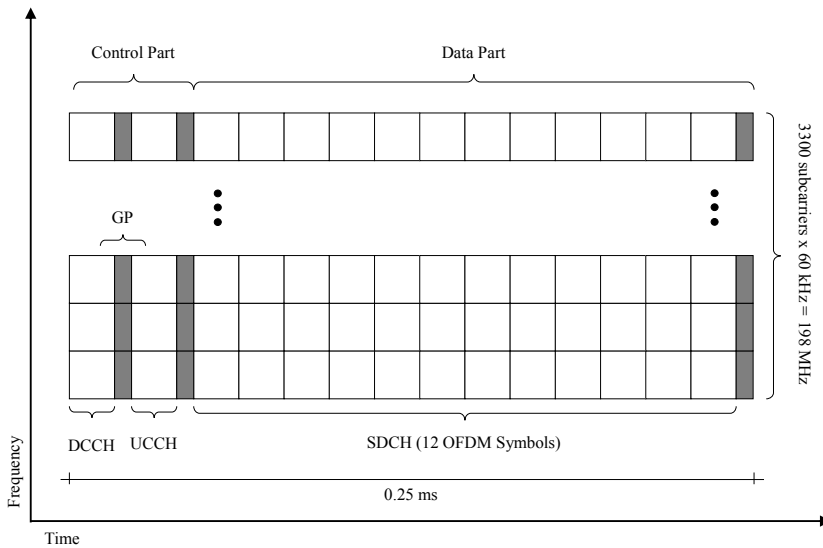
Fig. 3.6: Detailed schematic of the 5G RAT frame format.

Considering the 5G numerology presented in Table 3.1, the peak data rate target (10 Gbps) is reached if the system (i) uses 12 of the 14 symbols for

Table 3.1: 5G RAT concept numerology compared to LTE, LTE-A and IEEE 802.11ac [78] (based on similar table in [67]).

	5G	**LTE**	**LTE-A**[1]	**802.11ac**	
Carrier bandwidth [MHz]	200	20	100	20	160
Subcarrier spacing [kHz]	60	15	15	312.5	312.5
Symbol length [μs]	16.67	66.67	66.67	4	4
FFT size	4096	2048	5×2048	64	512
Effective subcarriers	3300	1200	5×1200	56	484
TTI duration [ms]	0.25	1	1	variable	variable
Number of GP	3	2	2	none	none
Number of symbols/frame	14	14	14	n.a.	n.a.
CP duration [μs][2]	1	4.7	4.7	0.4	0.4
GP duration [μs]	0.89	66.67	66.67	none	none
Overhead (CP+GP) [%]	6.67	7.25	7.25	11	11

[1] Based on a 5 Component Carrier (CC) configuration.
[2] Assuming the short Cyclic Prefix (CP) configuration.

data transmission (in the SDCH) and (ii) combines two 200 MHz carriers. In this case, the peak throughput at the physical layer is 10.1376 Gbps (20.8% overhead) [67].

3.3 Traditional interference mitigation support

The use of interference mitigation solutions is required for reaching high performance in small cell networks. The 5G cm-wave RAT concept was designed to support both traditional inter-cell interference coordination techniques and interference suppression receivers as the main interference mitigation solutions. This section deals with the traditional techniques.

The support for interference mitigation solutions was designed based on the assumption that it will be possible to synchronize the transmission and reception in different cells. In OFDM-based systems, synchronization is achieved if the OFDM symbols transmitted by different devices are received with a time misalignment τ_M that fulfils the following requirement [67]:

$$\tau_M < T_{CP} - \tau_D - \tau_{HW} - 2\tau_P \tag{3.2}$$

where T_{CP} is the duration of the CP, τ_D is the delay spread of the channel,

τ_{HW} is the delay response of the hardware filters and τ_P is the propagation delay. According to this formula, time misalignment τ_M must be within a fraction of T_{CP}. Assuming cells with 100 meters radius, which gives approximately 100 ns and 170 ns for τ_D and τ_P [79], respectively, and τ_{HW} in the order of 50 ns, the time misalignment τ_M must be less than 510 ns for 1 μs CP duration [67].

Network synchronization solutions, such as the IEEE 1588 PTP, cannot provide this synchronization accuracy level, whereas GPS-based synchronization is not possible due to high penetration losses in indoor scenarios. For these reasons, another solution for synchronizing the 5G small cells has been investigated and proposed [80, 81]. In this solution, multiple APs exchange over-the-air beacon messages that are used to correct the local timing reference. Using system-level simulations, this distributed synchronization methods has been shown to achieve residual synchronization error below 200 ns. The method was also tested in a testbed network using Software-Defined Radio (SDR) boards, confirming its feasibility [82].

The first benefit of inter-cell network synchronization is the possibility of separating the control and data parts of the frame, creating a protected control part that is only interfered by control parts of other transmissions. This separation simplifies the management of inter-cell interference levels in the control channels since UL-to-DL and DL-to-UL interference cannot occur.

A synchronized network also allows for the efficient use of inter-cell interference coordination techniques in the frequency and time domains. The advantage of synchronization for time-domain technique is obvious. In the frequency domain, inter-cell synchronization help to avoid the need for guard bands between different frequency allocation units. If cells are not synchronized, OFDM signals sent by multiple devices cannot be fully separated in the receiver; the interference signals in one allocation unit leak into other units. Therefore, guard bands would be required for minimizing this problem. If cells are synchronized, separating inter-cell signals in different allocation units become as simple as separating intra-cell signals and guard bands are not necessary.

For Frequency-domain ICIC (FD-ICIC), the frame may be divided in resource allocation units of approximately 10 MHz each. Both control and data parts are divided in blocks with independent allocation for each part (i.e. the frequency resources in the control part are not required to match the resources in the data part). This feature supports better adjustment for the different needs for interference protection in the different frame parts. FD-ICIC may be complemented by Inter-cell Interference Coordination (ICIC) in the component carrier domain in the same way as it is done in LTE-A [83].

Time-domain ICIC (TD-ICIC) is limited to frame by frame allocation. The ICIC allocation algorithm decides which frames shall be used by which cell, and if devices of a cell shall not use a frame, they can mute completely,

because no control information is transmitted in the data part. This is an advantage as compared to LTE-A because the use of Almost Blank Subframes (ABSs) is not necessary [84, 85].

The support for both FD-ICIC and TD-ICIC techniques also enables the use of mixed strategies that split resources in both domains. These strategies can be used to optimize the performance according to latency and energy consumption requirements. For example, FD-ICIC is generally better for lower latency requirements, whereas TD-ICIC increase the number of opportunities to apply energy saving strategies such as Discontinuous Reception (DRX) [86].

Another important aspect is the support for inter-cell message exchange, a feature used by ICIC techniques with centralized control and distributed ICIC techniques based on explicit coordination. The design of over-the-air control channels for this purpose is a topic that is still under investigation.

3.4   Support for interference suppression receivers

In this section, the design solutions used to provide the support necessary for interference suppression receivers are described. The idea behind such design is that the support will allow these receivers to perform as close to the ideal as possible, enabling their use as the main tools to deal with inter-cell interference in small cell networks.

3.4.1   Support for IRC receivers

As it was discussed in the previous chapter, the ideal IRC receiver can separate multiple received signals, achieving the optimal SINR for each of them. The performance of the receiver depends on the accuracy of the estimates of the channel response vectors and the received signal covariance matrix. The system design must therefore provide the means for obtaining highly accurate estimates at low complexity levels.

The first requirement is to guarantee inter-cell synchronization. This requirement is the same as the one discussed for other forms of inter-cell interference mitigation. Besides the aforementioned benefits of inter-cell synchronization, its use also enables the estimation of reference symbols transmitted by devices in other cells, facilitating the process of inter-cell interference estimation.

The main challenge for obtaining highly accurate interference signal estimates is the fact that long-term averages are not good enough to represent the interference conditions in small cell networks. Small cells usually serve few users at a time, causing received signal fluctuations much larger than those observed in macro cells. The small number of users also increases the

probability that a single (or few) interference signals will represent the largest part of the total interference and noise (i.e. the ratio between the power of the dominant interferer and the sum of the power of the rest of the interferers is usually very high in these scenarios). The use of Dynamic TDD makes the problem more complicated. Since cells are allowed to independently change the transmission direction at every frame, the interference sources may also change at every frame. Therefore, a better solution than long-term estimation is necessary.

Just-in-time estimation

The chosen design solution is to support "just-in-time" estimation, i.e. create the conditions to estimate with high accuracy all the required parameters that describe the interference conditions during a single frame using only information contained in that frame. Using this strategy, the interference source changes from frame to frame do not impact the estimation process; new estimations are made for each new frame.

To enable "just-in-time" estimation, the frame design enforces (i) the use of the SDCH for a single direction at a time, and (ii) the alignment of signal sources in the frequency domain (there cannot exist partial overlap of frequency allocation units in different cells). This enforcement guarantees that the interference sources will not change during a frame and that the estimates will represent the whole frame and not just part of it. By stabilizing interference sources, solutions for enabling the estimation of the parameters become much simpler.

Another important characteristic of the frame design is the use of identical frame formats for UL and DL transmissions. Using this approach, the problem created by UL-to-DL and DL-to-UL interference that may appear in TDD systems is eliminated; even if cells use Dynamic TDD, all received signals may be processed in the same way, regardless of link direction.

As a minimum requirement, the IRC receiver needs estimates of the channel response vectors regarding the desired signals and an estimate of the received signal covariance matrix. One possibility is to assume that the channel vectors will be estimated using reference symbols located at the control channels, whereas the covariance matrix will be obtained using the data symbols of the SDCH (using the DSB estimation method). This solution works, but due to the limited number of data symbols in a single frame, the number of samples may be insufficient to reach the required estimation accuracy level.

Another possibility is to transmit reference symbols in the SDCH, following the same principles as the UE-specific Demodulation Reference Signal (DMRS) in LTE-A [87, 48]. If all transmitters that are sending data in a specific channel also send reference symbols in the same frame, it is possible to estimate the currently active interference signals and calculate the received

signal covariance matrix using a RSB estimation method. This strategy requires that the multiple transmitters use orthogonal reference symbols to guarantee that channel vector estimates regarding different sources do not interfere with each other. Another important requirement is the use of precoded reference symbols. If non-precoded reference symbols were used, the receiver would need to know the rank and precoding matrix used by each signal source at each frame, a situation that would prove impracticable.

The greatest advantage of this approach is the higher estimation accuracy that can be reached. Since the estimation is based on reference symbols properly designed for the task, the number of samples required to reach the required accuracy is lower, providing a solution that better fits with "just-in-time" estimation in a very short frame.

The performance of both "just-in-time" estimation methods is investigated using system-level simulations and the receiver model presented in Appendix A (including the receiver front-end imperfections model). The receiver model takes into account the RAT concept numerology presented in Table 3.1 to define the number of estimation samples that are available at each frame, depending on the estimation method used.

The number of samples is calculated assuming that the frequency resolution of covariance matrix estimation will be 900 kHz, which is equivalent to 15 OFDM subcarriers [55]. Figure 3.7 shows the details of the SDCH, depicting the position of the DMRS. Using this configuration, the number of samples Q_{DS} for the estimation of the received signal covariance matrix $\hat{\mathbf{R}}_r$ using the DSB method is therefore 165 samples (11 OFDM symbols × 15 subcarriers). In the case of the RSB method, the number of samples Q_{RS} used to estimate the residual covariance matrix $\hat{\mathbf{R}}_n$ is 15 samples. The results of this evaluation are presented in Chapter 4.

Rank adaptation for IRC receivers

The use of inter-cell synchronization and "just-in-time" estimation helps the IRC receiver to operate close to its ideal performance. Nevertheless, the data rates that can be achieved still depend on the performance of the rank and precoding adaptation algorithm. As discussed in the previous chapter, the amount of interference that the IRC receiver is able to reject depends on the number of antennas and the number of received signals. Rank adaptation is therefore used for choosing the ideal number of transmitted data streams, balancing the interference rejection capability and the spatial multiplexing gains.

The implementation of IRC-aware rank adaptation algorithms become very simple when "just-in-time" estimation is used, because all the information necessary to estimate the expected performance for each possible rank (e.g. channel and covariance matrix estimates) is readily available. The only
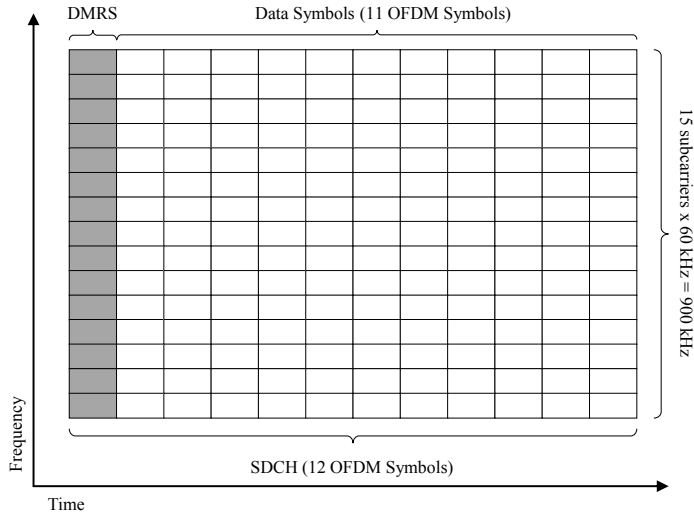
Fig. 3.7: Detailed schematic of the Shared Data Channel (SDCH).

performance limiting factor that remains is the delay between deciding the rank to be used and the actual transmission using that rank. Since the interference sources can change at every new frame, the rank adaptation algorithm should try to anticipate the changes to reach optimal performance.

Besides the individual link management role, the IRC-aware rank adaptation algorithm may also play a role in the management of network-wide inter-cell interference levels. By using victim-aware rank adaptation algorithms [59, 60, 61], the probability that the IRC receivers will have enough degrees of freedom to reject enough inter-cell interference may be increased. In this research work, the goal has been to identify simple victim-aware rank adaptation strategies that enable effective network-wide inter-cell interference management. The ultimate goal is to verify the hypothesis that inter-cell interference mitigation using interference suppression receivers may be easily applied as an alternative to mitigation in the frequency and time domains.

Maximum Rank Planning (MRP) The simplest of these victim-aware rank adaptation strategies is the Maximum Rank Planning (MRP) technique [59]. This technique consists in limiting the maximum number of data streams that may be used by a transmitter. This approach forces a reduction in the number of streams transmitted, increasing the probability that the victim receivers will be able to reject the interference.

The advantage of MRP is the improved performance in cells that are heavily interfered, because the small number of data streams have higher prob-

ability of been rejected. The ideal rank limit depends on the interference conditions. The limit may be applied network-wide, limiting all cells in the same way, or some method to select the limit for each cell can be devised.

Taxation-based Rank Adaptation (TRA)   Victim-aware rank adaptation algorithms may also be designed to apply simple weights to the each possible rank, artificially making higher ranks less attractive during the selection process. This weights may be constant or adjusted according to inter-cell interference levels [60].

A simple and practical example of a dynamic victim-aware rank adaptation algorithm is the Taxation-based Rank Adaptation (TRA) algorithm proposed in [61]. The principle of this algorithm is to introduce a taxation mechanism that discourages the selection of higher ranks when this would harm the neighbour cells. To select the rank for transmission, the j-th transmitting node selects the rank N_S^j that is expected to maximize Π_j, which is given by

$$\Pi_j = C_{N_S^j} - \underbrace{f_W(N_S^j)C(I)}_{\text{Taxation for rank } N_S^j} \tag{3.3}$$

where $C_{N_S^j}$ is the expected link capacity in case rank N_S^j is selected, $f_W(N_S^j)$ is a monotonically increasing weighting function, which quantifies the level of taxation, and $C(I)$ is a metric proportional to the inter-cell interference generated by the j-th transmitting node. Conservative and aggressive victim-aware rank adaptation strategies are obtained using different weight functions $f_W(N_S^j)$.

Ideally, the $C(I)$ metric should be calculated based on the actual instantaneous interference caused by the transmissions. However, obtaining such information is not feasible in practice, because it would require the exchange of impracticable amounts of information among neighbour cells. For this reason, the TRA algorithm proposed in [61] uses the interference received by the j-th node to calculate the $C(I)$ metric (even though it is admittedly a suboptimal approximation). Using this approximation, the $C(I)$ metric is calculated as

$$C(I) = \log_2\left(1 + \frac{tr\left(\sum_{k=1}^{N_T}\sum_{l=1}^{N_S^k}\hat{\mathbf{h}}_{k,l}\hat{\mathbf{h}}_{k,l}^H\right)}{tr\left(\hat{\mathbf{R}}_n\right)}\right) \tag{3.4}$$

where $tr(\cdot)$ is the matrix trace operator.

3.4.2 Support for IRC-SIC receivers

The proposed system design provides support for the cancellation of inter-stream interference. The support for inter-cell interference cancellation was not included in the design due to the reasons presented below.

As it was discussed in the previous chapter, interference cancellation requires the successful decoding of the signals before they can be removed from the overall received signal. The success of the decoding operation depends on the matching between the link capacity (between the interfering transmitter and the receiver) and the MCS used for the transmission of the signal. If the probability that this matching will occur is low, the benefits of inter-cell interference cancellation will also be low.

The probability of matching depends on the link adaptation strategy applied to adjust the MCS of the multiple transmitted signals. If the link adaptation is independent and selfish, the inter-cell interference cancellation becomes opportunistic and these opportunities rarely happen in small cell scenarios [63]. The other possibility is to choose the MCS of the multiple signals aiming at increasing the probability that they will be decodable at the victim receivers. However, this approach would required a centralized brute-force exhaustive search of all possible MCS combinations for the multiple links of the network. Considering the complexity of this approach, the use of victim-aware link adaptation was discarded and not considered in the concept design.

Considering that the benefits of inter-cell interference cancellation in the target scenarios are probably low, the incentive for including mechanisms for making the side information required for inter-cell interference cancellation available was also low. This mechanism would increase considerably the control channel overhead if over-the-air inter-cell messages were to be exchanged or would require wired connections between the multiple access points, a possibility that was ruled out due to the high costs and the increased deployment complexity.

Nevertheless, interference cancellation may be applied to inter-stream interference. This strategy surely does not deal directly with the small cell network's main problem (inter-cell interference), but it has the potential to indirectly help, by increasing the degrees-of-freedom of the MMSE combiner stage as the desired signals are decoded and removed from the total received signal.

The support for the use of IRC-SIC receiver to cancel inter-stream interference is much simpler than that required for inter-cell interference cancellation. In fact, all the side information required for decoding the desired signals must be transmitted even if interference cancellation is not used. There is no need to design additional control channels for the task. By enforcing different codewords in each spatial stream, the gain of inter-stream interference can-

cellation can be maximized. The remaining requirement is the use of a link adaptation algorithm that is aware of the interference cancellation process. Novel link adaptation algorithms that account for this new requirement are still under investigation.

3.5   Summary

By carefully designing the features necessary to support their operation, interference suppression receivers can operate close to their ideal performance. This condition leads to an air interface that presents very high robustness to strong inter-cell interference. With the additional aid of victim-aware rank adaptation algorithms to further improve network-wide interference conditions, this new interference-robust air interface is expected to be fundamental for the deployment of 5G ultra-dense small cell networks. The performance evaluation presented in next chapter verifies whether it is indeed possible to use of advanced receivers and victim-aware rank adaptation to manage inter-cell interference in these networks.

Chapter 4

Performance evaluation

4.1 Introduction

This chapter presents the performance evaluation study conducted to test the main hypothesis of this research work, i.e. whether the use of interference suppression receivers may be used as a valid alternative to traditional inter-cell interference coordination techniques in dense small cell networks. Before delving into the results, the simulator assumptions are briefly described (the detailed description is presented in Appendix B). The simulation results and the discussion regarding their implications are presented in the remaining sections.

4.2 General simulation assumptions

4.2.1 Simulation scenario

Three different representative dense indoor small cell scenarios are used in the performance evaluation. These scenarios are formed by the combination of a network topology, which may be either Indoor Hotspot or Indoor Office, and a cell access mode, which may be either Open Subscriber Group (OSG) or Closed Subscriber Group (CSG).

Figure 4.1(a) shows the schematic of the Indoor Hotspot network topology. This topology consists in a large open area, measuring 40 by 100 meters, which is similar to an airport check-in hall or a large conference hall. The total area of the hall is divided in 40 cells, each of them represented by a "virtual" square area measuring 10 by 10 meters. There are no walls in between the square areas. One AP is deployed in the middle of each area (fixed to the celling) and one UE randomly placed per area. This network topology uses

the Winner II Indoor Hotspot (B3) model [88] for both large and small scale propagation effects.

(a) Indoor Hotspot
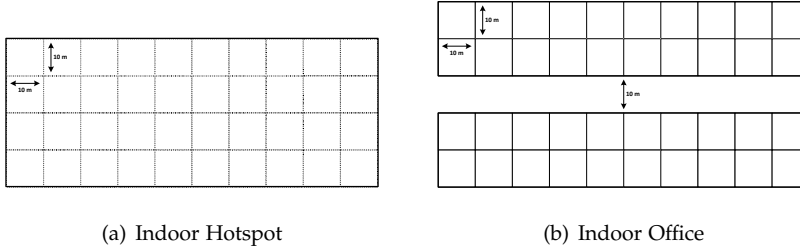
(b) Indoor Office

Fig. 4.1: Network topologies used in the performance evaluation.

The schematic of the Indoor Office network topology is presented in Figure 4.1(b). This topology emulates office or apartment buildings. The topology consists in two buildings separated by a ten-meter-wide street. Each building is formed by two rows of ten offices and each office measures 10 by 10 meters. One AP and one UE are deployed per office, summing up 40 cells per floor. In this study, only one floor is considered due to simulation time restrictions. This network topology uses the 3rd Generation Partnership Program (3GPP) Dual Stripe model [89] and the Winner II Indoor Hotspot (A1) model [88] for both large and small scale propagation effects, respectively.

When the CSG is enforced, the UEs may only connect to the AP located in the same office; when the OSG access mode is used instead, the UEs may freely connect to any cell. In the OSG case, a cell selection algorithm chooses the AP to which each UE should be connected based on the highest received power. If no UEs are connected to a certain AP, this AP is turned off during the simulation. If more than one UE connect to the same AP, a simple fair round-robin frequency-domain scheduling algorithm is used to assign the radio resources to each UE.

Table 4.1 describes the scenarios according to the combinations. Note that the combination of Indoor Hotspot network topology with CSG access mode is missing from the table. Although possible, this scenario is deemed as highly improbable and thus it is not considered in this study.

Table 4.1: Simulation scenarios used in the performance evaluation.

Scenario	Network Topology	Access Mode
Scenario A	Indoor Hotspot	OSG
Scenario B	Indoor Office	OSG
Scenario C	Indoor Office	CSG

The load of the network is controlled with the Activity Factor (AF) parameter. This parameter defines the probability that a cell will not be idle during a certain time frame, i.e. the probability that either the AP or the UE will transmit (in all simulations, UL and DL transmissions are equiprobable). The AF parameter is one of the parameters used to control the random data traffic model, which is used to model the Dynamic TDD frame structure, and affects the short-term interference conditions of the network.

4.2.2 Physical layer assumptions

The receiver model described in Appendix A is used to calculate the SINR of each received signal at each time frame. The SINR is adjusted using an Error Vector Magnitude (EVM) model to account for transceiver imperfections (EVM is 5% except when stated otherwise). The adjusted SINR is then used to calculate the approximate instantaneous cell throughput using the well-known Additive White Gaussian Noise (AWGN) channel capacity formulation. The maximum spectral efficiency efficiency is limited to 8 bps/Hz per spatial stream (which is equivalent to 256-QAM) and the minimum decodable SINR is -6 dB (the SINR required to decode Quadrature Phase Shift Keying (QPSK) with coding rate 1/6 [90]).

It is assumed that all devices are equipped with multi-antenna transceivers with 4 transmit and 4 receive antennas each. Each device may transmit up to 4 simultaneous spatial data streams and the LTE Release 8 precoding matrix codebook [48] is used to match the number of transmitted signals to the number of transmit antennas. The rank adaptation model assumes that the rank and precoding selection feedback from the receiver to the transmitter is ideal, i.e. each transmitter-receiver pair independently selects the rank and precoding matrix at each frame based on the current channel and interference conditions. Moreover, wideband feedback is assumed (the same matrix is used for all allocated frequency resources). The different types of rank adaptation algorithms used in the performance evaluation were the Selfish Rank Adaptation (SRA), the MRP [59] and the TRA [61] algorithms.

4.2.3 Simulation setup

A quasi-static system-level simulator is used for estimating the network performance. Each simulation consists in 200 snapshots of 200 time frames. The frequency-selective fast fading is updated at each time frame (block fading model is assumed), but the large scale propagation effects (pathloss and shadowing) are kept constant for the duration of the snapshot.

The average throughput of each cell is calculated for each snapshot as the average instantaneous throughput including transmissions in both directions (discarding idle frames). All average cell throughputs in all snapshots are

collected to create an empirical Cumulative Distribution Function (CDF) per simulation. The throughput values are also used to calculate the key performance indicators used in the performance evaluation: outage (5th percentile), average and peak (95th percentile) throughputs.

4.3   Inter-cell interference suppression performance

In the first part of this performance evaluation, the network performance is estimated in the three different scenarios considering different receiver types. The goal is to provide a general view of the potential benefits of the use of inter-cell interference suppression in each scenario.

Figures 4.2, 4.3 and 4.4 present the cumulative distribution probability of the average cell throughput (in the form of CDF curves) for Scenarios A, B and C, respectively. All simulation cases consider fully deployed networks with either low (25% AF) or maximum (100% AF) network traffic load. All cells use the same spectrum resources, i.e. Frequency Reuse 1 (FR1), and the rank adaptation method used is selfish (SRA) in all cases. The key performance indicators and the performance gains over the baseline are presented in Tables 4.2, 4.3 and 4.4 for Scenarios A, B and C, respectively.

This set of results clearly shows that interference suppression receivers (IRC and SIC) outperform the baseline receiver (MRC) in all three scenarios and different network traffic load conditions. Nevertheless, considerably different performance gains are observed in each scenario.

In Scenario A, the performance gain reduces as the load increases. This may be observed comparing the gains with 25% AF and 100% AF. This is explained by the large number of strong inter-cell signals that interfere the received signals (mostly due to the lack of walls separating the cells). As the network load increases from 25% to 100%, the number of inter-cell interference signals that are treated as spatially uncorrelated noise increases, getting close to a condition similar to the MRC receiver that treats all inter-cell interference as noise.

Another interesting fact about Scenario A is the behaviour of the selfish rank adaptation algorithm. When the network traffic is 100%, the rank adaptation algorithm rarely uses more than one spatial stream (rank 1). This is confirmed by the low peak data rates (which are bellow one fourth of the maximum data rate) and the almost identical CDFs regarding IRC and SIC receivers, suggesting that there are no inter-stream signals to be cancelled. This behaviour indicates that the interference condition in this scenario is balanced, i.e. as network load increases, the inter-cell interference affects homogeneously all the cells.

In Scenario B, the performance gains due to the use of interference suppression receivers increase as the network traffic load increases, as opposed

(a) Low load (25% AF)

(b) Maximum load (100% AF)
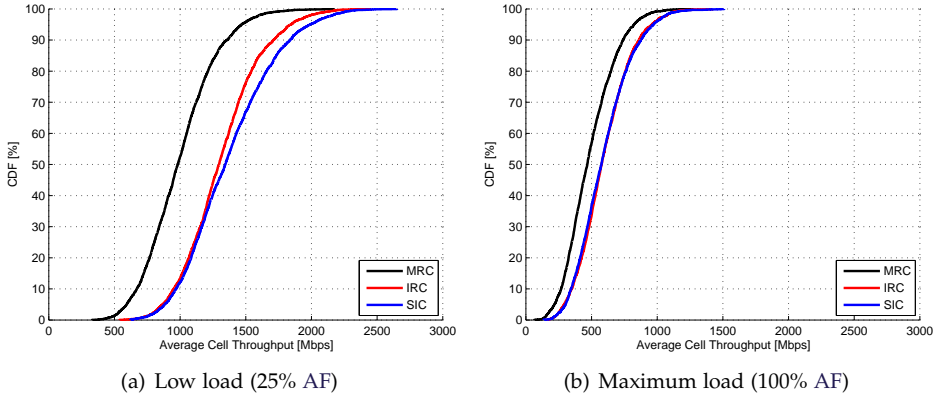
Fig. 4.2: Simulation results comparing the performance of different receiver types in Scenario A (Indoor Hotspot OSG) for different network traffic loads.

Table 4.2: Key performance indicators (in Mbps) for different receiver types and performance gains over the baseline receiver (MRC) in Scenario A (Indoor Hotspot OSG).

Load	Receiver	Outage	Average	Peak
25%	MRC	593.8	998.7	1468.1
	IRC	870.3 (+46.6%)	1314.8 (+31.6%)	1845.9 (+25.7%)
	SIC	881.4 (+48.4%)	1375.1 (+37.7%)	1990.4 (+35.6%)
100%	MRC	218.1	487.7	823.7
	IRC	291.4 (+33.6%)	595.8 (+22.2%)	959.9 (+16.5%)
	SIC	302.6 (+38.7%)	594.2 (+21.8%)	971.8 (+18.0%)

to Scenario A. This situation is explained by the signal power attenuation caused by the walls that separate the cells, which causes few inter-cell interference signals to dominate the overall interference power.

At low load, the number of cells that are affected by overwhelming inter-cell interference levels is very low. This is observed in the low outage gain when the IRC receiver is used. As the load increases, the interference level increases, but only few signals are relevant to the overall interference level and, by suppressing some or all of them, the SINR is significantly improved.

The performance gain due to the use of SIC also increases as the network load increases, but it is important to note that the difference between the outage gain when the IRC or the SIC receiver is used becomes marginal. This indicates that the rank adaptation algorithm is forced to select low rank for the cells in high interference conditions. In this situation, the potential benefits of SIC are reduced, but the use of SIC is still advantageous for a large number of cells.

(a) Low load (25% Deployment Ratio (DR))   (b) Maximum load (100% DR)
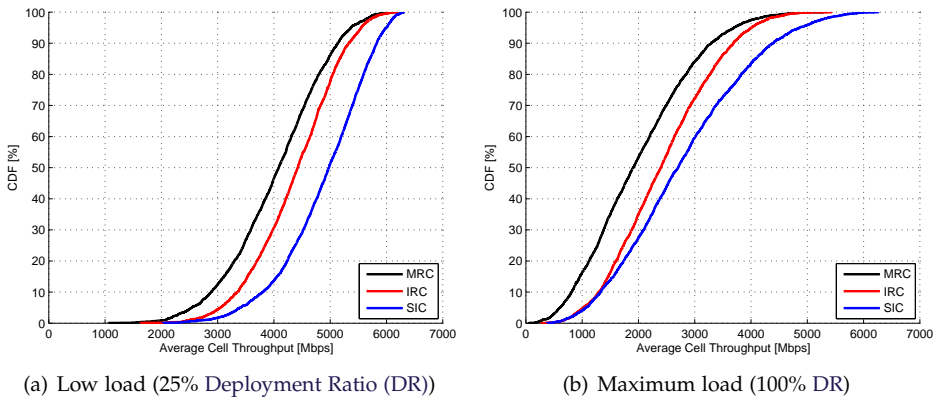
Fig. 4.3: Simulation results comparing the performance of different receiver types in Scenario B (Indoor Office OSG) for different network traffic loads.

Finally, in Scenario C, the results present the largest performance gains due to the use of interference suppression receivers, with up to 135% outage throughput gain. Once more, all performance indicators are improved, clearly indicating that the use of interference suppression receivers is highly recommended. The interference conditions in Scenario C are very similar to Scenario B. The walls cause few inter-cell interference signals to dominate the overall interference power, but in Scenario C the interference levels are even higher due to the use of CSG access mode.

The results also show that the use of SIC receiver may lead to unexpected negative effects in the network. Note that, at 100% load, the outage throughput (and the corresponding performance gain) when SIC is used is lower than

Table 4.3: Key performance indicators (in Mbps) for different receiver types and performance gains over the baseline receiver (MRC) in Scenario B (Indoor Office OSG).

Load	Receiver	Outage	Average	Peak
25%	MRC	2543.5	4041.7	5372.4
	IRC	3054.0 (+20.1%)	4374.3 (+8.2%)	5549.7 (+3.3%)
	SIC	3404.2 (+33.8%)	4885.2 (+20.9%)	5996.3 (+11.6%)
100%	MRC	605.5	1997.6	3700.4
	IRC	1023.3 (+69.0%)	2439.8 (+22.1%)	4009.7 (+8.4%)
	SIC	1068.0 (+76.4%)	2795.7 (+40.0%)	4862.7 (+31.4%)

when IRC is used. This occurs because the use of SIC increases the probability that higher ranks are used in the network, causing negative effects on the performance of the linear combining stage and reducing the inter-cell interference suppression performance. This effect is observed especially in the cells that have already exhausted the degrees of freedom to reject interference and are therefore forced to treat the extra interference signals as noise.

(a) Low load (25% DR)

(b) Maximum load (100% DR)
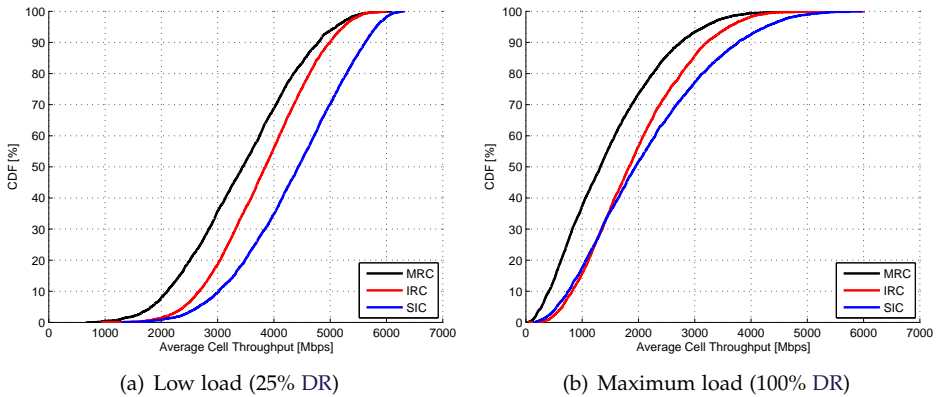
Fig. 4.4: Simulation results comparing the performance of different receiver types in Scenario C (Indoor Office CSG) for different network traffic loads.

4.4 Performance considering receiver imperfections

In this section, receiver imperfections are considered in the performance evaluation. In the first part of the section, performance obtained using the two different covariance matrix estimation methods are compared to the ideal performance. The objective is to identify which method performs best and

Table 4.4: Key performance indicators (in Mbps) for different receiver types and performance gains over the baseline receiver (MRC) in Scenario C (Indoor Office CSG).

Load	Receiver	Outage	Average	Peak
25%	MRC	1823.0	3439.5	5105.1
	IRC	2396.7 (+31.5%)	3830.5 (+11.4%)	5242.9 (+2.7%)
	SIC	2660.3 (+45.9%)	4367.2 (+27.0%)	5818.1 (+14.0%)
100%	MRC	277.5	1463.1	3175.3
	IRC	652.4 (+135.1%)	1942.7 (+32.8%)	3612.3 (+13.8%)
	SIC	549.0 (+97.8%)	2123.6 (+45.1%)	4265.6 (+34.3%)

whether the number of estimation samples per frame is sufficient. The rest of the section deals with the receiver front-end imperfections that may directly affect the interference suppression capability of the receivers.

In this part of the performance evaluation, only Scenario C is considered. This scenario was chosen due to the large performance gains of the advanced receivers observed in the first stage of the evaluation. The idea is to observe whether these gains are maintained when the imperfections are considered. The scenario is also considered due to the strong interference dominance condition observed in the network. In this condition, the combining stage is more susceptible to poor performance because small errors may lead to inefficient rejection of the relevant interferers.

The network traffic load is set to two thirds of the maximum (approximately 67%), which leads to equal probabilities of idle, DL and UL frames. This setup is used to create an interference scenario in which the interference level varies significantly from frame to frame. This large interference level variation is expected to be a problem for the receiver front-end.

In this part of the performance evaluation study, the EVM model is disabled, i.e. the only receiver imperfections considered are those modelled by the receiver model presented in Appendix A. Table 4.5 presents the values used to adjust the receiver model to emulate the expected conditions using the optimized frame structure.

Figure 4.5 shows a comparison of the performance of the IRC and SIC to the baseline receiver (MRC) when different received signal covariance matrix methods are used. In each figure, three different cases are shown for each receiver: ideal estimation, DSB estimation and RSB estimation. Table 4.6 summarizes the performance indicators and the losses due to imperfect estimation.

From the results, it is possible to conclude that the RSB method outperforms the DSB method, regardless of receiver type. This result is valid considering the number of estimation samples available for each method in the

Table 4.5: Physical layer parameters.

Number of samples for estimation		
Channel Vector	Q_{H}	4 samples
Covariance Matrix (DSB)	Q_{DSB}	165 samples
Covariance Matrix (RSB)	Q_{RSB}	15 samples
Receiver front-end parameters		
Noise Figure	*NF*	8 dB
ADC Full Range Amplitude	*A*	1 V
Back-off factor	ϵ	11.8 dB
AGC delay	τ	0 or 1 TTI
ADC resolution	*b*	6 or 10 bits

(a) IRC *vs.* MRC

(b) SIC *vs.* MRC
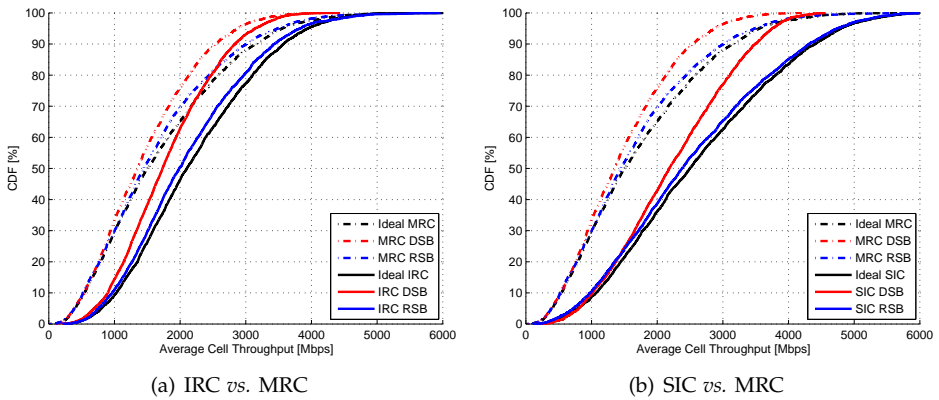
Fig. 4.5: Comparison between ideal, DSB and RSB covariance matrix estimation methods in Scenario C.

Table 4.6: Key performance indicators (in Mbps) for different covariance matrix estimation methods and performance gain/loss over the baseline (ideal estimation) in Scenario C.

Receiver	Method	Outage	Average	Peak
MRC	Ideal	406.6	1704.0	3556.4
	DSB	383.1 (-5.8%)	1457.3 (-14.5%)	2868.7 (-19.3%)
	RSB	393.2 (-3.3%)	1631.9 (-4.2%)	3486.6 (-2.0%)
IRC	Ideal	802.1	2220.5	3947.6
	DSB	689.5 (-14.0%)	1806.0 (-18.7%)	3142.8 (-20.4%)
	RSB	756.4 (-5.7%)	2120.6 (-4.5%)	3830.6 (-3.0%)
SIC	Ideal	792.5	2624.6	4795.0
	DSB	803.9 (+1.4%)	2230.2 (-15.0%)	3748.6 (-21.8%)
	RSB	722.8 (-8.8%)	2533.0 (-3.5%)	4737.9 (-1.2%)

optimized frame structure (assuming 900 KHz frequency resolution, there are 15 and 165 samples for RSB and DSB, respectively). The better performance with RSB is obtained despite the lower number of estimation samples; this occurs because the quality of the estimation depends on both the power (variance) of the estimated signal and the number of samples. With RSB, the covariance matrix is only calculated for the residual signal, a signal with much less power than the received signal used in the DSB method.

Observing the results for the SIC receiver, it is possible to notice that there is a slight increase in the outage performance when the DSB method is used. This counter-intuitive result is explained by the same mechanism that leads to lower outage throughput in comparison to the IRC receiver. When the DSB method is used, the use of higher ranks becomes less common and this impacts positively the performance of highly interfered receivers. Despite this result, the use of the RSB method provides the best overall network performance.

The impact of receiver front-end imperfections is observed in Figures 4.6 and 4.7 for both IRC and SIC receivers, respectively. The figures show the impact of ADC resolution when the AGC mechanism is assumed ideal or delayed. In all cases, the RSB covariance matrix estimation method is assumed. Tables 4.7 and 4.8 present the performance indicators for IRC and SIC cases, respectively.

When ideal AGC is assumed, the results show that ADC circuits with 10 bits resolution lead to low performance degradation (with up to 5.6% and 6.9% outage performance degradation for IRC and SIC, respectively). The results also show that the use of lower resolution will degrade much more the performance, as it is observed when 6 bits resolution ADC is used.

The performance degradation increases when the delayed AGC is as-

(a) Ideal AGC

(b) Delayed AGC
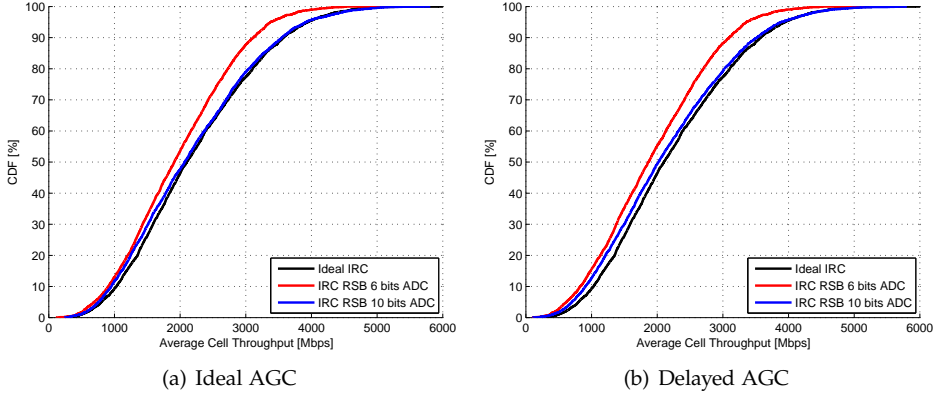
Fig. 4.6: Simulation results for different IRC receiver front-end parameters in Scenario C.

(a) Ideal AGC

(b) Delayed AGC
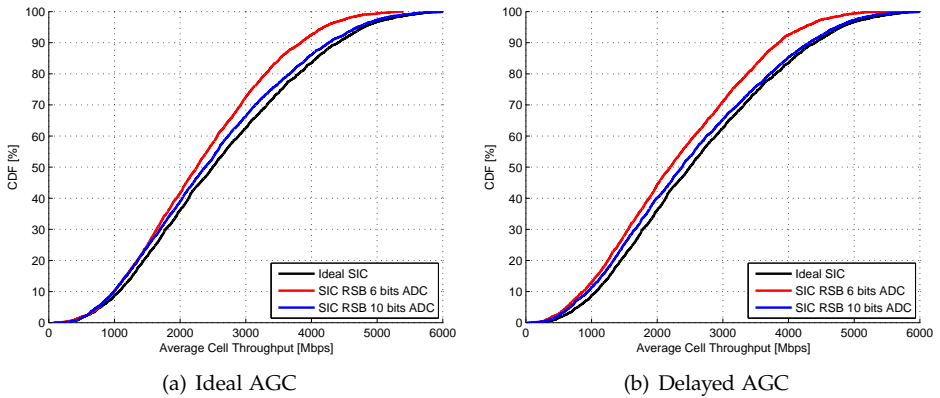
Fig. 4.7: Simulation results for different SIC receiver front-end parameters in Scenario C.

sumed, because the receivers ability to adjust the received signal to the dynamic range is reduced (the receiver is not able to predict changes in interference levels). In this case, the outage throughput losses increase to 12.6% and 14.7% for IRC and SIC cases, respectively. This losses are considerable and indicate that the use of higher-resolution ADC circuits or faster AGC mechanisms may be necessary.

Table 4.7: Key performance indicators (in Mbps) for IRC receiver with different ADC resolution values and AGC delay configurations and performance gain/loss over the baseline (ideal receiver front-end) in Scenario C.

AGC	ADC	Outage	Average	Peak
	Ideal	802.1	2220.5	3947.6
Ideal	6 bits	694.7 (-13.4%)	1970.3 (-11.3%)	3379.5 (-14.4%)
	10 bits	757.0 (-5.6%)	2173.5 (-2.1%)	3917.1 (-0.8%)
Delayed	6 bits	614.1 (-23.4%)	1926.6 (-13.2%)	3355.1 (-15.0%)
	10 bits	700.8 (-12.6%)	2138.3 (-3.7%)	3889.5 (-1.5%)

Table 4.8: Key performance indicators (in Mbps) for SIC receiver with different ADC resolution values and AGC delay configurations and performance gain/loss over the baseline (ideal receiver front-end) in Scenario C.

AGC	ADC	Outage	Average	Peak
	Ideal	792.5	2624.6	4795.0
Ideal	6 bits	761.9 (-3.9%)	2336.0 (-11.0%)	4186.3 (-12.7%)
	10 bits	738.1 (-6.9%)	2513.2 (-4.2%)	4704.2 (-1.9%)
Delayed	6 bits	624.2 (-21.2%)	2303.7 (-12.2%)	4245.3 (-11.5%)
	10 bits	676.2 (-14.7%)	2515.0 (-4.2%)	4732.9 (-1.3%)

To conclude the evaluation regarding the impact of receiver imperfections, the performance of the different receivers is compared assuming imperfect receivers, i.e. assuming channel and covariance matrix estimation errors (RSB method is assumed), and receiver front-end errors (10 bits ADC with delayed AGC). Figure 4.8 shows this comparison and Table 4.9 presents the performance indicators and the corresponding gains in both ideal and imperfect cases.

The results show that there is indeed degradation of the interference suppression capability, which is confirmed by the lower outage throughput gains. Besides, the results show that the SIC receiver suffers more with the imperfections than the IRC receiver. Nonetheless, the performance gains obtained

Fig. 4.8: Simulation results for different receiver types considering receiver imperfections (RSB covariance matrix estimation, 10 bits ADC resolution and delayed AGC) in Scenario C.

using interference suppression receivers are still high and indicate that these imperfections do not make their advantages disappear.

Table 4.9: Key performance indicators (in Mbps) for different ideal and imperfect receiver configurations and performance gains over the baseline receiver (MRC) in Scenario C. The imperfect receiver configuration assumes RSB covariance matrix estimation, 10 bits ADC resolution and delayed AGC.

Case	*Receiver*	*Outage*	*Average*	*Peak*
Ideal	MRC	406.6	1704.0	3556.4
	IRC	802.1 (+97.2%)	2220.5 (+30.3%)	3947.6 (+11.0%)
	SIC	792.5 (+94.9%)	2624.6 (+54.0%)	4795.0 (+34.8%)
Imperfect	MRC	385.4	1677.3	3501.5
	IRC	700.8 (+81.8%)	2138.3 (+27.5%)	3889.5 (+11.1%)
	SIC	676.2 (+75.4%)	2515.0 (+49.9%)	4732.9 (+35.2%)

4.5 Interference suppression *versus* Frequency Reuse Planning (FRP)

The next step in this performance evaluation is to compare the use of interference suppression receivers to Frequency Reuse Planning (FRP). Although other techniques could also be used in the comparison, FRP was chosen for this work as a representative inter-cell interference management technique. The reason for restricting the comparison to FRP was to reduce the complexity of the comparison process. If complex dynamic ICIC methods were used as baseline, the uncertainties regarding the parameters used to control the

methods and other practicalities would complicate the analysis of the results. By using FRP as baseline, this problems do not occur, since FRP is a well understood and simple-to-apply technique.

For this comparison, the term *network configuration* is used to refer to the combination of a receiver type and a frequency reuse plan. For each scenario and network traffic load condition, the baseline configuration is the combination of the baseline receiver (MRC) with the frequency reuse plan that provides the highest outage data rate (which is used as the target requirement in this comparison). This baseline configuration is compared with two configurations each formed by one of the interference suppression receivers and FR1.

Starting with Scenario A, it is possible to verify in Figure 4.9(a) that the use of FRP does not bring any benefit to the network. The same is confirmed by the performance indicators in Table 4.10; FR1 is the best performing configuration at all tested loads.

Using the combination of MRC and FR1 as baseline, Figure 4.9(b) confirms that interference suppression receivers do perform better than FRP in Scenario A. The complete comparison (for all different loads) is presented in Table 4.11. The numbers show that the use of interference suppression receivers can not only match the outage data rate performance, but also increase this performance indicator by up to 48.4% at low load condition (25%) and 38.7% in a fully loaded network (100%). Increases in average and peak throughputs are also observed, indicating overall network performance enhancement. Moreover, the fact that more conservative frequency reuse plans (Frequency Reuse 2 (FR2) and Frequency Reuse 4 (FR4)) do not improve the performance indicate that dynamic frequency reuse strategies would also not help in this case.

(a) MRC performance for different FRP   (b) IRC and SIC vs. MRC with FR1

Fig. 4.9: Simulation results comparing the best baseline configuration to interference suppression receivers in Scenario A (100% network traffic load).

Table 4.10: Key performance indicators (in Mbps) for the MRC receiver with different frequency reuse plans in Scenario A. The best configuration for each network traffic load is highlighted with **bold** fonts.

Load	FRP	Outage	Average	Peak
	FR1	**593.8**	**998.7**	**1468.1**
25%	FR2	487.0	764.7	1090.9
	FR4	408.1	611.4	842.1
	FR1	**355.7**	**682.0**	**1073.9**
50%	FR2	306.8	516.8	774.2
	FR4	248.8	395.0	566.0
	FR1	**266.8**	**556.0**	**919.1**
75%	FR2	226.8	423.0	656.6
	FR4	187.3	315.4	479.6
	FR1	**218.1**	**487.7**	**823.7**
100%	FR2	175.4	365.1	586.4
	FR4	151.9	271.8	423.2

In Scenario B, the best performing baseline configuration changes with the network load, as it is shown in Table 4.12. As the network load increases, the best performing configuration should go from FR1 at 25% to FR4 at 75% load and beyond. Figure 4.10(a) presents the average cell throughput CDFs for the different frequency reuse plans at 100% network traffic load.

Once more, the configurations that use interference suppression receivers outperform the baseline configuration, as it is shown in Table 4.12. All performance indicators are improved at all network traffic load conditions. The numbers also show that cells in good interference conditions are highly penalized by the frequency reuse scheme used to protect cells that are in bad interference conditions. This penalization is considerably minimized when interference suppression receivers are used, which results in very high average and peak data rate gains (up to 132.3% average throughput gain and 224.4% peak throughput gain). These results confirm that interference suppression receivers may also be used as an alternative to FRP in Scenario B, with highly improved average and peak throughputs as additional benefits.

Finally, the comparison is made in Scenario C. In this scenario, the best performing baseline configurations are the same as in Scenario B, as it is shown in Table 4.14. However, the difference in outage throughput with the different frequency reuse plans is more pronounced as it may be verified in Figure 4.11(a). When the network load is 100%, the outage throughput with FR4 is almost three times larger than the outage with FR1.

When comparing the baseline configurations to the interference suppression receiver configuration using the results presented in Table 4.15, it be-

Table 4.11: Key performance indicators (in Mbps) for different receiver types and performance gains over the baseline network configuration in Scenario A.

Load	Receiver	FRP	Outage	Average	Peak
25%	MRC	FR1	593.8	998.7	1468.1
	IRC	FR1	870.3 (+46.6%)	1314.8 (+31.6%)	1845.9 (+25.7%)
	SIC	FR1	881.4 (+48.4%)	1375.1 (+37.7%)	1990.4 (+35.6%)
50%	MRC	FR1	355.7	682.0	1073.9
	IRC	FR1	518.5 (+45.8%)	875.1 (+28.3%)	1306.8 (+21.7%)
	SIC	FR1	523.9 (+47.3%)	892.0 (+30.8%)	1351.9 (+25.9%)
75%	MRC	FR1	266.8	556.0	919.1
	IRC	FR1	378.6 (+41.9%)	701.3 (+26.1%)	1077.6 (+17.2%)
	SIC	FR1	374.9 (+40.5%)	708.3 (+27.4%)	1126.7 (+22.6%)
100%	MRC	FR1	218.1	487.7	823.7
	IRC	FR1	291.4 (+33.6%)	595.8 (+22.2%)	959.9 (+16.5%)
	SIC	FR1	302.6 (+38.7%)	594.2 (+21.8%)	971.8 (+18.0%)
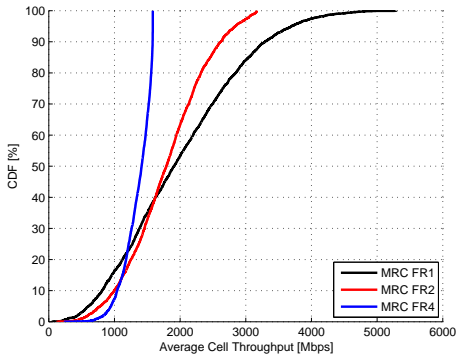
(a) MRC performance for different FRP

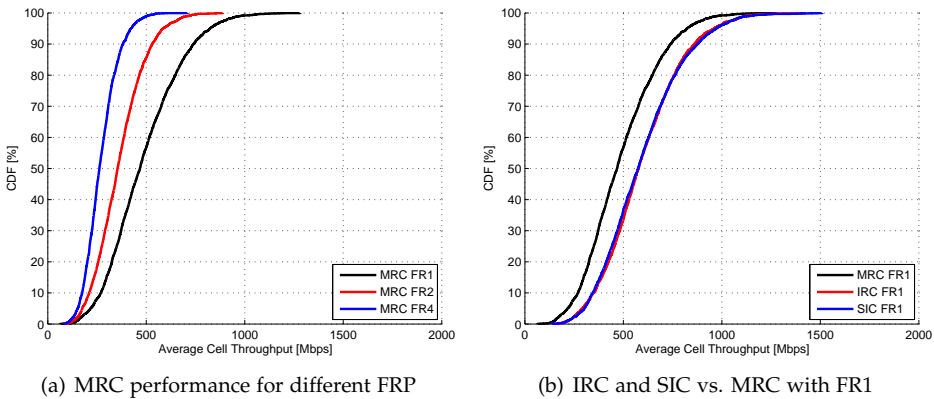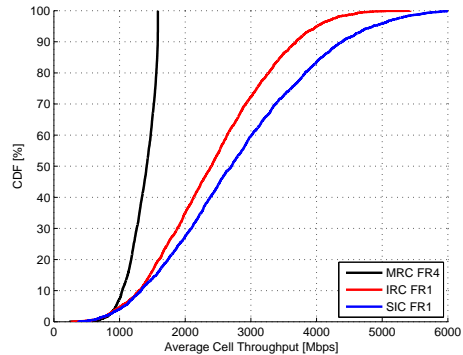(b) IRC and SIC vs. MRC with FR4

Fig. 4.10: Simulation results comparing the best baseline configuration to interference suppression receivers in Scenario B (100% network traffic load).

Table 4.12: Key performance indicators (in Mbps) for the MRC receiver with different frequency reuse plans in Scenario B. The best configuration for each network traffic load is highlighted with **bold** fonts.

Load	FRP	Outage	Average	Peak
25%	**FR1**	**2543.5**	**4041.7**	**5372.4**
	FR2	1952.0	2610.8	3104.9
	FR4	1320.9	1509.2	1584.0
50%	FR1	1441.2	3018.3	4678.0
	FR2	**1468.7**	**2276.7**	**2990.1**
	FR4	1164.0	1444.0	1584.0
75%	FR1	901.9	2403.6	4109.6
	FR2	1060.4	2004.8	2914.3
	FR4	**1062.8**	**1398.2**	**1584.0**
100%	FR1	605.5	1997.6	3700.4
	FR2	784.0	1794.4	2839.9
	FR4	**946.2**	**1357.7**	**1584.0**

Table 4.13: Key performance indicators (in Mbps) for different receiver types and performance gains over the baseline network configuration in Scenario B.

Load	Receiver	FRP	Outage	Average	Peak
25%	MRC	FR1	2543.5	4041.7	5372.4
	IRC	FR1	3054.0 (+20.1%)	4374.3 (+8.2%)	5549.7 (+3.3%)
	SIC	FR1	3404.2 (+33.8%)	4885.2 (+20.9%)	5996.3 (+11.6%)
50%	MRC	FR2	1468.7	2276.7	2990.1
	IRC	FR1	1986.2 (+ 35.2%)	3411.3 (+ 49.8%)	4846.5 (+ 62.1%)
	SIC	FR1	2175.4 (+ 48.1%)	3970.6 (+ 74.4%)	5628.6 (+ 88.2%)
75%	MRC	FR4	1062.8	1398.2	1584.0
	IRC	FR1	1420.7 (+ 33.7%)	2851.9 (+ 104.0%)	4387.5 (+ 177.0%)
	SIC	FR1	1510.9 (+ 42.2%)	3247.6 (+ 132.3%)	5138.3 (+ 224.4%)
100%	MRC	FR4	946.2	1357.7	1584.0
	IRC	FR1	1023.3 (+8.1%)	2439.8 (+79.7%)	4009.7 (+153.1%)
	SIC	FR1	1068.0 (+12.9%)	2795.7 (+105.9%)	4862.7 (+207.0%)

comes evident that interference suppression receivers are not capable of protecting the network as well as FRP when the network load is high. The outage throughputs are up to 32.9% lower when interference suppression receivers are used. This situation may also be observed in Figure 4.11(b). The other performance indicators (average and peak throughputs) are much higher when interference suppression receivers are used, but the main requirement of providing outage throughput that is greater than or equal to the throughput obtained with the use of frequency reuse plans is not met. It is therefore necessary to apply an inter-cell interference management mechanism to reach the required outage throughput target in Scenario C.

| (a) MRC performance for different FRP | (b) IRC and SIC vs. MRC FR4 |
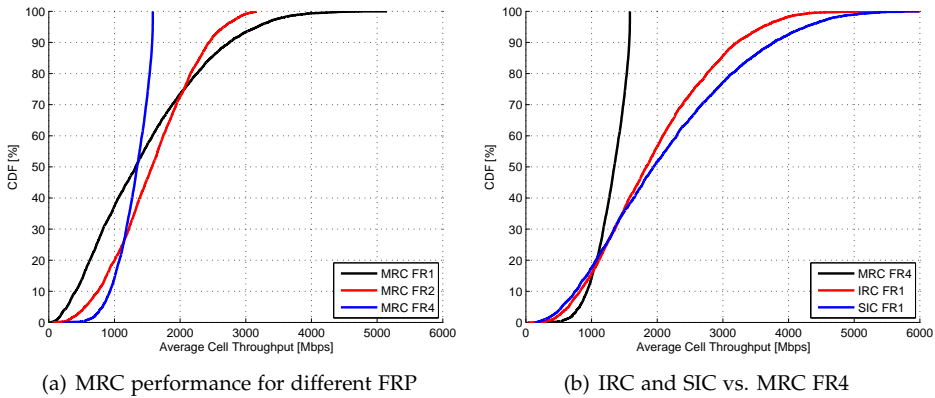
Fig. 4.11: Simulation results comparing the best baseline configuration to interference suppression receivers in Scenario C (100% network traffic load).

4.6 Using victim-aware rank adaptation

In this section, two different victim-aware rank adaptation algorithms are evaluated as tools for improving the outage performance obtained when interference suppression receivers are used in Scenario C. The Maximum Rank Planning (MRP) technique is evaluated first, followed by the Taxation-based Rank Adaptation (TRA) algorithm.

In this part of this performance evaluation work, the definition of the term *network configuration* is extended to include the rank adaptation technique used in combination with the other parameters. Therefore, a configuration is from here on the combination of a receiver type, a frequency reuse plan and a rank adaptation method. The baseline configuration used in this part of the evaluation is still the same: the combination of the MRC receiver with the best performing frequency reuse plan (from the outage performance point-of-view) and the selfish rank adaptation. The interference suppression receivers

Table 4.14: Key performance indicators (in Mbps) for the MRC receiver with different frequency reuse plans in Scenario C. The best configuration for each network traffic load is highlighted with **bold** fonts.

Load	FRP	Outage	Average	Peak
25%	**FR1**	**1823.0**	**3439.5**	**5105.1**
	FR2	1711.6	2457.5	3034.2
	FR4	1256.9	1482.2	1584.0
50%	FR1	837.8	2314.7	4103.0
	FR2	**1115.8**	**2051.5**	**2914.2**
	FR4	1087.4	1417.8	1583.6
75%	FR1	466.1	1848.4	3665.6
	FR2	770.8	1772.5	2765.8
	FR4	**913.3**	**1346.6**	**1583.4**
100%	FR1	277.5	1463.1	3175.3
	FR2	550.8	1586.8	2667.8
	FR4	**818.6**	**1294.7**	**1583.3**

Table 4.15: Key performance indicators (in Mbps) for different receiver types and performance gains over the baseline network configuration in Scenario C.

Load	Receiver	FRP	Outage	Average	Peak
25%	MRC	FR1	1823.0	3439.5	5105.1
	IRC	FR1	2396.7 (+31.5%)	3830.5 (+11.4%)	5242.9 (+2.7%)
	SIC	FR1	2660.3 (+45.9%)	4367.2 (+27.0%)	5818.1 (+14.0%)
50%	MRC	FR2	1115.8	2051.5	2914.2
	IRC	FR1	1350.8 (+21.1%)	2854.3 (+39.1%)	4482.5 (+53.8%)
	SIC	FR1	1396.2 (+25.1%)	3307.9 (+61.2%)	5270.9 (+80.9%)
75%	MRC	FR4	913.3	1346.6	1583.4
	IRC	FR1	**879.1 (-3.7%)**	2290.8 (+70.1%)	3938.8 (+148.7%)
	SIC	FR1	**853.8 (-6.5%)**	2573.7 (+91.1%)	4656.5 (+194.1%)
100%	MRC	FR4	818.6	1294.7	1583.3
	IRC	FR1	**652.4 (-20.3%)**	1942.7 (+50.1%)	3612.3 (+128.2%)
	SIC	FR1	**549.0 (-32.9%)**	2123.6 (+64.0%)	4265.6 (+169.4%)

are always combined with universal frequency reuse (FR1) and one of the rank adaptation algorithms.

4.6.1 Maximum Rank Planning (MRP)

Figure 4.12 shows the comparison of baseline configuration with configurations composed by interference suppression receivers and different rank adaptation strategies: selfish rank adaptation (SRA), maximum rank 2 (MR2) and maximum rank 1 (MR1). Tables 4.16 and 4.17 present the performance indicators and gains over the baseline for IRC and SIC receiver configurations, respectively.

| (a) Baseline *vs.* IRC with MRP | (b) Baseline *vs.* SIC with MRP |

Fig. 4.12: Simulation results comparing the baseline network configuration with Maximum Rank Planning (MRP) configurations in Scenario C (100% network traffic load).

The results confirm that the rank adaptation decisions in one cell can indeed affect the performance in other cells. By using Maximum Rank Planning, the outage throughput is increased, reaching up to 34.6% gain over baseline when MR1 is used. Considering the design target (outage throughput greater than or equal to the baseline), the use of MRP would suffice. Moreover, the technique is much simpler to apply than FRP because there is no need to decide resource allocations; the decision regarding the maximum number of data streams to use is all that is required.

Nevertheless, this technique presents a considerable drawback: as the network load changes, the rank limit must be adjusted to avoid penalizing the cells in good interference conditions (mostly in the same way as the frequency allocation is adjusted in the case of FRP). For this reason, the Maximum Rank Planning technique should be regarded as a first step towards the development of other victim-aware techniques that may provide a better balance of performance indicators.

Table 4.16: Key performance indicators (in Mbps) for IRC receiver with different MRP plans and performance gains over the baseline network configuration in Scenario C.

Load	Configuration	Outage	Average	Peak
75%	MRC/FR4/SRA	913.3	1346.6	1583.4
	IRC/FR1/SRA	879.1 (-3.7%)	2290.8 (+70.1%)	3938.8 (+148.7%)
	IRC/FR1/MR2	962.5 (+5.4%)	2137.0 (+58.7%)	3071.2 (+94.0%)
	IRC/FR1/MR1	1218.7 (+33.4%)	1502.6 (+11.6%)	1584.0 (+0.0%)
100%	MRC/FR4/SRA	818.6	1294.7	1583.3
	IRC/FR1/SRA	652.4 (-20.3%)	1942.7 (+50.1%)	3612.3 (+128.2%)
	IRC/FR1/MR2	674.4 (-17.6%)	1861.8 (+43.8%)	3001.2 (+89.6%)
	IRC/FR1/MR1	939.7 (+14.8%)	1423.0 (+9.9%)	1584.0 (+0.0%)

Table 4.17: Key performance indicators (in Mbps) for SIC receiver with different MRP plans and performance gains over the baseline network configuration in Scenario C.

Load	Configuration	Outage	Average	Peak
75%	MRC/FR4/SRA	913.3	1346.6	1583.4
	SIC/FR1/SRA	853.8 (-6.5%)	2573.7 (+91.1%)	4656.5 (+194.1%)
	SIC/FR1/MR2	1035.7 (+13.4%)	2240.4 (+66.4%)	3119.7 (+97.0%)
	SIC/FR1/MR1	1229.1 (+34.6%)	1507.7 (+12.0%)	1584.0 (+0.0%)
100%	MRC/FR4/SRA	818.6	1294.7	1583.3
	SIC/FR1/SRA	652.4 (-20.3%)	1942.7 (+50.1%)	3612.3 (+128.2%)
	SIC/FR1/MR2	660.2 (-19.3%)	1933.8 (+49.4%)	3047.5 (+92.5%)
	SIC/FR1/MR1	926.2 (+13.1%)	1410.2 (+8.9%)	1584.0 (+0.0%)

4.6.2 Taxation-based Rank Adaptation (TRA)

To test whether a simple victim-aware rank adaptation algorithm can adjust automatically the outage performance gains without penalizing excessively the other performance indicators, the Taxation-based Rank Adaptation (TRA) algorithm was configured using two sets of taxation weights: a conservative set (TRA-C) and a aggressive set (TRA-A), corresponding to high and low taxation settings, respectively. Table 4.18 present the weights for each configuration. These weights were heuristically selected as examples; they are not in any way regarded as optimal weights.

Table 4.18: Taxation weights for conservative and aggressive configurations.

Configuration	Label	Rank 1	Rank 2	Rank 3	Rank 4
Conservative	TRA-C	0	1/2	2/3	3/4
Aggressive	TRA-A	0	1/4	2/6	3/8

In Figure 4.13, the performance of the victim-aware rank adaptation algorithm is compared to the baseline. The figure shows that both configurations (TRA-C and TRA-A) outperform the baseline in all aspects. The TRA-C configuration performs almost identically to the MR1 configuration, whereas the TRA-A configuration provides better performance on the top of the curve and slightly worse performance on the bottom (though still better than the baseline). Tables 4.19 and 4.20 present the performance indicators for IRC and SIC configurations, respectively.

(a) Baseline *vs.* IRC with TRA
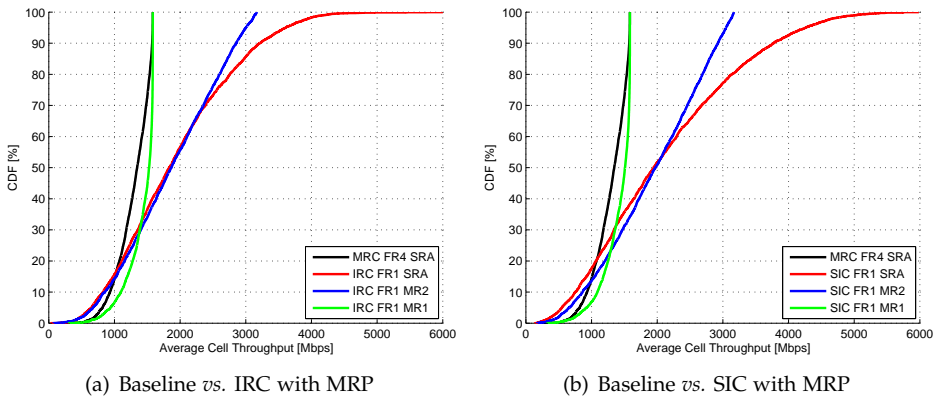
(b) Baseline *vs.* SIC with TRA

Fig. 4.13: Simulation results comparing the baseline network configuration with Taxation-based Rank Adaptation (TRA) configurations in Scenario C (100% network traffic load).

The performance indicators in Tables 4.19 and 4.20 show that either weight setting could be used to guarantee outage throughput greater than or equal

70

Table 4.19: Key performance indicators (in Mbps) for IRC receiver with different TRA configurations and performance gains over the baseline network configuration in Scenario C.

Load	Configuration	Outage	Average	Peak
25%	MRC/FR1/SRA	1823.0	3439.5	5105.1
	IRC/FR1/SRA	2396.7 (+31.5%)	3830.5 (+11.4%)	5242.9 (+2.7%)
	IRC/FR1/TRA-C	1841.3 (+1.0%)	2644.5 (-23.1%)	3775.8 (-26.0%)
	IRC/FR1/TRA-A	2276.6 (+24.9%)	3563.6 (+3.6%)	4931.8 (-3.4%)
50%	MRC/FR2/SRA	1115.8	2051.5	2914.2
	IRC/FR1/SRA	1350.8 (+21.1%)	2854.3 (+39.1%)	4482.5 (+53.8%)
	IRC/FR1/TRA-C	1478.8 (+32.5%)	1749.1 (-14.7%)	2243.4 (-23.0%)
	IRC/FR1/TRA-A	1436.5 (+28.7%)	2506.4 (+22.2%)	3945.8 (+35.4%)
75%	MRC/FR4/SRA	913.3	1346.6	1583.4
	IRC/FR1/SRA	879.1 (-3.7%)	2290.8 (+70.1%)	3938.8 (+148.7%)
	IRC/FR1/TRA-C	1217.8 (+33.3%)	1522.4 (+13.1%)	1688.6 (+6.6%)
	IRC/FR1/TRA-A	1102.5 (+20.7%)	1904.5 (+41.4%)	3113.9 (+96.7%)
100%	MRC/FR4/SRA	818.6	1294.7	1583.3
	IRC/FR1/SRA	652.4 (-20.3%)	1942.7 (+50.1%)	3612.3 (+128.2%)
	IRC/FR1/TRA-C	953.0 (+16.4%)	1422.6 (+9.9%)	1584.0 (+0.0%)
	IRC/FR1/TRA-A	883.1 (+7.9%)	1609.1 (+24.3%)	2818.0 (+78.0%)

to the baseline outage throughput. However, the conservative setting penalizes excessively the average and peak throughputs at lower network traffic load conditions (with up to 22.6% degradation), as it may be verified in Figure 4.14. The aggressive setting offers a more balanced situation; this configuration outperforms the baseline configurations, improving all performance indicators, when used with both types of interference suppression receivers in all the different network traffic load conditions (with the exception of a slight peak performance degradation with IRC receiver at 25% network load).

4.7 Summary

The results presented in this performance evaluation support the conclusion that interference suppression receivers may indeed be used as a valid alternative for traditional frequency reuse techniques with the additional benefit of better performance indicators in the scenarios considered in this study. This conclusion is only true if a system design that offers support for high-performance operation of interference suppression receivers, such as the optimized frame design presented in Chapter 3, is utilized, and victim-aware rank adaptation algorithms are applied to adjust the interference conditions

Table 4.20: Key performance indicators (in Mbps) for SIC receiver with different TRA configurations and performance gains over the baseline network configuration in Scenario C.

Load	Configuration	Outage	Average	Peak
25%	MRC/FR1/SRA	1823.0	3439.5	5105.1
	SIC/FR1/SRA	2660.3 (+45.9%)	4367.2 (+27.0%)	5818.1 (+14.0%)
	SIC/FR1/TRA-C	1900.1 (+4.2%)	2790.2 (-18.9%)	3951.4 (-22.6%)
	SIC/FR1/TRA-A	2463.1 (+35.1%)	3973.4 (+15.5%)	5488.2 (+7.5%)
50%	MRC/FR2/SRA	1115.8	2051.5	2914.2
	SIC/FR1/SRA	1396.2 (+25.1%)	3307.9 (+61.2%)	5270.9 (+80.9%)
	SIC/FR1/TRA-C	1469.2 (+31.7%)	1787.8 (-12.9%)	2426.5 (-16.7%)
	SIC/FR1/TRA-A	1445.7 (+29.6%)	2801.3 (+36.6%)	4523.2 (+55.2%)
75%	MRC/FR4/SRA	913.3	1346.6	1583.4
	SIC/FR1/SRA	853.8 (-6.5%)	2573.7 (+91.1%)	4656.5 (+194.1%)
	SIC/FR1/TRA-C	1216.0 (+33.1%)	1527.9 (+13.5%)	1743.1 (+10.1%)
	SIC/FR1/TRA-A	1072.6 (+17.4%)	2087.4 (+55.0%)	3730.9 (+135.6%)
100%	MRC/FR4/SRA	818.6	1294.7	1583.3
	SIC/FR1/SRA	549.0 (-32.9%)	2123.6 (+64.0%)	4265.6 (+169.4%)
	SIC/FR1/TRA-C	963.5 (+17.7%)	1424.2 (+10.0%)	1584.0 (+0.0%)
	SIC/FR1/TRA-A	866.2 (+5.8%)	1692.7 (+30.7%)	3263.3 (+106.1%)

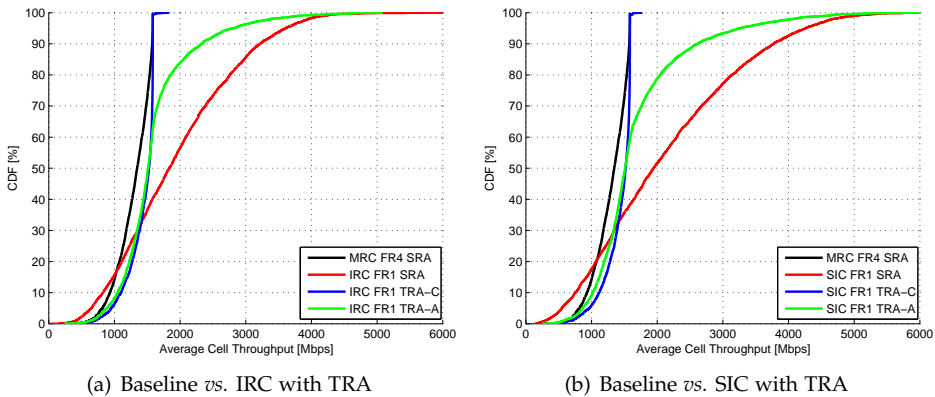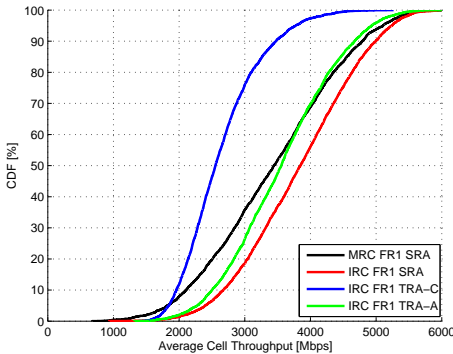(a) Baseline *vs.* IRC with TRA
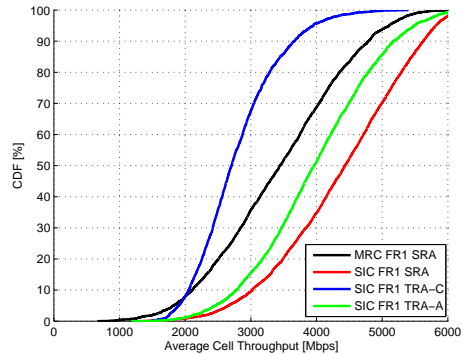
(b) Baseline *vs.* SIC with TRA

Fig. 4.14: Simulation results comparing the baseline network configuration with Taxation-based Rank Adaptation (TRA) configurations in Scenario C (25% network traffic load).

in scenarios with unbalanced interference conditions such as Scenario C (Indoor Office CSG). Moreover, the results also show that interference suppression receivers improve the network performance indicators even when receiver imperfections are considered in the evaluation, as long as the RSB covariance matrix estimation method and reasonably accurate ADC modules are used.

Chapter 5

Conclusions and future work

This project focused on the design of an interference-robust air interface for 5G ultra-dense small cell networks, using interference suppression receivers and victim-aware rank adaptation techniques as the main tools for coping with the inter-cell interference problem. In this brief final chapter, the project's main findings are summarized; general recommendations and suggestions for future studies are also provided.

5.1   Conclusions and recommendations

The main conclusion of this research work is the confirmation that interference suppression receivers are indeed a valid alternative to other types of inter-cell interference management techniques in ultra-dense small cell networks. The results show that a considerable amount of inter-cell interference is suppressed, leading to improved network performance indicators in all the scenarios. The frame structure optimized for "just-in-time" estimation and the victim-aware rank adaptation techniques are key aspects for reaching the main target.

The interference suppression receivers are shown to be robust to imperfections. The overall performance numbers are degraded due to the estimation errors and receiver front-end imperfections, but the results also show that the degradation is limited and the interference suppression receivers still perform much better than the baseline.

Finally, it is possible to conclude that the use of victim-aware rank adaptation algorithms is a new technique full of potential. The results show that simple techniques that do not require complex algorithms, large amounts of calculations or overly complicated protocols can provide a simple method to adjust the interference levels in the networks, providing fair overall network performance and high-quality services to the large majority of users.

The standardization process regarding 5G networks will start soon. Even before this time comes, companies will start discussions about their 5G visions as a first step towards consensus. Considering the results of the present research work, some recommendations for the standardization process may be formulated:

- **Consider how to deal with inter-cell interference from the very beginning of the system design** – Given the relevance of inter-cell interference problem in dense small-cell networks, it is rather important to search for methods to deal with it soon in the design process. By starting early, system designers have more opportunity to design the features required to support efficient inter-cell interference management methods.

- **Include the support for inter-cell interference suppression in the system design** – Interference suppression receivers require information about the interfering signals to perform well and providing this information may require the use of reference signals and control channel messages. This situation may indeed lead to higher control channel overhead, but care should be taken before deciding to minimize the overhead. Saving a few bits in overhead now may cost a large number of bits in the future.

- **Consider the spatial domain when designing inter-cell interference management techniques** – The spatial domain may be used to provide the degrees-of-freedom that are needed for interference management, in a similar way as do the other commonly used domains (frequency and time). By carefully considering the characteristics of each domain, adequate inter-cell interference management techniques may be designed for each scenario.

5.2 Future work

This section addresses some guidelines for future work concerning the use of interference suppression receiver in ultra-dense small cell networks.

In this thesis, it was assumed that orthogonal reference signals will be used by the different transmitters in order to allow for high-accuracy channel estimation. This assumption was considered adequate for the level of detail of the investigation, but in reality the number of orthogonal reference signals will be limited and this limitation may lead to reference signal interference (also know as the pilot contamination problem [91]). Therefore, further evaluation of the concept considering the impact of quasi-orthogonal and non-orthogonal reference signals is recommended. This investigation

should included the search for mechanisms for assigning the multiple reference signals for the different transmitters with the goal of minimizing their mutual interference. Ideally, such mechanism should be self-organizing to fit adequately with the rest of the concept.

Another important aspect is to study is the impact of narrow-band rank adaptation, which has the potential to improve even further the network performance. However, the study of narrow-band rank adaptation should consider the increased control channel overhead (due to the larger amount of necessary feedback information), trying to balance the benefits and drawbacks.

The analysis of the performance of the network should consider the existence of devices with different number of receive antennas. The number of antennas assumed in this work (four antennas) should be considered as the minimum requirement for the typical mobile broadband device. However, the existence of devices with more than four antennas should not be excluded from the investigation. Their existence will increase the complexity of the scenario and will make the design of victim-aware rank adaptation techniques more complex.

The careful design of link adaptation algorithms for this type of networks will be of paramount importance. The use of interference suppression receivers can provide robustness to quickly-changing interference sources, but also makes the link very sensible to the choices made by the rank adaptation algorithm. The study of link adaptation algorithms that jointly consider modulation, coding rate, number of streams (rank) and precoding matrix in the decisions is recommended.

Moreover, the comparison between interference suppression receivers with other candidate 5G techniques, such as the use of very large antenna arrays (also known as Massive MIMO) [92] and CoMP [42], is recommended. Performance evaluations comparing these techniques will be invaluable to decide if the additional costs of these more complex techniques are compensated by the additional performance gains. In these studies, the use of interference suppression receivers as suggested in this thesis may be used as a baseline for comparison.

Finally, the development of proof-of-concept experiments is highly recommended. Using testbed platforms consisting of multiple SDR devices, experiments may be designed to test the concepts presented in this thesis. In that respect, experimental activities have already started at the Wireless Communication Networks section at Aalborg University, where a testbed network consisting of four cells with MIMO devices with two transmit/receive antennas has been used to verify the benefits of the use of the IRC receiver [93] and the MRP rank adaptation technique [94]. This testbed will soon be upgraded to test larger networks and higher-order antenna configurations.

Bibliography

[1]   3GPP TS 25.308. *High Speed Downlink Packet Access (HSDPA); Overall description; Stage 2*. v12.2.0. Mar. 2015. URL: http://www.3gpp.org.

[2]   Heebyung Koh and Christopher L. Magee. "A functional approach for studying technological progress: Application to information technology". In: *Technological Forecasting and Social Change* 73.9 (2006), pp. 1061–1083.

[3]   B. Raaf, W. Zirwas, K.-J. Friederichs, E. Tiirola, M. Laitila, P. Marsch, and R. Wichman. "Vision for Beyond 4G broadband radio systems". In: *Personal Indoor and Mobile Radio Communications (PIMRC), 2011 IEEE 22nd International Symposium on*. Sept. 2011, pp. 2369–2373. DOI: 10.1109/PIMRC.2011.6139944.

[4]   Preben Mogensen, Kari Pajukoski, Bernhard Raaf, Esa Tiirola, Eeva Lähetkangas, Istvan Z. Kovács, Gilberto Berardinelli, Luis G. Uzeda Garcia, Liang Hu, and Andrea F. Cattoni. "B4G local area: High level requirements and system design". In: *Globecom Workshops (GC Wkshps), 2012 IEEE*. Dec. 2012, pp. 613–617. DOI: 10.1109/GLOCOMW.2012.6477644.

[5]   A. Osseiran, F. Boccardi, V. Braun, K. Kusume, P. Marsch, M. Maternia, O. Queseth, M. Schellmann, H. Schotten, H. Taoka, H. Tullberg, M.A. Uusitalo, B. Timus, and M. Fallgren. "Scenarios for 5G mobile and wireless communications: the vision of the METIS project". In: *Communications Magazine, IEEE* 52.5 (May 2014), pp. 26–35. ISSN: 0163-6804. DOI: 10.1109/MCOM.2014.6815890.

[6]   Preben Mogensen, Kari Pajukoski, Esa Tiirola, Jaakko Vihriälä, Eeva Lähetkangas, Gilberto Berardinelli, Fernando Menezes Leitão Tavares, Nurul Huda Mahmood, Mads Lauridsen, Davide Catania, and Andrea Fabio Cattoni. "Centimeter-wave concept for 5G ultra-dense small cells". In: *Vehicular Technology Conference (VTC Spring), 2014 IEEE 79th*. May 2014.

[7] F Boccardi, R.W. Heath, A. Lozano, T.L. Marzetta, and P. Popovski. "Five disruptive technology directions for 5G". In: *Communications Magazine, IEEE* 52.2 (Feb. 2014), pp. 74–80. ISSN: 0163-6804. DOI: 10.1109/MCOM.2014.6736746.

[8] Petar Popovski. "Ultra-Reliable Communication in 5G Wireless Systems". Accepted to the 1st International Conference on 5G for Ubiquitous Connectivity, November 2014.

[9] ITU 5D/TEMP/435-E. *IMT traffic estimates beyond the year 2020 - Working document towards a preliminary draft new report ITU-R M (IMT BEYOND2020 TRAFFIC)*. June 2014. URL: http://www.itu.int/.

[10] N. Bhushan, Junyi Li, D. Malladi, R. Gilmore, D. Brenner, A. Damnjanovic, R. Sukhavasi, C. Patel, and S. Geirhofer. "Network densification: the dominant theme for wireless evolution into 5G". In: *Communications Magazine, IEEE* 52.2 (Feb. 2014), pp. 82–89. ISSN: 0163-6804. DOI: 10.1109/MCOM.2014.6736747.

[11] T.S. Rappaport, Shu Sun, R. Mayzus, Hang Zhao, Y. Azar, K. Wang, G.N. Wong, J.K. Schulz, M. Samimi, and F. Gutierrez. "Millimeter Wave Mobile Communications for 5G Cellular: It Will Work!" In: *Access, IEEE* 1 (2013), pp. 335–349. ISSN: 2169-3536. DOI: 10.1109/ACCESS.2013.2260813.

[12] A. Damnjanovic, J. Montojo, Yongbin Wei, Tingfang Ji, Tao Luo, M. Vajapeyam, Taesang Yoo, Osok Song, and D. Malladi. "A survey on 3GPP heterogeneous networks". In: *Wireless Communications, IEEE* 18.3 (June 2011), pp. 10–21. ISSN: 1536-1284. DOI: 10.1109/MWC.2011.5876496.

[13] Liang Hu, L. Luque Sanchez, M. Maternia, I. Kovacs, B. Vejlgaard, P. Mogensen, and H. Taoka. "Heterogeneous LTE-Advanced Network Expansion for 1000x Capacity". In: *Vehicular Technology Conference (VTC Spring), 2013 IEEE 77th*. June 2013, pp. 1–5. DOI: 10.1109/VTCSpring.2013.6692578.

[14] G. Boudreau, J. Panicker, Ning Guo, Rui Chang, Neng Wang, and S. Vrzic. "Interference coordination and cancellation for 4G networks". In: *Communications Magazine, IEEE* 47.4 (Apr. 2009), pp. 74–81. ISSN: 0163-6804. DOI: 10.1109/MCOM.2009.4907410.

[15] 3GPP TR 36.932. *Scenarios and requirements for small cell enhancements for E-UTRA and E-UTRAN*. v12.1.0. Mar. 2013. URL: http://www.3gpp.org.

[16] 3GPP TR 36.872. *Small cell enhancements for E-UTRA and E-UTRAN - Physical layer aspects*. v12.1.0. Dec. 2013. URL: http://www.3gpp.org.

[17] 3GPP TR 36.842. *Study on Small Cell enhancements for E-UTRA and E-UTRAN; Higher layer aspects*. v12.0.0. Jan. 2014. URL: http://www.3gpp.org.

[18] Sergio Verdu. *Multiuser Detection*. 1st. New York, NY, USA: Cambridge University Press, 1998. ISBN: 0521593735.

[19] Jinho Choi. *Optimal Combining and Detection: Statistical Signal Processing for Communications*. Cambridge: Cambridge University Press, 2010.

[20] J. Winters. "Optimum Combining in Digital Mobile Radio with Cochannel Interference". In: *Selected Areas in Communications, IEEE Journal on* 2.4 (July 1984), pp. 528–539. ISSN: 0733-8716. DOI: 10.1109/JSAC.1984.1146095.

[21] J. Karlsson and J. Heinegard. "Interference rejection combining for GSM". In: *Universal Personal Communications, 1996. Record., 1996 5th IEEE International Conference on*. Vol. 1. Sept. 1996, 433–437 vol.1. DOI: 10.1109/ICUPC.1996.557950.

[22] M. Escartin and P.A. Ranta. "Interference rejection with a small antenna array at the mobile scattering environment". In: *Signal Processing Advances in Wireless Communications, First IEEE Signal Processing Workshop on*. Apr. 1997, pp. 165–168. DOI: 10.1109/SPAWC.1997.630223.

[23] J.D. Laster and J. Reed. "Interference rejection in digital wireless communications". In: *Signal Processing Magazine, IEEE* 14.3 (May 1997), pp. 37–62. ISSN: 1053-5888. DOI: 10.1109/79.587051.

[24] P. Patel and J. Holtzman. "Analysis of a simple successive interference cancellation scheme in a DS/CDMA system". In: *Selected Areas in Communications, IEEE Journal on* 12.5 (June 1994), pp. 796–807. ISSN: 0733-8716. DOI: 10.1109/49.298053.

[25] J.M. Holtzman. "DS/CDMA successive interference cancellation". In: *Spread Spectrum Techniques and Applications, 1994. IEEE ISSSTA '94., IEEE Third International Symposium on*. July 1994, 69–78 vol.1. DOI: 10.1109/ISSSTA.1994.379614.

[26] A.L.C. Hui and Khaled Letaief. "Successive interference cancellation for multiuser asynchronous DS/CDMA detectors in multipath fading links". In: *Communications, IEEE Transactions on* 46.3 (Mar. 1998), pp. 384–391. ISSN: 0090-6778. DOI: 10.1109/26.662644.

[27] G.E. Moore. "Cramming More Components Onto Integrated Circuits". In: *Proceedings of the IEEE* 86.1 (Jan. 1998), pp. 82–85. ISSN: 0018-9219. DOI: 10.1109/JPROC.1998.658762.

[28] 3GPP TR 36.829. *Enhanced performance requirement for LTE User Equipment (UE)*. v11.1.0. Jan. 2013. URL: http://www.3gpp.org.

[29]   3GPP TR 36.866. *Study on Network-Assisted Interference Cancellation and Suppression (NAIC) for LTE*. v12.0.1. Mar. 2014. URL: http://www.3gpp.org.

[30]   M. Lampinen, F. Del Carpio, T. Kuosmanen, T. Koivisto, and M. Enescu. "System-Level Modeling and Evaluation of Interference Suppression Receivers in LTE System". In: *Vehicular Technology Conference (VTC Spring), 2012 IEEE 75th*. May 2012, pp. 1–5. DOI: 10.1109/VETECS.2012.6239964.

[31]   K. Pietikainen, F. Del Carpio, H. Maattanen, M. Lampinen, T. Koivisto, and M. Enescu. "System-Level Performance of Interference Suppression Receivers in LTE System". In: *Vehicular Technology Conference (VTC Spring), 2012 IEEE 75th*. May 2012, pp. 1–5. DOI: 10.1109/VETECS.2012.6239969.

[32]   Y. Ohwatari, N. Miki, T. Abe, and H. Taoka. "Investigation on Advanced Receiver Employing Interference Rejection Combining in Asynchronous Network for LTE-Advanced Downlink". In: *Vehicular Technology Conference (VTC Spring), 2012 IEEE 75th*. May 2012, pp. 1–6. DOI: 10.1109/VETECS.2012.6240127.

[33]   Y. Ohwatari, N. Miki, T. Asai, T. Abe, and H. Taoka. "Performance of Advanced Receiver Employing Interference Rejection Combining to Suppress Inter-Cell Interference in LTE-Advanced Downlink". In: *2011 IEEE Vehicular Technology Conference (VTC Fall)*. Sept. 2011, pp. 1–7. DOI: 10.1109/VETECF.2011.6093196.

[34]   S. Golestaneh, H.M. Hafez, and S.A. Mahmoud. "The effect of adjacent channel interference on the capacity of FDMA cellular systems". In: *Vehicular Technology, IEEE Transactions on* 43.4 (Nov. 1994), pp. 946–954. ISSN: 0018-9545. DOI: 10.1109/25.330157.

[35]   G. Bauch and V. Franz. "Iterative equalization and decoding for the GSM-system". In: *Vehicular Technology Conference, 1998. VTC 98. 48th IEEE*. Vol. 3. May 1998, 2262–2266 vol.3. DOI: 10.1109/VETEC.1998.686160.

[36]   Timo Halonen, Javier Romero, and Juan Melero. *GSM, GPRS and EDGE performance: evolution towards 3G/UMTS*. John Wiley & Sons, 2004.

[37]   Mikko Saily, Guillaume Sebire, and Eddie Riddington. *GSM/EDGE: Evolution and performance*. John Wiley & Sons, 2011.

[38]   Abbas El Gamal and Young-Han Kim. *Network information theory*. Cambridge University Press, 2011.

[39]   Te Han and K. Kobayashi. "A new achievable rate region for the interference channel". In: *Information Theory, IEEE Transactions on* 27.1 (Jan. 1981), pp. 49–60. ISSN: 0018-9448. DOI: 10.1109/TIT.1981.1056307.

[40] F. Baccelli, A. El Gamal, and D.N.C. Tse. "Interference Networks With Point-to-Point Codes". In: *Information Theory, IEEE Transactions on* 57.5 (May 2011), pp. 2582–2596. ISSN: 0018-9448. DOI: 10.1109/TIT.2011. 2119230.

[41] S. Venkatesan, A. Lozano, and R. Valenzuela. "Network MIMO: Overcoming Intercell Interference in Indoor Wireless Systems". In: *Signals, Systems and Computers, 2007. ACSSC 2007. Conference Record of the Forty-First Asilomar Conference on*. Nov. 2007, pp. 83–87. DOI: 10. 1109/ACSSC.2007.4487170.

[42] R. Irmer, H. Droste, P. Marsch, M. Grieger, G. Fettweis, S. Brueck, H.P. Mayer, L. Thiele, and V. Jungnickel. "Coordinated multipoint: Concepts, performance, and field trial results". In: *Communications Magazine, IEEE* 49.2 (Feb. 2011), pp. 102–111. ISSN: 0163-6804. DOI: 10.1109/ MCOM.2011.5706317.

[43] O. El Ayach, S.W. Peters, and Jr. Heath R.W. "The practical challenges of interference alignment". In: *Wireless Communications, IEEE* 20.1 (Feb. 2013), pp. 35–42. ISSN: 1536-1284. DOI: 10.1109/MWC.2013.6472197.

[44] S.W. Peters and R.W. Heath. "Cooperative Algorithms for MIMO Interference Channels". In: *Vehicular Technology, IEEE Transactions on* 60.1 (Jan. 2011), pp. 206–218. ISSN: 0018-9545. DOI: 10.1109/TVT.2010. 2085459.

[45] Wei Yu, Wonjong Rhee, S. Boyd, and J.M. Cioffi. "Iterative water-filling for Gaussian vector multiple-access channels". In: *Information Theory, IEEE Transactions on* 50.1 (Jan. 2004), pp. 145–152. ISSN: 0018-9448. DOI: 10.1109/TIT.2003.821988.

[46] S. Haykin, M. Sellathurai, Y. de Jong, and T. Willink. "Turbo-MIMO for wireless communications". In: *Communications Magazine, IEEE* 42.10 (Oct. 2004), pp. 48–53. ISSN: 0163-6804. DOI: 10.1109/MCOM.2004. 1341260.

[47] M. Morelli and U. Mengali. "A comparison of pilot-aided channel estimation methods for OFDM systems". In: *Signal Processing, IEEE Transactions on* 49.12 (Dec. 2001), pp. 3065–3073. ISSN: 1053-587X. DOI: 10.1109/78.969514.

[48] 3GPP TS 36.211. *Evolved Universal Terrestrial Radio Access (E-UTRA); Physical channels and modulation*. v11.1.0. Dec. 2012. URL: http://www. 3gpp.org.

[49] 3GPP R1-062642. *Uplink Reference Signal Design in EUTRA*. Oct. 2006. URL: http://www.3gpp.org.

[50] 3GPP R1-080506. *UE specific reference signal pattern*. Jan. 2008. URL: http://www.3gpp.org.

[51] C.J. Hegarty and E. Chatre. "Evolution of the Global Navigation Satel-liteSystem (GNSS)". In: *Proceedings of the IEEE* 96.12 (Dec. 2008), pp. 1902–1917. ISSN: 0018-9219. DOI: 10.1109/JPROC.2008.2006090.

[52] S. Chia, M. Gasparroni, and P. Brick. "The next challenge for cellular networks: backhaul". In: *Microwave Magazine, IEEE* 10.5 (Aug. 2009), pp. 54–66. ISSN: 1527-3342. DOI: 10.1109/MMM.2009.932832.

[53] P. Briggs, R. Chundury, and J. Olsson. "Carrier ethernet for mobile backhaul". In: *Communications Magazine, IEEE* 48.10 (Oct. 2010), pp. 94–100. ISSN: 0163-6804. DOI: 10.1109/MCOM.2010.5594683.

[54] "IEEE Standard for a Precision Clock Synchronization Protocol for Networked Measurement and Control Systems". In: *IEEE Std 1588-2002* (2002), pp. i–144. DOI: 10.1109/IEEESTD.2002.94144.

[55] Fernando M.L. Tavares, Gilberto Berardinelli, Nurul H. Mahmood, Troels B. Sørensen, and Preben Mogensen. "On the Impact of Re-ceiver Imperfections on the MMSE-IRC Receiver Performance in 5G Networks". In: *Vehicular Technology Conference (VTC Spring), 2014 IEEE 79th*. May 2014, pp. 1–6. DOI: 10.1109/VTCSpring.2014.7023014.

[56] L. Thiele, M. Schellmann, S. Schiffermuller, V. Jungnickel, and W. Zir-was. "Multi-Cell Channel Estimation using Virtual Pilots". In: *Vehic-ular Technology Conference, 2008. VTC Spring 2008. IEEE*. May 2008, pp. 1211–1215. DOI: 10.1109/VETECS.2008.256.

[57] A. Ghosh, R. Ratasuk, B. Mondal, N. Mangalvedhe, and T. Thomas. "LTE-advanced: next-generation wireless broadband technology [In-vited Paper]". In: *Wireless Communications, IEEE* 17.3 (June 2010), pp. 10–22. ISSN: 1536-1284. DOI: 10.1109/MWC.2010.5490974.

[58] Thien-Toan Tran, Yoan Shin, and Oh-Soon Shin. "Overview of en-abling technologies for 3GPP LTE-advanced". In: *EURASIP Journal on Wireless Communications and Networking* 2012.1 (2012), p. 54. ISSN: 1687-1499. DOI: 10.1186/1687-1499-2012-54. URL: http://jwcn.eurasipjournals.com/content/2012/1/54.

[59] F.M.L. Tavares, G. Berardinelli, N.H. Mahmood, T.B. Sørensen, and P. Mogensen. "Inter-cell interference management using Maximum Rank Planning in 5G small cell networks". In: *Wireless Communica-tions Systems (ISWCS), 2014 11th International Symposium on*. Aug. 2014, pp. 628–632. DOI: 10.1109/ISWCS.2014.6933430.

[60] N.H. Mahmood, G. Berardinelli, F.M.L. Tavares, and P. Mogensen. "A distributed interference-aware rank adaptation algorithm for lo-cal area MIMO systems with MMSE receivers". In: *Wireless Commu-nications Systems (ISWCS), 2014 11th International Symposium on*. Aug. 2014, pp. 697–701. DOI: 10.1109/ISWCS.2014.6933443.

[61]   Davide Catania, Andrea Fabio Cattoni, Nurul Huda Mahmood, Gilberto Berardinelli, Frank Frederiksen, and Preben Mogensen. "A Distributed Taxation Based Rank Adaptation Scheme for 5G Small Cells". Accepted to the 2015 IEEE 81st Vehicular Technology Conference (VTC Spring), May 2015.

[62]   3GPP TS 36.211. *Evolved Universal Terrestrial Radio Access (E-UTRA); Medium Access Control (MAC) protocol specification*. v12.4.0. Jan. 2015. URL: http://www.3gpp.org.

[63]   N.H. Mahmood, L.G. Uzeda Garcia, P. Popovski, and P.E. Mogensen. "On the performance of successive interference cancellation in 5G small cell networks". In: *Wireless Communications and Networking Conference (WCNC), 2014 IEEE*. Apr. 2014, pp. 1154–1159. DOI: 10.1109/WCNC.2014.6952292.

[64]   P. Popovski, H. Yomo, K. Nishimori, R. Di Taranto, and R. Prasad. "Opportunistic Interference Cancellation in Cognitive Radio Systems". In: *New Frontiers in Dynamic Spectrum Access Networks, 2007. DySPAN 2007. 2nd IEEE International Symposium on*. Apr. 2007, pp. 472–475. DOI: 10.1109/DYSPAN.2007.68.

[65]   D. Dardari. "Joint clip and quantization effects characterization in OFDM receivers". In: *Circuits and Systems I: Regular Papers, IEEE Transactions on* 53.8 (2006), pp. 1741–1748. ISSN: 1549-8328. DOI: 10.1109/TCSI.2006.875170.

[66]   Chun-Tao Lin and Wen-Rong Wu. "Clipping ratio estimation for OFDM receivers". In: *Vehicular Technology Conference (VTC Spring), 2005 IEEE 61st*. 2005. DOI: 10.1109/VETECS.2005.1543414.

[67]   P. Mogensen, K. Pajukoski, E. Tiirola, E. Lahetkangas, J. Vihriala, S. Vesterinen, M. Laitila, G. Berardinelli, G.W.O. Da Costa, L.G.U. Garcia, F.M.L. Tavares, and A.F. Cattoni. "5G small cell optimized radio design". In: *Globecom Workshops (GC Wkshps), 2013 IEEE*. Dec. 2013, pp. 111–116. DOI: 10.1109/GLOCOMW.2013.6824971.

[68]   D. Catania, M.G. Sarret, A.F. Cattoni, F. Frederiksen, G. Berardinelli, and P. Mogensen. "The Potential of Flexible UL/DL Slot Assignment in 5G Systems". In: *Vehicular Technology Conference (VTC Fall), 2014 IEEE 80th*. Sept. 2014, pp. 1–6. DOI: 10.1109/VTCFall.2014.6966202.

[69]   Davide Catania, Marta Gatnau, Andrea Fabio Cattoni, Frank Frederiksen, Gilberto Berardinelli, and Preben Mogensen. "Flexible UL/DL in Small Cell TDD Systems: A Performance Study with TCP Traffic". Accepted to the 2015 IEEE 81st Vehicular Technology Conference (VTC Spring), May 2015.

[70]   E. Lahetkangas, K. Pajukoski, J. Vihriala, G. Berardinelli, M. Laurid-
       sen, E. Tiirola, and P. Mogensen. "Achieving low latency and en-
       ergy consumption by 5G TDD mode optimization". In: *Communica-
       tions Workshops (ICC), 2014 IEEE International Conference on*. June 2014,
       pp. 1–6. DOI: 10.1109/ICCW.2014.6881163.

[71]   Eeva Lahetkangas, Kari Pajukoski, Jaakko Vihriala, and Esa Tiirola.
       "On the flexible 5G dense deployment air interface for mobile broad-
       band". In: *5G for Ubiquitous Connectivity (5GU), 2014 1st International
       Conference on*. Nov. 2014, pp. 57–61. DOI: 10.4108/icst.5gu.2014.
       258101.

[72]   B. Farhang-Boroujeny. "OFDM Versus Filter Bank Multicarrier". In:
       Signal Processing Magazine, IEEE 28.3 (May 2011), pp. 92–112. ISSN:
       1053-5888. DOI: 10.1109/MSP.2011.940267.

[73]   F. Schaich. "Filterbank based multi carrier transmission (FBMC) - evolv-
       ing OFDM: FBMC in the context of WiMAX". In: *Wireless Conference
       (EW), 2010 European*. Apr. 2010, pp. 1051–1058. DOI: 10.1109/EW.2010.
       5483518.

[74]   V. Vakilian, T. Wild, F. Schaich, S. Ten Brink, and J. F. Frigon. "Universal-
       filtered multi-carrier technique for wireless systems beyond LTE". In:
       Globecom Workshops (GC Wkshps), 2013 IEEE. Dec. 2013, pp. 223–228.
       DOI: 10.1109/GLOCOMW.2013.6824990.

[75]   Gilberto Berardinelli, Kari Pajukoski, Eeva Lahetkangas, Risto Wich-
       man, Olav Tirkkonen, and Preben Mogensen. "On the Potential of
       OFDM Enhancements as 5G Waveforms". In: *Vehicular Technology Con-
       ference (VTC Spring), 2014 IEEE 79th*. May 2014, pp. 1–5. DOI: 10.1109/
       VTCSpring.2014.7023019.

[76]   G. Berardinelli, F.M.L. Tavares, T.B. Sørensen, P. Mogensen, and K.
       Pajukoski. "Zero-tail DFT-spread-OFDM signals". In: *Globecom Work-
       shops (GC Wkshps), 2013 IEEE*. Dec. 2013, pp. 229–234. DOI: 10.1109/
       GLOCOMW.2013.6824991.

[77]   G. Berardinelli, F.M.L. Tavares, T.B. Sørensen, P. Mogensen, and K.
       Pajukoski. "On the Potential of Zero-Tail DFT-Spread-OFDM in 5G
       Networks". In: *Vehicular Technology Conference (VTC Fall), 2014 IEEE
       80th*. Sept. 2014, pp. 1–6. DOI: 10.1109/VTCFall.2014.6966089.

[78]   "IEEE Standard for Information technology - Telecommunications and
       information exchange between systemsLocal and metropolitan area
       networks - Specific requirements - Part 11: Wireless LAN Medium Ac-
       cess Control (MAC) and Physical Layer (PHY) Specifications - Amend-
       ment 4: Enhancements for Very High Throughput for Operation in
       Bands below 6 GHz." In: *IEEE Std 802.11ac-2013 (Amendment to IEEE*

Std 802.11-2012, as amended by IEEE Std 802.11ae-2012, IEEE Std 802.11aa-2012, and IEEE Std 802.11ad-2012) (Dec. 2013), pp. 1–425. DOI: `10.1109/IEEESTD.2013.6687187`.

[79] H. Hashemi. "The indoor radio propagation channel". In: *Proceedings of the IEEE* 81.7 (July 1993), pp. 943–968. ISSN: 0018-9219. DOI: `10.1109/5.231342`.

[80] G. Berardinelli, F.M.L. Tavares, N.H. Mahmood, O. Tonelli, A.F. Cattoni, T.B. Sørensen, and P. Mogensen. "Distributed synchronization for beyond 4G indoor femtocells". In: *Telecommunications (ICT), 2013 20th International Conference on*. May 2013, pp. 1–5. DOI: `10.1109/ICTEL.2013.6632081`.

[81] Gilberto Berardinelli, Fernando M.L. Tavares, Olav Tirkkonen, Troels B. Sørensen, and Preben Mogensen. "Distributed Initial Synchronization for 5G Small Cells". In: *Vehicular Technology Conference (VTC Spring), 2014 IEEE 79th*. May 2014, pp. 1–5. DOI: `10.1109/VTCSpring.2014.7022884`.

[82] G. Berardinelli, J.L. Buthler, F.M.L. Tavares, O. Tonelli, D. Assefa, F. Hakhamaneshi, T.B. Sørensen, and P. Mogensen. "Distributed Synchronization of a testbed network with USRP N200 radio boards". In: *Asilomar Conference on Signals, Systems and Computers. Conference Record*. Nov. 2014.

[83] L.G.U. Garcia, IZ. Kovacs, K.I Pedersen, G. W O Costa, and P.E. Mogensen. "Autonomous Component Carrier Selection for 4G Femtocells - A Fresh Look at an Old Problem". In: *Selected Areas in Communications, IEEE Journal on* 30.3 (Apr. 2012), pp. 525–537.

[84] K.I. Pedersen, Yuanye Wang, B. Soret, and F. Frederiksen. "eICIC Functionality and Performance for LTE HetNet Co-Channel Deployments". In: *Vehicular Technology Conference (VTC Fall), 2012 IEEE*. Sept. 2012, pp. 1–5. DOI: `10.1109/VTCFall.2012.6399106`.

[85] K.I. Pedersen, Yuanye Wang, S. Strzyz, and F. Frederiksen. "Enhanced inter-cell interference coordination in co-channel multi-layer LTE-advanced networks". In: *Wireless Communications, IEEE* 20.3 (June 2013), pp. 120–127.

[86] Mads Lauridsen, Gilberto Berardinelli, Troels B. Sorensen, and Preben Mogensen. "Ensuring Energy Efficient 5G User Equipment by Technology Evolution and Reuse". In: *Vehicular Technology Conference (VTC Spring), 2014 IEEE 79th*. May 2014, pp. 1–6. DOI: `10.1109/VTCSpring.2014.7022914`.

[87]   Young-Han Nam, Y. Akimoto, Younsun Kim, Moon-il Lee, K. Bhattad, and A. Ekpenyong. "Evolution of reference signals for LTE-advanced systems". In: *Communications Magazine, IEEE* 50.2 (Feb. 2012), pp. 132–138. ISSN: 0163-6804. DOI: 10.1109/MCOM.2012.6146492.

[88]   P. Kyösti et al. *WINNER II Channel Models*. D1.1.2 v1.1. IST-WINNER, Sept. 2007. URL: https://www.ist-winner.org/WINNER2-Deliverables/D1.1.2v1.1.pdf.

[89]   3GPP TR 36.814. *Evolved Universal Terrestrial Radio Access (E-UTRA); Further advancements for E-UTRA physical layer aspects*. v9.0.0. Mar. 2010. URL: http://www.3gpp.org.

[90]   Harri Holma and Antii Toskala. *LTE for UMTS: Evolution to LTE-Advanced*. Wiley, 2011.

[91]   J. Jose, A. Ashikhmin, T.L. Marzetta, and S. Vishwanath. "Pilot contamination problem in multi-cell TDD systems". In: *Information Theory, 2009. ISIT 2009. IEEE International Symposium on*. June 2009, pp. 2184–2188. DOI: 10.1109/ISIT.2009.5205814.

[92]   E. Larsson, O. Edfors, F. Tufvesson, and T. Marzetta. "Massive MIMO for next generation wireless systems". In: *Communications Magazine, IEEE* 52.2 (Feb. 2014), pp. 186–195. ISSN: 0163-6804. DOI: 10.1109/MCOM.2014.6736761.

[93]   Dereje Assefa Wassie, Gilberto Berardinelli, Fernando Menezes Leitão Tavares, Oscar Tonelli, Troels Bundgaard Sørensen, and Preben Mogensen. "Experimental Evaluation of Interference Rejection Combining for 5G Small Cells". Accepted to the 2015 IEEE Wireless Communications and Networking Conference (WCNC), March 2015.

[94]   Dereje Assefa Wassie, Gilberto Berardinelli, Fernando Menezes Leitão Tavares, Troels Bundgaard Sørensen, and Preben Mogensen. "Experimental Verification of Interference Mitigation techniques for 5G Small Cells". Accepted to the 2015 IEEE 81st Vehicular Technology Conference (VTC Spring), May 2015.

[95]   R. Gold. "Optimal binary sequences for spread spectrum multiplexing (Corresp.)" In: *Information Theory, IEEE Transactions on* 13.4 (Oct. 1967), pp. 619–621. ISSN: 0018-9448. DOI: 10.1109/TIT.1967.1054048.

[96]   D. Chu. "Polyphase codes with good periodic correlation properties (Corresp.)" In: *Information Theory, IEEE Transactions on* 18.4 (July 1972), pp. 531–532. ISSN: 0018-9448. DOI: 10.1109/TIT.1972.1054840.

[97]   Antonio M Tulino and Sergio Verdú. "Random matrix theory and wireless communications". In: *Communications and Information theory* 1.1 (2004), pp. 1–182.

[98] WB Smith and RR Hocking. "Algorithm as 53: Wishart variate generator". In: *Applied Statistics* (1972), pp. 341–345.

[99] D. Morales-Jimenez, J.F. Paris, J.T. Entrambasaguas, and Kai-Kit Wong. "On the Diagonal Distribution of a Complex Wishart Matrix and its Application to the Analysis of MIMO Systems". In: *Communications, IEEE Transactions on* 59.12 (2011), pp. 3475–3484. ISSN: 0090-6778. DOI: 10.1109/TCOMM.2011.100611.100641.

[100] B. Widrow, I. Kollar, and Ming-Chang Liu. "Statistical theory of quantization". In: *Instrumentation and Measurement, IEEE Transactions on* 45.2 (1996), pp. 353–361. ISSN: 0018-9456. DOI: 10.1109/19.492748.

[101] F.M.L. Tavares, G. Berardinelli, N.H. Mahmood, T.B. Sørensen, and P. Mogensen. "On the Potential of Interference Rejection Combining in B4G Networks". In: *Vehicular Technology Conference (VTC Fall), 2013 IEEE 78th*. Sept. 2013, pp. 1–5. DOI: 10.1109/VTCFall.2013.6692318.

[102] 3GPP TR 25.951. *FDD Base Station (BS) classification*. v12.0.0. Oct. 2014. URL: http://www.3gpp.org.

[103] Stefania Sesia, Matthew Baker, and Issam Toufik. *LTE - The UMTS Long Term Evolution: from theory to practice*. Chichester, West Sussex: Wiley, 2009. ISBN: 9780470697.

Part II

Appendices

Appendix A

Receiver model

In this appendix, the receiver model used for system-level simulations is presented. The baseband signal model is described first, followed by the description of the general received signal combining method. Channel response and received signal covariance matrix estimation are then discussed, including the error models for both types of estimation. Finally, the model for SIC is described and the equations used to calculate the SINR used in the simulations are presented in the last section of this appendix.

A.1 Baseband signal model

The baseband signal model assumes a network composed of multiple transmitting and receiving devices. Each device is equipped with N_{tx} transmit and N_{rx} receive antennas. All devices transmit time-aligned OFDM symbols. The received baseband signal vector $\mathbf{r}(f, t)$ with dimension $[N_{rx} \times 1]$ is given in the frequency domain by

$$\mathbf{r}(f, t) = \sum_{k=1}^{N_T} \sum_{l=1}^{N_S^k} \mathbf{h}_{k,l}(f, t) s_{k,l}(f, t) + \mathbf{n}(f, t) \tag{A.1}$$

where N_T is the number of devices transmitting at the same time and N_S^k is the number of data streams transmitted by the k-th device, which is limited to $1 \leq N_S^k \leq min(N_{rx}, N_{tx})$. The indexes f and t represent the OFDM subcarrier and OFDM time symbol indexes, respectively[1]. These indexes are omitted in the following equations for the sake of simplicity. The scalar $s_{k,l}$ represents

---

[1]Note that this model is a discrete time and frequency representation of the received baseband signal. Both indexes f and t are integers, with $0 \leq f \leq N_{sc} - 1$ and $-\infty \leq t \leq \infty$, where N_{sc} is the total number of OFDM subcarriers.

the data symbol of the l-th stream transmitted by the k-th transmitter through the equivalent complex channel given by the vector $\mathbf{h}_{k,l}$ $[N_{rx} \times 1]$.

The equivalent complex channel vector $\mathbf{h}_{k,l}$ is assumed to include the effects of signal precoding, transmit power amplification, transmit and receive antenna gains, and large and small scale propagation effects (path loss, shadowing and fast fading). The vectors $\mathbf{h}_{k,l}$ are assumed to be constant for the duration of the transmission interval, i.e. a block fading model is assumed.

The model assumes that transmitted signals $s_{k,l}$ have zero mean and unity power, and that the signals transmitted by the multiple devices are uncorrelated, i.e.

$$\mu_{s_{k,l}} = \mathbb{E}\{s_{k,l}\} = 0 \tag{A.2}$$

$$\sigma_{s_{k,l}s_{i,j}} = \mathbb{E}\{s_{k,l}s_{i,j}^*\} = \begin{cases} 1 & \text{if } k = i \text{ and } l = j \\ 0 & \text{if } k \neq i \text{ or } l \neq j \end{cases} \tag{A.3}$$

where $\mathbb{E}\{\cdot\}$ is the expectation operator.

The vector $\mathbf{n}$ $[N_{rx} \times 1]$ represents the additive noise. The m-th element of $\mathbf{n}$, which is relative to the m-th receive antenna, has power $\sigma_{n_m}^2$ and all elements of $\mathbf{n}$ are uncorrelated, i.e.

$$\mu_{n_x} = \mathbb{E}\{n_x\} = 0 \tag{A.4}$$

$$\sigma_{n_x n_y} = \mathbb{E}\{n_x n_y^*\} = \begin{cases} \sigma_{n_x}^2 & \text{if } y = x \\ 0 & \text{if } y \neq x \end{cases} \tag{A.5}$$

If the simplified receiver front-end model is used, the power $\sigma_{n_m}^2$ is equal to the additive thermal noise power σ_0^2 (which may be adjusted based on a noise figure model). In the case of the detailed receiver front-end model, $\sigma_{n_m}^2$ will depend on the characteristics of both the receiver and the input signal.

Note that the formula for the received signal vector $\mathbf{r}$ may be split in multiple parts depending on the intended desired signal. Assuming that the desired signal is the symbol on the j-th stream sent by the i-th transmitter, i.e. $s_{i,j}$, the received signal vector may be described as follows

$$\mathbf{r} = \underbrace{\mathbf{h}_{i,j}s_{i,j}}_{\substack{\text{desired} \\ \text{signal}}} + \underbrace{\sum_{\substack{l=1 \\ l \neq j}}^{N_S^i} \mathbf{h}_{i,l}s_{i,l}}_{\substack{\text{inter-stream} \\ \text{interference}}} + \underbrace{\sum_{\substack{k=1 \\ k \neq i}}^{N_T} \sum_{l=1}^{N_S^k} \mathbf{h}_{k,l}s_{k,l}}_{\substack{\text{other} \\ \text{interference}}} + \mathbf{n} \tag{A.6}$$

A.2 Received signal combining

To generate an estimate of the j-th signal sent by the i-th transmitter, the elements of the received signal $\mathbf{r}$ are combined using vector $\mathbf{w}_{i,j}$. The estimate

$\hat{s}_{i,j}$ is given by

$$\hat{s}_{i,j} = \mathbf{w}_{i,j}^H \mathbf{r} \tag{A.7}$$

where $(\cdot)^H$ is the Hermitian conjugate operator.

The optimal combining vector $\mathbf{w}_{i,j}$ is obtained using the MMSE estimate [19], given by

$$\mathbf{w}_{i,j} = \mathbf{R}_r^{-1} \mathbf{h}_{i,j} \tag{A.8}$$

where $\mathbf{h}_{i,j}$ is the equivalent complex channel vector through which the j-th signal transmitted by the i-th transmitter was sent, and $\mathbf{R}_r$ $[N_{rx} \times N_{rx}]$ is the covariance matrix of the received signal $\mathbf{r}$, defined as

$$\mathbf{R}_r = \mathbb{E}\{\mathbf{r}\mathbf{r}^H\} \tag{A.9}$$

In reality, the receiver uses estimates of the equivalent complex channel vector $\mathbf{h}_{i,j}$ and the received signal covariance matrix $\mathbf{R}_r$. Therefore, the combining vector used in practical receivers is given by

$$\mathbf{w}_{i,j} = \hat{\mathbf{R}}_r^{-1} \hat{\mathbf{h}}_{i,j} \tag{A.10}$$

where $\hat{\mathbf{R}}_r$ is the estimate of $\mathbf{R}_r$ and $\hat{\mathbf{h}}_{i,j}$ is the estimate of $\mathbf{h}_{i,j}$.

A.3 Channel response estimation

The channel response is estimated using reference symbols that are known to both the transmitter and the receiver. These symbols, also known as pilots, are transmitted in predefined positions in the frame. When these pilots are transmitted, the received signal $\mathbf{r}$ in the frequency domain is given by

$$\mathbf{r}(f,t) = \sum_{k=1}^{N_T} \sum_{l=1}^{N_S^k} \mathbf{h}_{k,l}(f,t) p_{k,l}(f,t) + \mathbf{n}(f,t) \tag{A.11}$$

where N_T is the number of devices transmitting reference symbols at the same time and N_S^k is the number of reference symbols transmitted on the spatial domain by the k-th device. The scalar $p_{k,l}$ represents the l-th pilot symbol transmitted by the k-th transmitter[2].

Assuming $p_{i,j} p_{i,j}^* = 1$, the channel estimate $\hat{\mathbf{h}}_{i,j}$ obtained using the received signal $\mathbf{r}$ and the pilot $p_{i,j}$ known at the receiver side is given by

$$\hat{\mathbf{h}}_{i,j} = \mathbf{r} p_{i,j}^* \tag{A.12}$$

---

[2]Note that in Eq. A.11 the value of pilots $p_{k,l}(f,t)$ is zero in most of the (f,t) positions. The non-zero (f,t) positions are defined by the pilot spacing configuration in the time and frequency domains.

where $(\cdot)^*$ is the conjugate operator. Ideally, the pilot symbols $p_{k,l}$ should be designed to guarantee that the different pilots transmitted by the multiple devices (including those in other cells) do not interfere with each other. This requirement is fulfilled if the pilots transmitted by each device do not overlap, i.e. they use different different positions in the frame (different f and t indexes) or different frames. The other possibility is to use orthogonal reference sequences, such as Gold codes [95] or Zadoff-Chu [96, 48] sequences. If the pilots fulfil this requirement then it is possible to obtain the channel estimate $\hat{\mathbf{h}}_{i,j}$ without any interference, i.e. the estimate is given by

$$\hat{\mathbf{h}}_{i,j} = (\sum_{k=1}^{N_T} \sum_{l=1}^{N_S^k} \mathbf{h}_{k,l} p_{k,l} + \mathbf{n}) p_{i,j}^* \tag{A.13}$$

$$= \sum_{k=1}^{N_T} \sum_{l=1}^{N_S^k} \mathbf{h}_{k,l} p_{k,l} p_{i,j}^* + \mathbf{n} p_{i,j}^* \tag{A.14}$$

$$= \mathbf{h}_{i,j} + \mathbf{n} p_{i,j}^* \tag{A.15}$$

$$= \mathbf{h}_{i,j} + \mathbf{e} \tag{A.16}$$

where $\mathbf{e}_{i,j}$ is the residual estimation error. This error is modelled using the covariance of the vector $\mathbf{e}_{i,j}$, given by

$$\mathbf{R}_e = \mathbb{E}\{(\mathbf{n} p_{i,j}^*)(\mathbf{n} p_{i,j}^*)^H\} \tag{A.17}$$

$$= \mathbb{E}\{\mathbf{n}(p_{i,j}^* p_{i,j})\mathbf{n}^H\} \tag{A.18}$$

$$= \mathbb{E}\{\mathbf{n}\mathbf{n}^H\} \tag{A.19}$$

$$= \mathbf{R}_n \tag{A.20}$$

where $\mathbf{R}_n$ is the covariance of the noise vector $\mathbf{n}$.

The model assumes that the estimation method may use multiple samples of the same pilot (received in different positions of the frame) to obtain the channel estimate. The use of multiple estimates helps to improve the quality of the estimation by reducing the power of the noise error $\mathbf{e}$. This possibility is also considered in the model. In the simulations, the vector $\mathbf{e}_{i,j}$ is modelled as a circularly-symmetric Complex Normal random vector with zero mean and covariance equal to $\mathbf{R}_n/Q_H$, where Q_H is the number of samples used to estimate the channel response vector [50]. The number of samples Q_H depends on the reference symbol design as well as on the frequency correlation of the channel [49].

$$\mathbf{e}_{i,j} \sim \mathcal{CN}(0, \mathbf{R}_n/Q_H) \tag{A.21}$$

If ideal estimation is assumed, the channel estimates match exactly with the channel coefficients, i.e. the equivalent channel vector $\hat{\mathbf{h}}_{i,j}$ is given by

$$\hat{\mathbf{h}}_{i,j} = \mathbf{h}_{i,j} \tag{A.22}$$

A.4 Covariance matrix estimation

Different methods for the estimation of the received signal covariance matrix $\mathbf{R}_r$ can be used depending on the assumptions made about the received signals, and by extension, about the received signal covariance matrix. The covariance matrix estimation model for the IRC receiver is presented first, followed by the model used for the Maximal Ratio Combining (MRC) receiver.

A.4.1 IRC Receiver

Assuming that the channel response vectors $\mathbf{h}_{k,l}$ are constant, the received signal covariance matrix $\mathbf{R}_r$ is given by

$$\mathbf{R}_r = \mathbb{E}\{\mathbf{r}\mathbf{r}^H\} \tag{A.23}$$

$$= \mathbb{E}\{(\sum_{k=1}^{N_T}\sum_{l=1}^{N_S^k}\mathbf{h}_{k,l}s_{k,l} + \mathbf{n})(\sum_{k=1}^{N_T}\sum_{l=1}^{N_S^k}\mathbf{h}_{k,l}s_{k,l} + \mathbf{n})^H\} \tag{A.24}$$

$$= \mathbb{E}\{(\sum_{k=1}^{N_T}\sum_{l=1}^{N_S^k}\mathbf{h}_{k,l}s_{k,l})(\sum_{k=1}^{N_T}\sum_{l=1}^{N_S^k}\mathbf{h}_{k,l}s_{k,l})^H\} + \mathbb{E}\{\mathbf{n}\mathbf{n}^H\} \tag{A.25}$$

$$= \sum_{k=1}^{N_T}\sum_{l=1}^{N_S^k}\mathbb{E}\{(\mathbf{h}_{k,l}s_{k,l})(\mathbf{h}_{k,l}s_{k,l})^H\} + \mathbb{E}\{\mathbf{n}\mathbf{n}^H\} \tag{A.26}$$

$$= \sum_{k=1}^{N_T}\sum_{l=1}^{N_S^k}\mathbf{h}_{k,l}\mathbb{E}\{s_{k,l}s_{k,l}^*\}\mathbf{h}_{k,l}^H + \mathbb{E}\{\mathbf{n}\mathbf{n}^H\} \tag{A.27}$$

$$= \sum_{k=1}^{N_T}\sum_{l=1}^{N_S^k}\mathbf{h}_{k,l}\mathbf{h}_{k,l}^H + \mathbf{R}_n \tag{A.28}$$

where $\mathbf{R}_n$ is the covariance matrix of the noise vector $\mathbf{n}$.

In practice, the receiver must use an estimate of the covariance matrix $\mathbf{R}_r$. In this model, two estimation methods are considered: DSB and RSB methods [30].

Data-Symbol Based (DSB) Estimation The DSB method is the most direct method of estimation. The method uses the samples of the received signal at the many different positions of the frame that contain data symbols to estimate the covariance matrix. The estimate of the covariance matrix using the DSB method is given by

$$\hat{\mathbf{R}}_r = \frac{1}{Q_{DS}} \sum_{\substack{<f,t> \\ \in \mathcal{P}_{DS}}} \mathbf{r}(f,t)\mathbf{r}(f,t)^H \tag{A.29}$$

97

where $\mathcal{P}_{DS}$ is the set of indexing pairs for the subcarriers of the OFDM symbols in which data symbols are transmitted and Q_{DS} is the cardinality of $\mathcal{P}_{DS}$.

The covariance matrix estimate is modelled in the simulations as a random matrix sample drawn from a Wishart distribution [97, 98] with covariance matrix $\mathbf{R}_r$ (as in Eq. A.28) and Q_{DS} degrees of freedom.

$$\hat{\mathbf{R}}_r \sim \frac{1}{Q_{DS}} \mathcal{W}(\mathbf{R}_r, Q_{DS}) \tag{A.30}$$

Reference-Symbol Based (RSB) Estimation The RSB method uses the channel response estimates to improve the accuracy of the received signal covariance matrix estimate. If only the channel response estimates relative to the desired signals ($k = i$) are known, the estimate of the covariance matrix using the RSB method is given by

$$\hat{\mathbf{R}}_r = \sum_{l=1}^{N_S^i} \hat{\mathbf{h}}_{i,l} \hat{\mathbf{h}}_{i,l}^H + \hat{\mathbf{R}}_z \tag{A.31}$$

where $\hat{\mathbf{R}}_z$ is the estimate of the covariance matrix relative to the residual interference plus noise signal vector. This estimate is given by

$$\hat{\mathbf{R}}_z = \frac{1}{Q_{RS}} \sum_{\substack{<f,t> \\ \in \mathcal{P}_{RS}}} (\mathbf{r}(f,t) - \sum_{l=1}^{N_S^i} \hat{\mathbf{h}}_{i,l} p_{i,l}(f,t))(\mathbf{r}(f,t) - \sum_{l=1}^{N_S^i} \hat{\mathbf{h}}_{i,l} p_{i,l}(f,t))^H \tag{A.32}$$

where $\mathcal{P}_{RS}$ is the set of indexing pairs for the subcarriers of the OFDM symbols in which reference symbols (used for covariance matrix estimation) are transmitted and Q_{RS} is the cardinality of $\mathcal{P}_{RS}$.

The covariance matrix estimate $\hat{\mathbf{R}}_z$ is also modelled in simulations as a random matrix sample drawn from a Wishart distribution with covariance matrix $\mathbf{R}_z$ and Q_{RS} degrees of freedom, i.e.

$$\hat{\mathbf{R}}_z \sim \frac{1}{Q_{RS}} \mathcal{W}(\mathbf{R}_z, Q_{RS}) \tag{A.33}$$

where the covariance matrix $\mathbf{R}_z$ is calculated as

$$\mathbf{R}_z = \sum_{\substack{k=1 \\ k \neq i}}^{N_T} \sum_{l=1}^{N_S^k} \mathbf{h}_{k,l} \mathbf{h}_{k,l}^H + \mathbf{R}_n \tag{A.34}$$

If the channel response estimates are known for all signals, including the interferers ($k \in \{1, \dots, N_T\}$), the estimate of the covariance matrix using the

RSB method is given by

$$\hat{\mathbf{R}}_r = \sum_{k=1}^{N_T} \sum_{l=1}^{N_S^k} \hat{\mathbf{h}}_{k,l} \hat{\mathbf{h}}_{k,l}^H + \hat{\mathbf{R}}_n \tag{A.35}$$

where $\hat{\mathbf{R}}_n$ is the estimate of $\mathbf{R}_n$, which is calculated as

$$\hat{\mathbf{R}}_n = \frac{1}{Q_{RS}} \sum_{\substack{<f,t> \\ \in \mathcal{P}_{RS}}} (\mathbf{r}(f,t) - \sum_{k=1}^{N_T} \sum_{l=1}^{N_S^k} \hat{\mathbf{h}}_{k,l} p_{k,l}(f,t))(\mathbf{r}(f,t) - \sum_{k=1}^{N_T} \sum_{l=1}^{N_S^k} \hat{\mathbf{h}}_{k,l} p_{k,l}(f,t))^H \tag{A.36}$$

The covariance matrix estimate $\hat{\mathbf{R}}_n$ is modelled in simulations as a random matrix sample drawn from Wishart distribution with covariance matrix $\mathbf{R}_n$ and Q_{RS} degrees of freedom.

$$\hat{\mathbf{R}}_n \sim \frac{1}{Q_{RS}} \mathcal{W}(\mathbf{R}_n, Q_{RS}) \tag{A.37}$$

Since the covariance matrix $\mathbf{R}_n$ is diagonal (there is no correlation between the elements of the additive noise vector $\mathbf{n}$), each one of the diagonal elements may be estimated individually to reduce the complexity of the estimation. If this approach is used to estimate $\mathbf{R}_n$, the diagonal elements may be modelled using random samples drawn from a Chi-squared distribution [99], where the index m indicates the m-th receive antenna.

$$\hat{\sigma}_{n_m}^2 \sim \frac{\sigma_{n_m}^2}{Q_{RS} - 1} \chi^2(Q_{RS} - 1) \tag{A.38}$$

A.4.2   MRC Receiver

The MRC receiver assumes the sum of all interference coming from other transmitters may be modelled as additive noise, i.e. it assumes there is no correlation between the signals received by the different receive antennas, leading to the assumption of a diagonal covariance matrix $\mathbf{R}_z$. This assumption simplifies the estimation process because the diagonal elements may be estimated individually.

In this case, the estimate of the m-th diagonal element of the $\mathbf{R}_z$ matrix is given by

$$\hat{\sigma}_{z_m}^2 = \frac{1}{Q_{RS}} \sum_{\substack{<f,t> \\ \in \mathcal{P}_{RS}}} (r_m(f,t) - \sum_{l=1}^{N_S^i} \hat{h}_{i,l,m} p_{i,l}(f,t))(r_m(f,t) - \sum_{l=1}^{N_S^i} \hat{h}_{i,l,m} p_{i,l}(f,t))^H \tag{A.39}$$

where r_m and $\hat{h}_{i,l,m}$ are the m-th elements of the vectors $\mathbf{r}$ and $\hat{\mathbf{h}}_{i,l}$, respectively. The estimate of the $\mathbf{R}_z$ matrix is then obtained as

$$\hat{\mathbf{R}}_z = diag(\hat{\sigma}_{z_1}^2, \hat{\sigma}_{z_1}^2, \ldots, \hat{\sigma}_{z_{Nrx}}^2) \tag{A.40}$$

In simulations, the diagonal elements of the $\hat{\mathbf{R}}_z$ matrix are modelled using a Chi-squared distribution. The m-th element is given by

$$\hat{\sigma}_{z_m}^2 \sim \frac{\sigma_{z_m}^2}{Q_{RS} - 1} \chi^2(Q_{RS} - 1) \tag{A.41}$$

where the variance $\sigma_{z_m}^2$ is calculated as

$$\sigma_{z_m}^2 = \sum_{\substack{k=1 \\ k \neq i}}^{N_T} \sum_{l=1}^{N_S^k} h_{k,l,m} h_{k,l,m}^* + \sigma_{n_m}^2 \tag{A.42}$$

A.5 Receive front-end imperfections model

This part of the model is used to account for the errors due to imperfections in the receiver front-end. These imperfections exist due to limitations in the AGC and ADC mechanisms. Depending on the characteristics of the receiver, these limitations may increase the received signal noise floor, leading to higher estimation errors, inaccurate receiver combining and poor interference suppression.

The model is divided in two parts: the amplification part, that includes the effect of power estimation delay, signal amplification and corresponding SNR degradation, and the analog-to-digital conversion part, that includes the signal quality degradation due to quantization and clipping errors. Figure A.1 presents a schematic for the model, depicting the input and output signals of each stage.

The input baseband signal at the m-th antenna (before the receiver front-end components) is given by

$$r_m^{(1)}(f,t) = \sum_{k=1}^{N_T} \sum_{l=1}^{N_S^k} h_{k,l,m}(f,t) s_{k,l}(f,t) + v_m(f,t) \tag{A.43}$$

where v_m is the additive thermal noise with power σ_0^2. The mean received power of the t-th OFDM symbol is given by

$$\sigma_{r_m^{(1)}}^2(t) = \frac{1}{N_{sc}} \sum_{f=1}^{N_{sc}} \left(\sum_{k=1}^{N_T} \sum_{l=1}^{N_S^k} |h_{k,l,m}(f,t)|^2 + \sigma_0^2 \right) \tag{A.44}$$

A.5. Receive front-end imperfections model
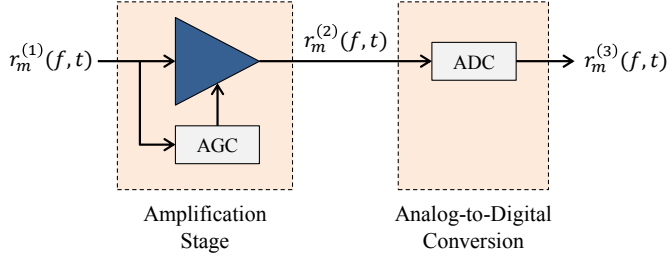
Fig. A.1: Receiver Front-End Model

where N_{sc} is the number of OFDM subcarriers.

In the amplification stage, AGC mechanism attempts to adjust the amplification gain to make best use of the ADC dynamic range. In practice, there is a delay between the estimation of the received signal power and the adjustment of the gain. The amplification gain applied to the signal received at the m-th antenna at time t is given by [65]

$$g_m(t) = \frac{A}{\sqrt{\epsilon \sigma^2_{r_m^{(1)}}(t - \tau)}} \tag{A.45}$$

where A is the ADC full range amplitude, ϵ is the back-off factor and τ is the AGC estimation delay. The back-off ϵ is use to account for the difference between the peak and average values of the received signal. In ideal conditions, this value controls the probability that the input signal will be clipped by the ADC. The value of ϵ may be calculated for a desired probability by assuming the OFDM signal to be a band-limited zero-mean Gaussian stationary process [65].

The output signal power after the amplification stage is given by

$$\sigma^2_{r_m^{(2)}}(t) = \frac{1}{N_{sc}} \sum_{f=1}^{N_{sc}} \left(\sum_{k=1}^{N_T} \sum_{l=1}^{N_S^k} g_m^2(t) |h_{k,l,m}(f,t)|^2 + g_m^2(t) F \sigma_0^2 \right) \tag{A.46}$$

where F is the the noise factor of the amplification stage.

In the quantization stage, the quantization noise due to the analog-to-digital conversion process is included. The model assumes the quantization noise to be independently and uniformly distributed [65, 100]. This noise is included as an extra additive noise term with power given by

$$\sigma_q^2 = \frac{A^2 2^{-2b}}{3} \tag{A.47}$$

where b is the ADC word-length in bits. This parameter defines the resolution of the ADC process.

The clipping stage accounts for the noise generated when the amplitude of the input signal at the ADC input is higher than the ADC full range amplitude. This process causes two types of effects: signal amplitude compression and additive noise power enhancement. The amplitude compression of the input signal relative to the m-th antenna at time t is calculated as [66]

$$\alpha_m(t) = 1 - e^{-\beta_m^2(t)} + \frac{\sqrt{\pi}}{2}\beta_m(t)\text{erfc}(\beta_m(t)) \tag{A.48}$$

where $\text{erfc}(\cdot)$ is the complementary error function and $\beta_m(t)$ is the clipping ratio given by

$$\beta_m(t) = \sqrt{\frac{A^2}{\sigma_{r_m^{(2)}}^2(t)}} \tag{A.49}$$

The power of the clipping noise is calculated as a function of the input signal signal power $\sigma_{r_m^{(2)}}^2(t)$ and is given by [66]

$$\sigma_{c_m}^2(t) = (1 - e^{-\beta_m^2(t)} - \alpha_m^2(t))\sigma_{r_m^{(2)}}^2(t) \tag{A.50}$$

The output signal power after the analog-to-digital conversion stage is given by

$$\sigma_{r_m^{(3)}}^2(t) = \frac{1}{N_{sc}}\sum_{f=1}^{N_{sc}}(\sum_{k=1}^{N_T}\sum_{l=1}^{N_S^k}\alpha_m^2(t)g_m^2(t)|h_{k,l,m}(f,t)|^2 + g_m(t)^2 F\sigma_0^2 + \sigma_q^2 + \sigma_{c_m}^2(t)) \tag{A.51}$$

When the receiver front-end error model is used, the received signal after the ADC stage relative to the m-th antenna at time t is given by

$$r_m^{(3)}(f,t) = \sum_{k=1}^{N_T}\sum_{l=1}^{N_S^k}\alpha_m(t)g_m(t)h_{k,l,m}(f,t)s_{k,l}(f,t) + n_m(f,t) \tag{A.52}$$

and the power of the additive noise term $n_m(f,t)$ is given by

$$\sigma_{n_m}^2(t) = g_m(t)^2 F\sigma_0^2 + \sigma_q^2 + \sigma_{c_m}^2(t) \tag{A.53}$$

A.6 Successive interference cancellation

If SIC is used, a iterative process takes place in the receiver. In each iteration, the receiver attempts to decode one of the multiple $s_{k,l}$ signals that composes the received signal **r** using the estimated signal $\hat{s}_{k,l}$. If successful, this signal

is reconstructed and removed from the received signal $\mathbf{r}$, eliminating its interfering contribution to the decoding of the other signals. Therefore, after each iteration, the received signal $\mathbf{r}$ is given by

$$\mathbf{r}(f,t) = \sum_{k=1}^{N_T} \sum_{l=1}^{N_S^k} \mathbf{h}_{k,l} s_{k,l} + \mathbf{n} - \underbrace{\sum_{k=1}^{N_T} \sum_{l=1}^{N_S^k}}_{<k,l> \in \mathcal{D}} \mathbf{h}_{k,l} s_{k,l} \qquad (A.54)$$

where $\mathcal{D}$ is the set of indexing pairs of the signals that have already been decoded. A practical receiver that uses SIC must use estimates of the channel response vectors $\mathbf{h}_{k,l}$ and the transmitted symbols $s_{k,l}$. Therefore, in the practical receiver, the received signal $\mathbf{r}$ is given after each iteration by

$$\mathbf{r}(f,t) = \sum_{k=1}^{N_T} \sum_{l=1}^{N_S^k} \mathbf{h}_{k,l} s_{k,l} + \mathbf{n} - \underbrace{\sum_{k=1}^{N_T} \sum_{l=1}^{N_S^k}}_{<k,l> \in \mathcal{D}} \hat{\mathbf{h}}_{k,l} \hat{s}_{k,l} \qquad (A.55)$$

i.e. the effectiveness of the interference cancellation depends both on the quality of the channel estimation and on the correctness of the signal decoding process. In this model, it is assumed that a verification mechanism is used to guarantee that only correctly decoded codewords are used for cancellation, i.e. set $\mathcal{D}$ only contains the indexes of correctly decoded symbols.

A.7 Signal-to-interference-plus-noise ratio

The SINR of the estimated signal $\hat{s}_{i,j}$ is obtained through the decomposition of the total power of the estimated signal into desired and interference plus

noise contributions. The total power of $\hat{s}_{i,j}$ is given by

$$\sigma_{\hat{s}_{i,j}}^2 = \mathbb{E}\{(\mathbf{w}_{i,j}^H \mathbf{r})(\mathbf{w}_{i,j}^H \mathbf{r})^H\} \tag{A.56}$$

$$= \mathbf{w}_{i,j}^H \mathbb{E}\{\mathbf{r}\mathbf{r}^H\}\mathbf{w}_{i,j} \tag{A.57}$$

$$= \mathbf{w}_{i,j}^H \mathbf{R}_r \mathbf{w}_{i,j} \tag{A.58}$$

$$= \mathbf{w}_{i,j}^H \left(\sum_{k=1}^{N_T}\sum_{l=1}^{N_S^k} \mathbf{h}_{k,l}\mathbf{h}_{k,l}^H + \mathbf{R}_n\right)\mathbf{w}_{i,j} \tag{A.59}$$

$$= \mathbf{w}_{i,j}^H \left(\sum_{l=1}^{N_S^i} \mathbf{h}_{i,l}\mathbf{h}_{i,l}^H + \sum_{\substack{k=1\\k\neq i}}^{N_T}\sum_{l=1}^{N_S^k} \mathbf{h}_{k,l}\mathbf{h}_{k,l}^H + \mathbf{R}_n\right)\mathbf{w}_{i,j} \tag{A.60}$$

$$= \mathbf{w}_{i,j}^H \left(\mathbf{h}_{i,j}\mathbf{h}_{i,j}^H + \sum_{\substack{l=1\\l\neq j}}^{N_S^i} \mathbf{h}_{i,l}\mathbf{h}_{i,l}^H + \sum_{\substack{k=1\\k\neq i}}^{N_T}\sum_{l=1}^{N_S^k} \mathbf{h}_{k,l}\mathbf{h}_{k,l}^H + \mathbf{R}_n\right)\mathbf{w}_{i,j} \tag{A.61}$$

$$= \mathbf{w}_{i,j}^H (\mathbf{h}_{i,j}\mathbf{h}_{i,j}^H)\mathbf{w}_{i,j} + \mathbf{w}_{i,j}^H \left(\sum_{\substack{l=1\\l\neq j}}^{N_S^i} \mathbf{h}_{i,l}\mathbf{h}_{i,l}^H + \sum_{\substack{k=1\\k\neq i}}^{N_T}\sum_{l=1}^{N_S^k} \mathbf{h}_{k,l}\mathbf{h}_{k,l}^H + \mathbf{R}_n\right)\mathbf{w}_{i,j} \tag{A.62}$$

This equation may be simplified to separate the desired signal part from the interference and noise part, as follows

$$\sigma_{\hat{s}_{i,j}}^2 = \underbrace{\mathbf{w}_{i,j}^H (\mathbf{h}_{i,j}\mathbf{h}_{i,j}^H)\mathbf{w}_{i,j}}_{\substack{\text{desired signal}\\\text{power}}} + \underbrace{\mathbf{w}_{i,j}^H (\mathbf{R}_r - \mathbf{h}_{i,j}\mathbf{h}_{i,j}^H)\mathbf{w}_{i,j}}_{\substack{\text{interference and noise}\\\text{power}}} \tag{A.63}$$

Using this formulation, the SINR of the estimated signal $\hat{s}_{i,j}$ is given by

$$\gamma_{i,j} = \frac{\mathbf{w}_{i,j}^H (\mathbf{h}_{i,j}\mathbf{h}_{i,j}^H)\mathbf{w}_{i,j}}{\mathbf{w}_{i,j}^H (\mathbf{R}_r - \mathbf{h}_{i,j}\mathbf{h}_{i,j}^H)\mathbf{w}_{i,j}} \tag{A.64}$$

If SIC is used, the covariance matrix used in the SINR formula is updated at every iteration to remove the contribution from the cancelled interferers.

$$\mathbf{R}_r = \sum_{k=1}^{N_T}\sum_{l=1}^{N_S^k} \mathbf{h}_{k,l}\mathbf{h}_{k,l}^H + \mathbf{R}_n - \underbrace{\sum_{k=1}^{N_T}\sum_{l=1}^{N_S^k} \hat{\mathbf{h}}_{k,l}\hat{\mathbf{h}}_{k,l}^H}_{<k,l>\in\mathcal{D}} \tag{A.65}$$

Appendix B

Detailed simulation assumptions

The simulation tool used to generate the results presented in this thesis and in the related publications was initially developed for inter-cell interference coordination studies. The main focus was to evaluate different distributed mechanisms for the allocation of time/frequency resources among neighbour cells. The simulator was coded in Matlab and was designed to be modular and testable.

During this research project, this simulator was modified to include the new features necessary for the investigation on the use of interference suppression receivers as a tool to manage inter-cell interference, such as the receiver model presented in Appendix A. A detailed description of the simulation tool and the models used for system-level simulations is presented in the following sections.

B.1   Simulation tool

The high-level flowchart of the simulation tool is presented in Figure B.1(a). The simulator uses a Monte Carlo simulation approach in which many different trials are used to achieve statistical reliability. These different trials, also known as "snapshots", generate data that is collected and post-processed to derive the statistical indicators used to analyse the network when different sets of input parameters are used.

For each snapshot, the simulator generates a new network topology, i.e. the APs and UEs are positioned in different positions following a set of positioning rules that depend on the scenario selected for simulation. During this step, every variable that is not time dependent is pre-calculated to save simu-

lation time. For example, the large scale propagation effects are calculated at this point, since device mobility is not considered in these simulations due to the short time span of each snapshot. For the same reason, the cell association process is also performed only once at the beginning of each snapshot.

In each snapshot a predefined number of frames is simulated. Each frame consists in a sequence of steps, as shown in Figure B.1(b). The final result of each frame is a set of variables that describe the status of the network at the end of that time frame. This set includes for example the instantaneous SINR and throughput of each link at that specific frame. After enough frames have been simulated, a new snapshot starts with a new topology. This process is repeated until the end of the simulation.
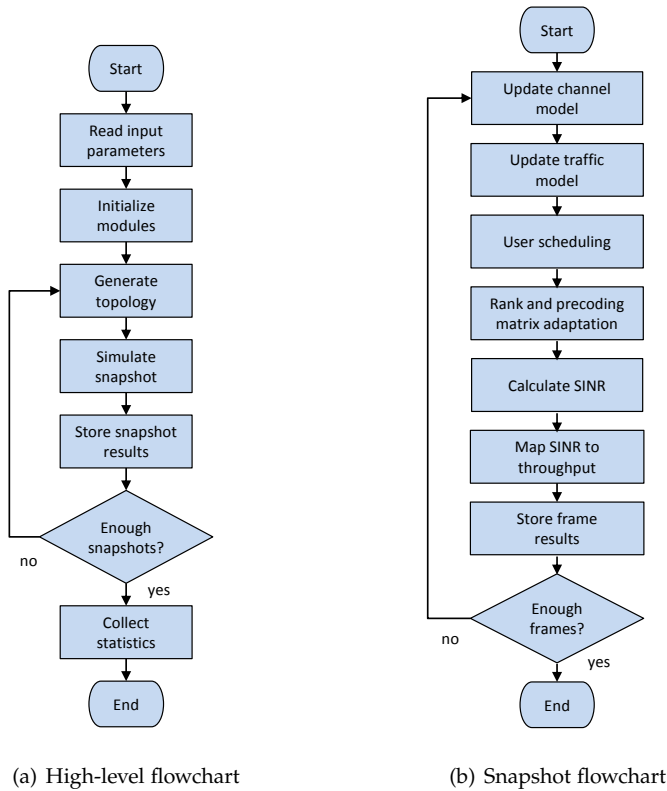

(a) High-level flowchart   (b) Snapshot flowchart

Fig. B.1: Simulation flowcharts

Fig. B.2: Indoor Office [89]

B.2 Simulation scenario

The general simulation scenario consists of a small-cell network operating over a 200 MHz frequency band at 3.5 GHz. This frequency band is dedicated for the operation of the small-cell network, i.e. it is assumed that the band is free of interference coming from other networks or layers (such as a macro cell layer, for example).

Two different indoor deployment scenarios are considered in this study. The first scenario, hereby referred to as the Indoor Office scenario, is a standard 3GPP scenario that was first used for the evaluation of LTE femtocells [89]. This scenario is also known as the dual-stripe scenario in the literature. The scenario, depicted in Figure B.2, consists in two office buildings separated by a ten-meter-wide street. Each building is composed of two rows of ten offices per floor. Each office measures ten meters by ten meters.

In this scenario, one AP and a configurable number of UEs are dropped uniformly at random positions in each office. Devices are not dropped outdoors. The position of the APs is random in this scenario to emulate the users deploying their APs at any place in the offices (i.e. the network operator has no control over the location of the APs in this scenario). Although the number of UEs per office may be configured, the simulations in this research work were always configured with one UE per office.

The second scenario, hereby referred to as the Indoor Hotspot scenario, is a simple modification of the first scenario [101]. This scenario mimics a large hall in which multiple APs are deployed to cover the area of the hall. Figure B.3 depicts the scenario. The scenario consists of four rows of ten virtual square spaces (there are no walls separating the square spaces in this scenario). One AP is deployed in the middle of each virtual square space, creating a uniform coverage area throughout the hall. The UEs are then dropped uniformly at random positions. Again, no devices are dropped
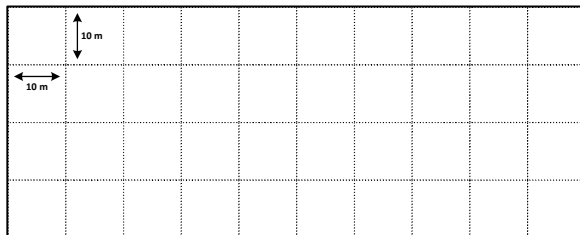
Fig. B.3: Indoor Hotspot [101]

outdoors.

Each deployment scenario may be configured to assume either CSG or OSG access modes. In CSG mode, the UEs are only allowed to connect to the AP located in the same office, whereas in OSG mode, the UEs may freely connect to any AP. In the OSG case, the UEs are connected to the AP that will lead to the link with the smallest total propagation loss.

The Indoor Office scenario may also be configured to emulate different network densities by changing the cell DR, i.e. the probability that an AP will exist in either each office. This probability is modelled as the outcome of a Bernoulli trial. Therefore, the actual number of APs deployed per snapshot is given by a Binomial distribution with number of trials equal to the number of offices or spaces and probability equal to the deployment ratio.

B.3 Propagation model

The propagation model includes both large-scale (deterministic path loss and log-normal shadowing) and small-scale (frequency-selective time-varying signal fading) effects.

B.3.1 Deterministic path loss

For the Indoor Office scenario, the deterministic path loss model for the standard 3GPP dual-stripe scenario [89] is used. This model takes into account the attenuation loss due to the walls that may exist in between devices. The model provides path loss formulas for links between devices in the same building and devices in different buildings. The path loss in decibels [dB] is given by

$$PL = 38.46 + 20\log_{10} R + 0.7d_{2D_{indoor}} + qL_{iw} + 18.3n^{((n+2)/(n+1)-0.46)} \quad \text{(B.1)}$$

and

$$PL = \max(15.3 + 37.6 \log_{10} R, 38.46 + 20 \log_{10} R) \tag{B.2}$$

$$+ 0.7 d_{2D_{\text{indoor}}} + q L_{\text{iw}} + 2 L_{\text{ow}} + 18.3 n^{((n+2)/(n+1)-0.46)} \tag{B.3}$$

for devices in the same building and devices in different buildings, respectively. In these formulas, R is the linear distance between transmitter and receiver in meters (considering the three spatial dimensions) and $d_{2D_{\text{indoor}}}$ is the linear indoor distance in the xy-plane (excluding height) also in meters. This additional loss of 0.7 dB per meter models the loss due to furniture and other obstacles found indoors. The model also accounts for the loss due to internal walls (L_{iw}) and external walls (L_{ow}), where q is the total number of internal walls traversed by the signal. Finally, n is the number of floors separating the transmitter from the receiver in multi-floor deployments. The Minimum Coupling Loss (MCL) in this scenario is 45 dB [102].

The model for the Indoor Hotspot scenario is the Winner II Indoor Hotspot (B3) model [88]. In this model the formula used depends on the line-of-sight conditions. The path in decibels [dB] is given in this case by

$$PL = \max(70, 13.9 \log_{10} R + 64.4 + 20 \log_{10}(f_c/5)) \tag{B.4}$$

and

$$PL = \max(60, 37.8 \log_{10} R + 36.5 + 23 \log_{10}(f_c/5)) \tag{B.5}$$

if the links are in line-of-sight and non-line-of-sight conditions, respectively. The variable f_c is the carrier frequency in GHz. In this scenario, the MCL is 70 dB. The probability of line-of-sight is calculated for each link based on the distance between transmitter and receiver, according to the following rule.

$$P(LOS) = \begin{cases} 1 & \text{if } R \leq 10 \\ e^{-(R-10)/45} & \text{if } R > 10 \end{cases} \tag{B.6}$$

B.3.2 Log-normal shadowing

The shadowing for each link is given by a random sample drawn from log-normal distributions. In the Indoor Office scenario, the parameters of this distribution depend on whether the link is an interfering link or not. The values are 8 dB for interfering links and 6 dB for the other [89]. In the Indoor Hotspot scenario, the parameter depends on the line-of-sight-condition. The values are 3 dB for line-of-sight links and 4 dB for non-line-of-sight links [88].

B.3.3 Frequency-selective time-varying signal fading

Signal fading is modelled as a frequency-selective time-varying process, using the channel model developed during the Winner II project [88]. The

fading channel samples are pre-calculated and saved in a large binary file in order to reduce simulation time. In each simulation snapshot, different parts of the file are selected randomly to emulate the signal fading for the different links. Care was taken to guarantee that the samples used in different snapshots have very low correlation and that this correlation does not affect the accuracy of the results.

Different files were created for the different scenarios and for different line-of-sight conditions. The Winner II scenario used for the Indoor Office and the Indoor Hotspot scenarios were the Indoor Office (A1) and Indoor Hotspot (B3), respectively [88]. It was assumed that all devices of the network use the same type of antenna: a simple uniform linear array with four dipole elements, with half wave-length distance between adjacent elements.

A fading sample generator script (which is a deliverable of the Winner II project) was used to create the fading files for the MIMO channel. The script was configured to generate channel samples for each possible path between the four transmit antennas and the four receive antennas at every tenth time frame, which for the proposed 5G RAT concept means every 2.5 ms. This time resolution was chosen to reduce file size, taking advantage of the fact that the channel varies slowly in indoor scenarios. Each channel sample is given in the time domain in the form of a power delay profile. The carrier frequency was set to 3.5 GHz and the device speed was assumed to be 3 km/h, even though devices are static, to account for moving objects or people in the indoor spaces.

The time-domain channel samples were converted to the frequency domain, taking the proposed 5G RAT concept as the base model for the frequency-domain signal. The conversion assumed that the FFT size of OFDM transceiver is 4096 and that each subcarrier is 60 kHz wide. The system uses 3300 subcarriers in total, using 198 MHz of the 200 MHz frequency band allocated for the system. The frequency resolution of the file is equal to 900 kHz (15 subcarriers).

B.4 Frequency allocation

Frequency allocation according to static frequency reuse plans was used in the simulations to evaluate the benefits of interference suppression receivers in different inter-cell interference conditions. Three basic plans were used during the project: universal frequency reuse (or simply Reuse 1) and planned frequency reuse with reuse factors equal to 2 and 4 (referred to as Reuse 2 and Reuse 4, respectively). Figures B.4 and B.5 show the frequency allocation plans for Reuse 2 and Reuse 4 cases in the Indoor Office and Indoor Hotspot scenarios, respectively.

(a) Frequency Reuse 2   (b) Frequency Reuse 4
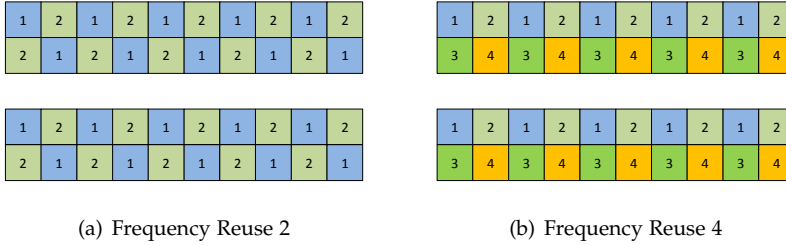
Fig. B.4: Frequency Allocation Plans - Indoor Office Scenario

(a) Frequency Reuse 2   (b) Frequency Reuse 4
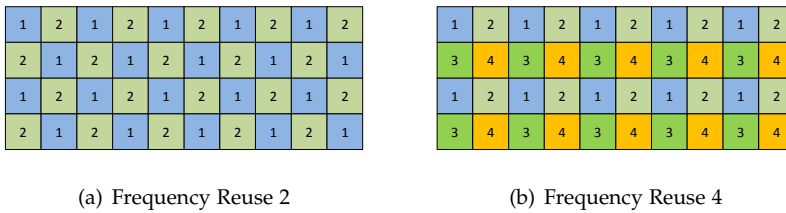
Fig. B.5: Frequency Allocation Plans - Indoor Hotspot Scenario

B.5 Traffic model

Two different traffic models were used in the simulations: a downlink-only full-buffer traffic model, that assumes all APs transmit in all time frames during the simulation period, and a three-state random traffic model, that assumes that the state of each cell may randomly change between DL, UL or idle at every time frame. In the three-state random traffic model, the probability that the state of the cell will change from one state to the other is modelled as a discrete-time Markov process. Figure B.6 shows the schematic for the process.

The three-state random traffic model was included in the simulator to mimic the effect of Dynamic TDD on the inter-cell interference conditions of the network. This model is also used to control the average load of the network by determining the average number of times that a cell will not be in the idle state i.e. there will be either a DL or a UL transmission. This average is hereby referred to as the AF of the network.

Although the three-state random traffic model implemented in the simulator may be used with any transition probability matrix, the simulations regarding this thesis always used transition matrices with identical rows. This setup leads to a three-state Bernoulli scheme in which the probability of transition does not depend on the current state. Therefore, the AF can be

111
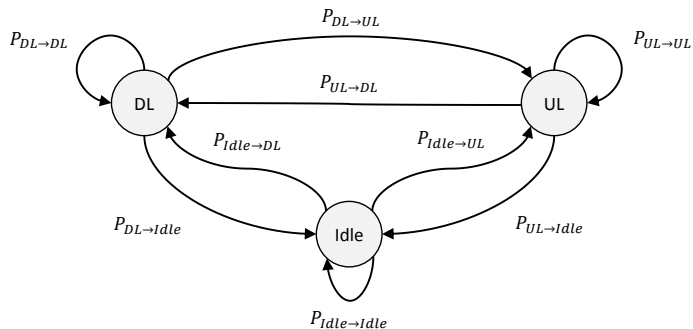
Fig. B.6: Three-state Traffic Model

defined in this cases simply as the probability of not choosing the idle state, i.e. choosing either the DL or the UL states.

B.6 User scheduling model

The user scheduling model implements a simple frequency-domain channel-blind fair-resource scheduler that operates independently in each cell. The scheduler always allocates an equal share of resources for the active users. Moreover, all the resources are always used at every time frame.

B.7 Physical layer model

The physical layer model uses the concept of resource blocks to calculate the instantaneous throughput of each link. Each resource block is defined as 15 subcarriers (900 kHz) for the duration of one time frame (0.25 ms). In this description of the model, the index φ is used to identify the multiple resource blocks of a single time frame.

At every time frame, the SINR of all relevant received signals is calculated using the receiver model described in Appendix A. These SINR values are then adjusted using the EVM model [103] to avoid unrealistically high SINR values.[1] The EVM is a widely accepted model to emulate the expected quality of the communication system devices. Using this model, a EVM value in percentage is used to derive a maximum asymptotic value that the SINR may reach. This value is given by

$$\gamma_{\max} = -20 \log_{10}(\text{EVM}/100) \tag{B.7}$$

[1]The EVM model is only used when the receiver front-end model presented in Appendix A is not used.

The EVM-adjusted SINR value for the j-th stream transmitted by the i-th transmitter at the φ-th resource block is then given by

$$\gamma_{i,j_{\text{EVM}}}(\varphi) = \frac{\gamma_{i,j}(\varphi)\gamma_{\text{max}}}{\gamma_{i,j}(\varphi) + \gamma_{\text{max}}} \tag{B.8}$$

These values are then used to calculate the spectral efficiency of the links. The spectral efficiency for the j-th stream transmitted by the i-th transmitter at the φ-th resource block is then given in bits/s/Hz by

$$\eta_{i,j}(\varphi) = \begin{cases} \eta_{\text{max}} & \text{if } \gamma_{i,j_{\text{EVM}}} \geq \gamma_{\text{max}} \\ \log_2(1 + \gamma_{i,j_{\text{EVM}}}(\varphi)) & \text{if } \gamma_{\text{min}} \leq \gamma_{i,j_{\text{EVM}}} < \gamma_{\text{max}} \\ 0 & \text{if } \gamma_{i,j_{\text{EVM}}} < \gamma_{\text{min}} \end{cases} \tag{B.9}$$

where γ_{min} is the minimum required SINR for decoding any signal and γ_{max} is the maximum SINR given by

$$\gamma_{\text{max}} = 2^{\eta_{\text{max}}} - 1 > \gamma_{\text{min}} \tag{B.10}$$

where η_{max} is the maximum spectral efficiency that the link may reach. The values γ_{min} and η_{max} are derived from the Adaptive Modulation and Coding (AMC) scheme used by the communication system.

The spectral efficiency values are used to calculate the data rate for each individual stream. The data rate for the j-th stream transmitted by the i-th transmitter is calculated using the average spectral efficiency over the multiple allocated resource blocks and is given in bits/s/Hz by

$$R_{i,j} = \frac{Bw}{N_\varphi} \sum_{\varphi=1}^{N_\varphi} \eta_{i,j}(\varphi) \tag{B.11}$$

where Bw is the total allocated bandwidth used by the signal and N_φ is the number of allocated resource blocks. Finally, the instantaneous total data rate for the signals transmitted by the i-th transmitter is given by

$$R_i = \sum_{l=1}^{N_S^i} R_{i,j} \tag{B.12}$$

where N_S^i is the number of data streams transmitted by the i-th transmitter.

B.8 Rank and precoding matrix adaptation model

The aim of the rank and precoding matrix adaptation model is to emulate the effect of the adaptation algorithms that are used to find the ideal rank

and precoding matrices for the transmission of signals. The model implemented in the simulator assumes independent adaptation for each link, i.e. each transmitter-receiver pair tries to choose a matrix to maximize the data rate of their links. In this model, the receiver chooses the best matrix and sends to the transmitter through a feedback channel the index that identifies this matrix in a larger set of matrices. The set of precoding matrices used by the simulator is the LTE codebook for downlink closed-loop Single-User Multiple-Input Multiple-Output (SU-MIMO) transmissions []. This set of precoding matrices is used for both DL and UL transmissions.

The following algorithm describes the rank and precoding adaptation process in the simulation.

1. **Initialization**

    At the first time frame of the snapshot, a random matrix $\mathbf{C}_k \ [N_{tx} \times N_S^k]$ is selected for the k-th transmitter from the set of all Rank 1 matrices. The first time frames of each snapshot are discarded from the collection of results to avoid the transient effect due to this initial setup;

2. **Update channel vectors**

    All equivalent channel vectors $\mathbf{h}_{k,l}$ are updated to account for the selected matrices. This update is performed using the non-precoded channel matrix $\tilde{\mathbf{H}}_k \ [N_{rx} \times N_{tx}]$ that is output by the channel model. The precoded channel matrix $\mathbf{H}_k \ [N_{rx} \times N_S^k]$ is then given by

    $$\mathbf{H}_k = \tilde{\mathbf{H}}_k \mathbf{C}_k \qquad (B.13)$$

    and the precoded equivalent channel vectors $\mathbf{h}_{k,l}$ are the columns of $\mathbf{H}_k$, i.e.

    $$\mathbf{H}_k = \begin{bmatrix} \mathbf{h}_{k,1} & \mathbf{h}_{k,2} & \dots & \mathbf{h}_{k,N_S^k} \end{bmatrix} \qquad (B.14)$$

3. **Search best matrix for each link**

    The search for the best matrix for each link is performed by testing which matrix would have led to the highest throughput assuming all the rest was constant. Therefore, for the search relative to the i-th transmitter, all possible $\mathbf{C}_i$ are tested while $\mathbf{C}_k$ for $k \neq i$ are constant. The $\mathbf{C}_i$ matrix that leads to the highest throughput is selected for transmission at the next time frame;

4. **Repeat steps 2 and 3 per each frame until the end of the snapshot**

In the case that the MRP technique [59] is used, the algorithm is modified to limit the set of rank and precoding matrices that may be used by each link, whereas in the case of TRA [61], the algorithm is uses the taxation metric to decide which matrix to use.

Part III

Papers

Paper A

On the Potential of Interference Rejection Combining
in B4G Networks

Fernando M. L. Tavares, Gilberto Berardinelli, Nurul H.
Mahmood, Troels B. Sørensen, and Preben Mogensen

Abstract

Beyond 4th Generation (B4G) local area networks will be characterized by the dense uncoordinated deployment of small cells. This paper shows that inter-cell interference, which is a main limiting factor in such networks, can be effectively contained using Interference Rejection Combining (IRC) receivers. By simulation we investigate two significantly different interference scenarios with dense small cell deployment. The results show that IRC brings considerable improvement in outage as well as in peak and median throughputs in both scenarios, and thus has a big potential as a capacity and coverage enhancing technique for B4G. The IRC gain mechanism depends strongly on the interference scenario and to some extent on the use of frequency reuse. These results are achieved with no coordination among cells and suggests that Multiple Input Multiple Output (MIMO) rank adaptation and IRC can be performed independently.

I. Introduction

In the last decades, several generations of Radio Access Networks (RANs) have been designed to cope with the growing demand for wireless services. A new disruptive system has emerged approximately every 10 years to alleviate backward compatibility problems and to take advantage of the evolution of the technology components. Considering that the specifications of the Long Term Evolution - Advanced (LTE-A) radio standard were submitted in 2010, a novel Beyond 4th Generation (B4G) RAN is then expected to emerge in the market around 2020 [1].

This new RAN should be designed to support the massive deployment of small cells, since this type of deployment is foreseen as a solution for meeting the future capacity expansion requirements [1]. As deployments become denser, their uncoordinated nature will inevitably aggravate the inter-cell interference problem, causing considerable impact on the network performance. The allocation of orthogonal spectrum resources to cells that strongly interfere with each other is often considered as the solution for this problem [2, 3].

With the evolution of electronic hardware and Multiple-Input Multiple-Output (MIMO) techniques, inter-cell interference suppression techniques, whose application was previously limited by their large computational burden, may now be cost-effectively implemented in receivers. It is reasonable to believe that this kind of receivers can offer high performance gains in interference limited scenarios, but, to the best of our knowledge, all the system level performance evaluation studies on the topic focus on macro cell and heterogeneous Long Term Evolution (LTE) and LTE-A network scenarios [4, 5, 6, 7].

Different baseband processing techniques may be used to suppress the inter-cell interference. For instance, Successive Interference Cancellation (SIC) and Parallel Interference Cancellation (PIC) techniques decode both the desired and the interfering signal to cancel their mutual interference contribution [8]. Conversely, Interference Rejection Combining (IRC) is a linear combining technique that relies on multiple receive antennas and the estimate of the interfering channels to project the received signals on a subspace in which the Mean Square Error (MSE) is minimized [9]. IRC is attractive given its simplicity and maturity, and it represents a straightforward add-on to the known Minimum Mean Square Error (MMSE) detector, which is now considered the baseline detector in LTE networks [10].

In this paper, we present the first system level downlink performance evaluation of inter-cell interference suppression for different local area small cell B4G scenarios. Specifically, we consider scenarios with dense small cell deployment and two modes of operation: one with closed subscriber mode of relevance for office buildings (or private apartments) and one with open subscriber mode of relevance for public hot spots. We use a signal model that includes spatial multiplexing precoding with multiple data layers (both for the desired and the interfering signals) to verify their effects on the interference rejection capabilities of IRC and contrast it with the use of different frequency reuse schemes. Our ultimate goal is to address the effective potential of this detector on the performance of B4G networks, providing information that will help guide the design of this new RAN.

The paper is organized as follows. We first describe the signal model used in the simulations in Section II and the details related to the simulation setup in Section III; we present and analyse the simulation results in Section IV; finally, we draw our conclusions in Section V.

II. Signal Model

In this section, we present the analytical signal model of the detectors that are used in our system evaluation.

We assume that the generic i-th network node is equipped with N_{tx} transmit antennas and N_{rx} receive antennas, and can transmit $1 \leq N_{streams_i} \leq min(N_{rx}, N_{tx})$ data streams. The number of transmitted streams is also often referred as transmission *rank*. For simplicity, we present the system model for a generic Orthogonal Frequency Division Multiplexing (OFDM) frequency subcarrier.

Let us denote with $\mathbf{s}_i$ the $N_{streams_i} \times 1$ data column vector of the i-th node. The vector $\mathbf{s}_i$ is mapped over the N_{tx} antennas by the $N_{tx} \times N_{streams_i}$ precoding matrix $\mathbf{C}_i$. Let us assume that the subscript D denotes the desired signal at the receiver side, and the subscript I_q the q-th interfering signal. After

transmission over the fading channel, the $N_{rx} \times 1$ frequency domain received column vector at a particular receiver can then be expressed as

$$\mathbf{r} = \tilde{\mathbf{H}}_D \mathbf{s}_D + \tilde{\mathbf{H}}_I \mathbf{s}_I + \mathbf{n} \tag{A.1}$$

where

- $\mathbf{n}$ is the $N_{rx} \times 1$ Additive White Gaussian Noise (AWGN) contribution vector with power σ_0^2;

- $\tilde{\mathbf{H}}_D$ and $\tilde{\mathbf{H}}_{I_q}$ are the equivalent channel matrices which include the precoding matrices, i.e. $\tilde{\mathbf{H}}_D = \mathbf{H}_D \mathbf{C}_D$ and $\tilde{\mathbf{H}}_{I_q} = \mathbf{H}_{I_q} \mathbf{C}_{I_q}$, with $\mathbf{H}_D$ and $\mathbf{H}_{I_q}$ being the $N_{rx} \times N_{tx}$ fading channel matrices;

- $\mathbf{s}_I$ and $\tilde{\mathbf{H}}_I$ represent the concatenation of the N_I received interfering signals and the concatenation of their equivalent N_I channels, respectively, i.e.

$$\mathbf{s}_I = [\mathbf{s}_{I_1}^T \ldots \mathbf{s}_{I_q}^T \ldots \mathbf{s}_{I_{N_I}}^T]^T \tag{A.2}$$

$$\tilde{\mathbf{H}}_I = [\tilde{\mathbf{H}}_{I_1} \ldots \tilde{\mathbf{H}}_{I_q} \ldots \tilde{\mathbf{H}}_{I_{N_I}}] \tag{A.3}$$

where $(\cdot)^T$ denotes the transpose operator.

Let us also define the generic MMSE combining matrix [11]:

$$\mathbf{W} = (\hat{\mathbf{H}}_D \hat{\mathbf{H}}_D^H + \mathbf{R}_n)^{-1} \hat{\mathbf{H}}_D \tag{A.4}$$

where $(\cdot)^H$ is the hermitian operator and $\hat{\mathbf{H}}_D$ represents the estimated equivalent channel matrix of the desired signal.

The desired $\hat{\mathbf{s}}_D$ is then estimated by using the combining matrix $\mathbf{W}$:

$$\hat{\mathbf{s}}_D = \mathbf{W}^H \mathbf{r} \tag{A.5}$$

The following detectors can be specified according to the nature of the matrix $\mathbf{R}_n$:

- *MMSE - Interference Rejection Combining (MMSE-IRC):*

$$\mathbf{R}_n = E\{\hat{\mathbf{H}}_I \hat{\mathbf{H}}_I^H\} + \sigma_0^2 \mathbf{I}_{\mathbf{N_{rx}}} \tag{A.6}$$

where $\mathbf{I}_{\mathbf{N_{rx}}}$ denotes the $N_{rx} \times N_{rx}$ identity matrix.

- *MMSE - Maximal Ratio Combining (MMSE-MRC):*

$$\mathbf{R}_n = \text{diag}([m_1 \cdots m_{N_{rx}}]) \tag{A.7}$$

where

$$m_z = E\Big\{\sum_{q=1}^{N_I} \sum_{k=1}^{N_{streamsq}} \Big|\hat{\mathbf{H}}_{I_{q(z,k)}}\Big|^2\Big\} + \sigma_0^2 \tag{A.8}$$

with $\hat{\mathbf{H}}_{I_{q(z,k)}}$ corresponding to the element in the z-th row and the k-th column of $\hat{\mathbf{H}}_{I_q}$.

While in the MMSE-MRC detector the matrix $\mathbf{R}_n$ can be computed by estimating the total interference plus noise power at each receive antenna, $\mathbf{R}_n$ in the MMSE-IRC detector corresponds to the estimated covariance matrix of the interfering signals. Therefore, MMSE-IRC assumes knowledge of each interfering channel at each antenna which may impose strict requirements on the system design since each node would need to discriminate the reference sequences sent by multiple interferers. We assume here that such a system design is possible, and consider it to be a topic for future work.

III. Simulation Setup

As mentioned in the introduction, the usage of IRC detectors is foreseen as particularly beneficial in scenarios characterized by a dense uncoordinated deployment of small cells. This paper aims at addressing such potential with an extensive system level evaluation. In this section, we describe in details the physical layer assumptions, scenarios and simulation setup used in our simulation campaign.

A. Physical Layer Assumptions

We assume ideal channel estimation of both desired and interfering signals based on the aforementioned reference sequences. Rank and precoding adaptation feedback with no errors and one frame delay is assumed. The precoding matrices used are those defined in [12] for downlink closed-loop single-user MIMO in LTE, and are applied per Physical Resource Block (PRB) in frequency domain for the assumed OFDM based system [1].

We calculate the Signal-to-Interference-plus-Noise Ratio (SINR) for the j-th stream as follows [11]:

$$\text{SINR}_j = \frac{\mathbf{W}_{(j)}^H \mathbf{H}_{D_{(j)}} \mathbf{H}_{D_{(j)}}^H \mathbf{W}_{(j)}}{\mathbf{W}_{(j)}^H (\bar{\mathbf{H}}_{D_{(j)}} \bar{\mathbf{H}}_{D_{(j)}}^H + \mathbf{H}_I \mathbf{H}_I^H + \sigma_0^2 \mathbf{I}_{\mathbf{N_{rx}}}) \mathbf{W}_{(j)}} \tag{A.9}$$

where $\mathbf{A}_{(j)}$ denotes the j-th column of matrix $\mathbf{A}$ and $\bar{\mathbf{A}}_{(j)}$ is the matrix obtained by removing the j-th column from matrix $\mathbf{A}$.

The SINR values are then adjusted using the following Error Vector Magnitude (EVM) model to account for transceiver implementation imperfections.

$$\text{SINR}_{\text{evm},j} = \frac{\text{SINR}_j \cdot \text{SINR}_{\text{max}}}{\text{SINR}_j + \text{SINR}_{\text{max}}} \tag{A.10}$$

Based on the resulting SINR we calculate the corresponding data rate using the Shannon formula, with maximum spectral efficiency limited to 6 bits/s/Hz (uncoded 64QAM modulation). All streams are added, resulting in the total data rate per User Equipment (UE). Table A.1 summarizes these physical layer details.

Table A.1: Physical Layer Assumptions

Physical Layer Model [1]		
Spectrum Allocation	200 MHz at 3.5 GHz	
Frame Duration	0.25 ms	
Access Scheme	Downlink OFDMA	
	3000 subcarrriers	60 kHz each
	15 subcarriers per PRB	
Transmission Power	20 dBm	
Receiver Noise Figure	9 dB	
MIMO Scheme	Closed-loop SU-MIMO with	
	dynamic rank and precoder adaptation	
Spectral Efficiency Model		
Maximum Spectral Efficiency	6 bits/s/Hz	64 QAM (1/1)
Error Vector Magnitude	5%	$\text{SINR}_{\text{max}} \approx 26\text{dB}$

B. Simulation Scenarios

Two simulation scenarios were selected for this study. Scenario A is an indoor office scenario used for the study of femtocells [13]. This scenario is depicted in Figure A.1(a). It consists of two office buildings, each located at one side of a 10 meter wide street. Each building is modelled as two rows of 10 square offices. For simplicity, only one floor was simulated with one UE and one Access Point (AP) randomly placed in each office. Each office may have one

active cell under Closed Subscriber Group (CSG) access mode, i.e. the UE can only connect to the AP in the same office and not to any of the neighbour's APs. Large scale propagation effects (pathloss and shadowing) are calculated using the 3GPP Dual Stripe model [13].

(a) Scenario A - Indoor Office   (b) Scenario B - Indoor Hotspot
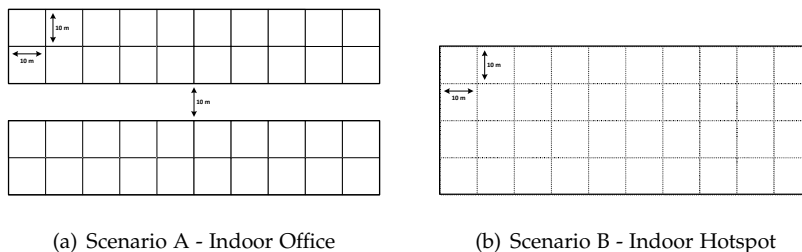
Fig. A.1: Simulation Scenarios

Figure A.1(b) depicts Scenario B. This scenario simulates an indoor hotspot scenario, similar to an airport check-in hall or a large conference hall, for example. The total area of the hall is divided in square areas and one AP is installed in the center of each of them, summing up 40 APs. In this scenario, the user may connect to any of the available APs, i.e. the network operates in Open Subscriber Group (OSG) access mode. One UE is randomly placed in each square area and each UE selects which AP to connect to based on the highest received power. In case an AP does not serve any UE, it is switched off. In this scenario, pathloss and shadowing are calculated according to the WINNER II Indoor Hotspot (B3) channel model [14].

Small scale fading samples used in the simulation were computed using the WINNER II channel model (Indoor Office (A1) for Scenario A and the Indoor Hotspot (B3) for Scenario B) [14]. We assume uniform linear antenna arrays with four elements separated by $\lambda/2$ in both APs and UEs. In both scenarios, we assume 3 Km/h mobility that may be due to device mobility or other objects moving in the same area causing the channel to change. Table A.2 presents further details on the simulation scenarios.

C. Simulation Results

The network downlink performance was evaluated using a quasi-static system level simulator. The statistical reliability of the simulations is ensured by collecting results from 500 snapshots. Each snapshot evaluates a time span of 50 frames in which the fast fading channel values are updated every frame, but pathloss and shadowing remain constant. An Empirical Cumulative Distribution Function (ECDF) is then calculated using the throughput of all cells in all snapshots. Three key performance indicators (KPIs) were

Table A.2: Simulation Setup

Scenario A - Indoor Office		
Access Mode	Closed Subscriber Group (CSG)	
Data Generation	Full Buffer Traffic	
Path Loss	3GPP Dual Stripe Model	
	45 dB Minimum Coupling Loss	
Wall Loss	Internal Walls	5 dB attenuation
	External Walls	10 dB attenuation
Shadowing Std. Deviation	Serving Cell	6 dB
	Other Cells	8 dB
Fast Fading	WINNER II CDL Model	
	Indoor Office (A1) - 3 Km/h	
Antenna Configuration	Uniform Linear Array (ULA)	
	4 antenna elements (0.5λ spacing)	
Scenario B - Indoor Hotspot		
Access Mode	Open Subscriber Group (OSG)	
Data Generation	Full Buffer Traffic	
Path Loss	WINNER II Indoor Hotspot (B3) Model	
	70 dB Minimum Coupling Loss	
Shadowing Std. Deviation	Line of Sight	3 dB
	Non Line of Sight	4 dB
Fast Fading	WINNER II CDL Model	
	Indoor Hotspot (B3) - 3 Km/h	
Antenna Configuration	Uniform Linear Array (ULA)	
	4 antenna elements (0.5λ spacing)	

extracted from the ECDFs, namely peak (95%-tile), median (50%-tile) and outage (5%-tile) data rates.

In both network scenarios, we simulate different frequency reuse schemes by splitting the total bandwidth and assigning only part of the Physical Resource Blocks (PRBs) to each cell. We simulate the scenarios with Reuse 1 (R1), Reuse 2 (R2) and Reuse 4 (R4). In the case of R1, all PRBs are used by all cells, but in the case of R2 and R4, each cell will use only a half and a quarter of all PRBs, respectively. In these two cases, the frequency allocation follows a geometrical pattern that maximizes the distance between two cells using the same set of PRBs.

IV. Performance Evaluation

In this section, we present the numerical simulation results using different combinations of receiver type and planned frequency reuse schemes. First, we discuss the results for Scenario A. Figure A.2(a) displays the network throughput performance assuming MMSE-MRC and MMSE-IRC detectors, for different frequency reuse patterns, while Table A.3 presents the KPIs and the relative gains of MMSE-IRC over MMSE-MRC for all Scenario A simulation cases. The MMSE-IRC detector shows considerable gain in terms of outage data rate with respect to MMSE-MRC when R1 is adopted. Such improvement diminishes with higher reuse factors, due to the lower total interference to be rejected. However, the relative data rate gains that MMSE-IRC provides over MMSE-MRC are very large, with improvements of 267.5%, 82.2% and 28.3% in R1, R2 and R4 cases, respectively.

The large data rate gain of MMSE-IRC in scenario A is due to its capability of rejecting the strongest interfering signals. The particular setup with multiple walls and CSG access mode (i.e., the signal from the serving AP may be weaker than the interferer signals) reduces the overall interference power at the UE and let the most significant interference components be suppressed.

The results also suggest that the negative effects due to multi-stream inter-cell interference on the performance of MMSE-IRC are limited. IRC provides significant outage data rate improvement despite the fact that many cells consistently use spatial multiplexing to transmit multiple data stream to reach higher data rates in this scenario.

Figure A.2(b) shows the performance results of both detectors for Scenario B, which represents a different interference situation. As the results in Table A.4 show, the use of MMSE-IRC improves the outage data rates by 25.0%, 33.5% and 51.0% for the R1, R2 and R4 cases, respectively. Notice that the outage data rate gains actually improve as higher reuse factors are used. In this scenario, the OSG access mode reduces the probability of very strong interference, but on the other hand there are no walls to attenuate the inter-
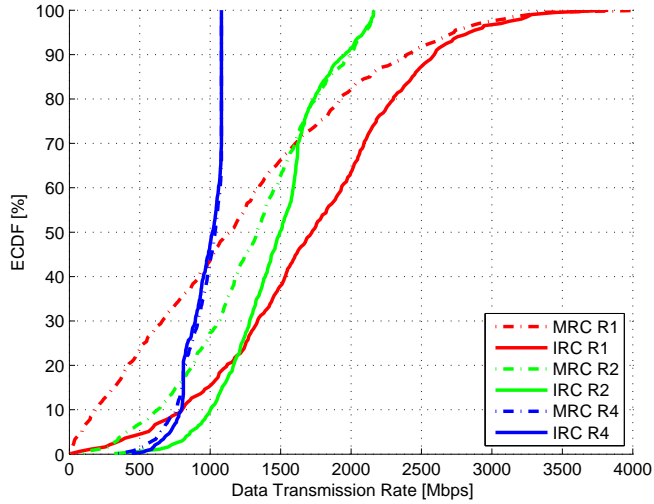
(a) Scenario A - Indoor Office
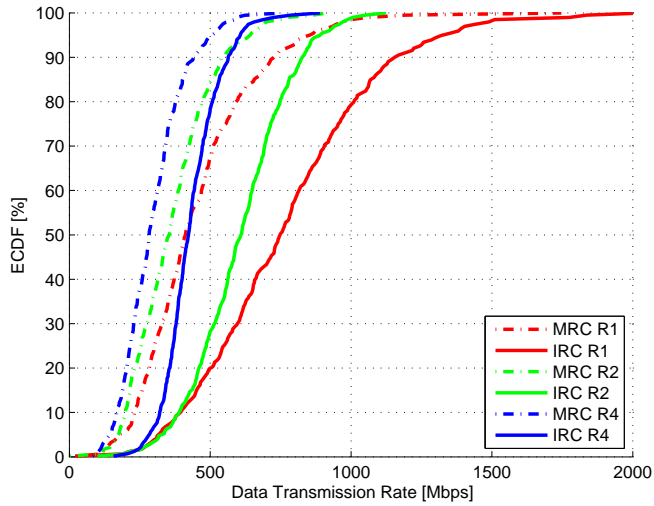
(b) Scenario B - Indoor Hotspot

Fig. A.2: ECDFs showing the data transmission rates in Mbps for both detector types (MMSE-MRC and MMSE-IRC) and different frequency reuse schemes.

Table A.3: Data Rates - Scenario A [Mbps]

Outage	MMSE-MRC	MMSE-IRC	*Gains*
R1	91.8	337.4	(+267.5%)
R2	314.7	573.6	(+82.2%)
R4	543.4	697.1	(+28.3%)
Median	MMSE-MRC	MMSE-IRC	*Gains*
R1	837.5	1261.2	(+50.6%)
R2	1178.4	1402.4	(+19.0%)
R4	1026.0	1029.6	(+0.3%)
Peak	MMSE-MRC	MMSE-IRC	*Gains*
R1	2576.7	2804.2	(+8.8%)
R2	2058.3	2065.1	(+0.3%)
R4	1080.0	1080.0	-

ference generated by the multiple cells that transmit in the same hall. These conditions lead to a situation in which the interference is actually spatially whiter than in Scenario A. As the reuse factor increases, the number of interferers is reduced and the interference becomes less white, i.e. the received signal is dominated by a few strong interferers, and this is the situation in which interference rejection works better.

Furthermore, all cells experience considerable throughput gains, as opposed to Scenario A where the cells in the worst conditions (i.e., lower part of the ECDF) benefit much more than the others. The median data rates are improved by 23.5%, 25.6% and 36.6% and the peak data rates are improved by 23.3%, 23.6% and 29.8% for R1, R2 and R4 cases, respectively. In this scenario, the cells in the top half of the ECDF also experience high interference levels, limiting the throughput to about half of the maximum link capacity. MMSE-IRC rejects more interference in this situation than in the case of the cells in the top half of the ECDFs in Scenario A. However, the median and peak data rate gains are actually reduced as higher reuse factor schemes are used and the overall interference level is reduced.

The results also show that, if higher reuse factors are used in an attempt to reduce the interference levels in Scenario B, the throughputs are actually reduced, because the improvement in SINR is not sufficient to compensate for the reduction in the available bandwidth per cell. Thus, a technique that

Table A.4: Data Rates - Scenario B [Mbps]

Outage	MMSE-MRC	MMSE-IRC	Gains
R1	113.7	142.1	(+25.0%)
R2	104.7	139.8	(+33.5%)
R4	87.4	131.9	(+51.0%)
Median	MMSE-MRC	MMSE-IRC	Gains
R1	233.1	287.9	(+23.5%)
R2	201.7	253.3	(+25.6%)
R4	162.8	222.4	(+36.6%)
Peak	MMSE-MRC	MMSE-IRC	Gains
R1	435.4	536.6	(+23.3%)
R2	346.3	428.0	(+23.6%)
R4	272.3	353.3	(+29.8%)

is capable of reducing the interference levels without limiting the bandwidth is particularly interesting in this scenario.

V.   Conclusion

In this paper, we discussed the potential benefits of IRC as a baseline detector for Beyond 4G small cell networks, where inter-cell interference is identified as the main limiting factor for the throughput performance. Performance results in indoor office and indoor hotspot scenarios have shown the effectiveness of the MMSE-IRC receiver in improving the network throughput with respect to baseline MMSE-MRC detector. The gains are observed even when frequency reuse is used to combat the high interference levels, suggesting that both techniques may be used together to improve the network performance. Also, MIMO rank coordination among neighbour cells does not seem to be required to reach very good results, although it may provide additional gains over those presented in this paper.

The results confirm that the benefits of IRC are large enough to substantiate further studies that will evaluate its performance in situations that are closer to reality, including the effects of channel and interference covariance matrix estimation errors and limitations. Further studies will also address the design of a B4G frame structure that provides the support for IRC to per-

form consistently, including the adequate design of reference symbols and the necessary means to stabilize the interference during the transmission of a frame.

References

[1] Preben Mogensen, Kari Pajukoski, Bernhard Raaf, Esa Tiirola, Eeva Lähetkangas, Istvan Z. Kovács, Gilberto Berardinelli, Luis G. Uzeda Garcia, Liang Hu, and Andrea F. Cattoni. "B4G local area: High level requirements and system design". In: *Globecom Workshops (GC Wkshps), 2012 IEEE*. Dec. 2012, pp. 613–617. DOI: 10.1109/GLOCOMW.2012.6477644.

[2] G. Boudreau, J. Panicker, Ning Guo, Rui Chang, Neng Wang, and S. Vrzic. "Interference coordination and cancellation for 4G networks". In: *Communications Magazine, IEEE* 47.4 (Apr. 2009), pp. 74–81. ISSN: 0163-6804. DOI: 10.1109/MCOM.2009.4907410.

[3] V. Chandrasekhar, J. Andrews, and A. Gatherer. "Femtocell networks: a survey". In: *Communications Magazine, IEEE* 46.9 (Sept. 2008), pp. 59–67. ISSN: 0163-6804. DOI: 10.1109/MCOM.2008.4623708.

[4] M. Lampinen, F. Del Carpio, T. Kuosmanen, T. Koivisto, and M. Enescu. "System-Level Modeling and Evaluation of Interference Suppression Receivers in LTE System". In: *Vehicular Technology Conference (VTC Spring), 2012 IEEE 75th*. May 2012, pp. 1–5. DOI: 10.1109/VETECS.2012.6239964.

[5] K. Pietikainen, F. Del Carpio, H. Maattanen, M. Lampinen, T. Koivisto, and M. Enescu. "System-Level Performance of Interference Suppression Receivers in LTE System". In: *Vehicular Technology Conference (VTC Spring), 2012 IEEE 75th*. May 2012, pp. 1–5. DOI: 10.1109/VETECS.2012.6239969.

[6] Y. Ohwatari, N. Miki, T. Abe, and H. Taoka. "Investigation on Advanced Receiver Employing Interference Rejection Combining in Asynchronous Network for LTE-Advanced Downlink". In: *Vehicular Technology Conference (VTC Spring), 2012 IEEE 75th*. May 2012, pp. 1–6. DOI: 10.1109/VETECS.2012.6240127.

[7] Yousuke Sano, Yusuke Ohwatari, Nobuhiko Miki, Akihito Morimoto, and Yukihiko Okumura. "Investigation on link performance modeling of advanced receiver employing interference rejection combining in system level evaluation for LTE-Advanced downlink". In: *2012 International Symposium on Wireless Communication Systems (ISWCS)*. Aug. 2012, pp. 919–923. DOI: 10.1109/ISWCS.2012.6328502.

[8]   S. Haykin, M. Sellathurai, Y. de Jong, and T. Willink. "Turbo-MIMO for wireless communications". In: *Communications Magazine, IEEE* 42.10 (Oct. 2004), pp. 48–53. ISSN: 0163-6804. DOI: 10 . 1109 / MCOM . 2004 . 1341260.

[9]   J. Winters. "Optimum Combining in Digital Mobile Radio with Cochannel Interference". In: *Selected Areas in Communications, IEEE Journal on* 2.4 (July 1984), pp. 528–539. ISSN: 0733-8716. DOI: 10.1109/JSAC.1984. 1146095.

[10] 3GPP TR 36.829. *Enhanced performance requirement for LTE User Equipment (UE)*. v11.1.0. Jan. 2013. URL: http://www.3gpp.org.

[11] Jinho Choi. *Optimal Combining and Detection: Statistical Signal Processing for Communications*. Cambridge: Cambridge University Press, 2010.

[12] 3GPP TS 36.211. *Evolved Universal Terrestrial Radio Access (E-UTRA); Physical channels and modulation*. v11.1.0. Dec. 2012. URL: http://www. 3gpp.org.

[13] 3GPP TR 36.814. *Evolved Universal Terrestrial Radio Access (E-UTRA); Further advancements for E-UTRA physical layer aspects*. v9.0.0. Mar. 2010. URL: http://www.3gpp.org.

[14] P. Kyösti et al. *WINNER II Channel Models*. D1.1.2 v1.1. IST-WINNER, Sept. 2007. URL: https://www.ist-winner.org/WINNER2-Deliverables/ D1.1.2v1.1.pdf.

Paper B

On the impact of receiver imperfections on the MMSE-IRC receiver performance in 5G networks

Fernando M. L. Tavares, Gilberto Berardinelli, Nurul H. Mahmood, Troels B. Sørensen, and Preben Mogensen

Abstract

The usage of Minimum Mean Square Error – Interference Rejection Combining (MMSE-IRC) receivers is expected to be a significant performance booster in the ultra-dense deployment of small cells envisioned by an upcoming 5th generation (5G) Radio Access Technology (RAT). However, hardware limitations of the radio-frequency front-end and poor covariance matrix estimation may severely compromise its ideal gains. In this paper, we evaluate the network performance of MMSE-IRC receivers by including the effects of the receiver imperfections as well as realistic co-variance matrix estimates. System level simulation results confirm that a realistic MMSE-IRC receiver can achieve throughput gains close to ideal, provided a rea-sonably high resolution Analog-to-Digital Converter (ADC) as well as a supportive radio frame format design are used.

I. Introduction

The growing demand for wireless communications services is the main driver for the design of a novel 5th Generation (5G) Radio Access Technology (RAT). This novel system is expected to operate in ultra-dense small cell network scenarios, providing Gbps data rates with very low latency [1].

5G networks will employ different techniques for mitigating the inter-cell interference, which is considered the main performance limiting factor in such dense scenarios. One very promising technique is the use of ad-vanced receivers capable of suppressing interference, such as the Minimum Mean Square Error – Interference Rejection Combining (MMSE-IRC) receiver. This receiver has the potential to significantly improve the 5G network per-formance, as was demonstrated in [2], but its performance depends on the accuracy of the channel response and the received signal covariance matrix estimates, as shown in [3, 4, 5] for Long Term Evolution (LTE) networks. The estimation accuracy is affected by the quality of the receiver components, as well as on the radio frame format used by the network.

In this paper, we study the performance of the MMSE-IRC receiver in 5G local area networks using system level simulations that model in detail the effects of receiver imperfections and the effects of channel response and covariance matrix estimation errors. Our aim is to address the potential of the MMSE-IRC receiver in realistic conditions in order to justify its natural inclusion in the 5G design.

This paper is organized as follows. Section II describes how the radio frame format may affect the performance of the MMSE-IRC receiver. We present the receiver model used in the simulations in Section III and we describe the simulation setup in Section IV. In Section V, we present and discuss the simulation results. Section VI closes the paper with conclusions

and future work.

II. Radio Frame Format

The design for a new 5G radio frame format was proposed in [6]. This new design was driven by two main requirements. The frame format must provide the means for accurate channel response and covariance matrix estimation, enabling the possibility of achieving high IRC gains. Further, very low latency is required, suggesting the design of a radio frame format with very short Transmit Time Interval (TTI) and flexible Uplink (UL) and Downlink (DL) resource allocation. Using this flexibility, each AP may decide the transmission direction at each TTI, reducing the Round Trip Time (RTT). However, such increased flexibility leads to network scenarios with rapidly varying interference sources, which may impact the accuracy of the covariance matrix estimation.

In design proposed in [6], a very short TTI duration (0.25 ms) is used to meet the latency requirement. To meet the other requirement, the same frame format is used for UL and DL, and the transmission direction is set to be constant within the TTI. Thus, provided all the transmitting devices (both APs and UEs) are synchronized, the interference is stabilized for the duration of a TTI. By assuming that all APs and UEs which are transmitting simultaneously use orthogonal reference sequences, an accurate covariance matrix estimation method can be applied.

Even though this frame format provides inbuilt support for the MMSE-IRC receiver, the short TTI size limits the number of samples that may be used in practical covariance matrix estimation methods, resulting in estimation errors. Also, the potentially very different power levels observed in each TTI due to varying interference sources may degrade the radio frequency (RF) front-end performance due to dynamic range limitations. Therefore, our aim is to evaluate the performance degradation caused by these imperfections, using a signal model that includes the effects of estimation errors and RF front-end imperfections. We present this model in the next section.

III. Signal Model

Let us consider a network composed by devices with N_{tx} transmit and N_{rx} receive antennas each. All devices are time aligned and transmit MIMO OFDM signals. The received baseband signal column vector $\mathbf{r}$ with dimension $[N_{rx} \times 1]$ at a generic device is then given by

$$\mathbf{r} = \sum_{k=1}^{N_T} \sum_{l=1}^{N_S^k} \mathbf{h}_{k,l} s_{k,l} + \mathbf{n} \tag{B.1}$$

where N_T is the number of transmitters and N_S^k is the number of data streams transmitted by the k-th device (also denoted as its rank), which is limited by $min(N_{rx}, N_{tx})$. The scalar $s_{k,l}$ represents the l-th symbol transmitted by the k-th transmitter through the equivalent complex channel represented by the vector $\mathbf{h}_{k,l}$ $[N_{rx} \times 1]$. The vector $\mathbf{n}$ $[N_{rx} \times 1]$ represents the additive noise. Note that this equation holds for a generic subcarrier in a generic OFDM symbol, whose indexes are omitted for the sake of simplicity.

We assume that the transmitted symbols $s_{k,l}$ have unit power, which holds for typical symbol constellations, and that there is no correlation between the multiple symbols sent by all the transmitters. We also assume that the channel response is constant for the duration of a TTI and that the equivalent channel vectors include the effect of the transmit power amplification, large scale and small scale propagation effects, and the $[N_{tx} \times N_S^k]$ precoding matrix at the transmitter.

A. Received Signal Combining

An estimate of the j-th signal sent by the i-th transmitter can be obtained by applying the combining vector $\mathbf{w}_{i,j}$ $[N_{rx} \times 1]$.

$$\hat{s}_{i,j} = \mathbf{w}_{i,j}^H \mathbf{r} \tag{B.2}$$

Using the MMSE criterion to maximize the SINR [7], the combining vector $\mathbf{w}_{i,j}$ is given by

$$\mathbf{w}_{i,j} = \mathbf{R}_r^{-1} \mathbf{h}_{i,j} \tag{B.3}$$

where $\mathbf{h}_{i,j}$ is the equivalent channel vector relative to the j-th symbol transmitted by the i-th transmitter and $\mathbf{R}_r$ $[N_{rx} \times N_{rx}]$ is the covariance matrix of the received signal vector $\mathbf{r}$, defined as

$$\mathbf{R}_r = \mathbb{E}\{\mathbf{r}\mathbf{r}^H\} \tag{B.4}$$

where $\mathbb{E}\{\cdot\}$ denotes the expectation operator.

B. Covariance Matrix Estimation

Ideally, if an infinite number of samples were available, the received signal covariance matrix would be given by

$$\mathbf{R}_r = \sum_{k=1}^{N_T} \sum_{l=1}^{N_S^k} \mathbf{h}_{k,l} \mathbf{h}_{k,l}^H + \mathbf{R}_n \tag{B.5}$$

where $\mathbf{R}_n$ is the covariance of the additive noise vector $\mathbf{n}$. However, in practice the estimation process is prone to errors due to the limited number of

data symbols. In this paper, we consider two covariance matrix estimation approaches for the MMSE-IRC receiver: Data Symbol Based (DSB) and Reference Symbol Based (RSB) [3].

The DSB method is a direct estimation of the covariance matrix using a finite number of data symbols $s_{k,l}$ as samples. As suggested in [3], we model the DSB covariance matrix with estimation errors as a random matrix sample drawn from the Wishart distribution $\mathcal{W}$ with covariance matrix $\mathbf{R}_r$ and Q_{DSB} degrees of freedom. The number of degrees of freedom is given by the number of resource elements (OFDM subcarriers) per frame designated for data transmission in the frame format.

$$\hat{\mathbf{R}}_r \sim \frac{1}{Q_{DSB}} \mathcal{W}(\mathbf{R_r}, Q_{DSB}) \tag{B.6}$$

The RSB method estimates the covariance matrix using only the reference symbols. This method uses an estimate of the equivalent channel $\mathbf{h}_{i,j}$, obtained from such reference symbols, to indirectly calculate the contribution of the desired signal to the covariance matrix. Thus, the RSB covariance matrix estimate is

$$\hat{\mathbf{R}}_r = \sum_{l=1}^{N_S^i} \hat{\mathbf{h}}_{i,l} \hat{\mathbf{h}}_{i,l}^H + \hat{\mathbf{R}}_{z+n} \tag{B.7}$$

where $\hat{\mathbf{h}}_{i,l}$ are the estimates of $\mathbf{h}_{i,l}$ and $\hat{\mathbf{R}}_{z+n}$ the estimate of the matrix $\mathbf{R}_{z+n}$, which represents the contribution of the interference and the noise to the total covariance matrix. The matrix $\mathbf{R}_{z+n}$ can be expressed as

$$\mathbf{R}_{z+n} = \sum_{\substack{k=1 \\ k \neq i}}^{N_T} \sum_{l=1}^{N_S^k} \mathbf{h}_{k,l} \mathbf{h}_{k,l}^H + \mathbf{R}_n \tag{B.8}$$

where the first term is the covariance of the inter-cell interference and the last is the covariance of the additive noise. Since in practice the number of samples for the estimation of $\mathbf{R}_{z+n}$ is also limited, we also model $\hat{\mathbf{R}}_{z+n}$ as a random matrix drawn from a Wishart distribution. In this case, the distribution has covariance $\mathbf{R}_{z+n}$ and Q_{RSB} degrees of freedom, which corresponds to the number of resource elements per frame designated for reference symbol transmission.

$$\hat{\mathbf{R}}_{z+n} \sim \frac{1}{Q_{RSB}} \mathcal{W}(\mathbf{R}_{z+n}, Q_{RSB}) \tag{B.9}$$

We also use the Minimum Mean Square Error – Maximum Ratio Combining (MMSE-MRC) receiver as a baseline receiver in our simulations. The MMSE-MRC receiver assumes no correlation between the signals received on different antennas, leading to the assumption of a diagonal covariance matrix. In this case, the m-th diagonal elements (for the m-th receive antenna)

are given by

$$\sigma_m^2 = \sum_{k=1}^{N_T} \sum_{l=1}^{N_S^k} h_{k,l,m} h_{k,l,m}^* + \sigma_{n_m}^2 \qquad \text{(B.10)}$$

where $h_{k,l,m}$ is the m-th antenna equivalent channel component from vector $\mathbf{h}_{k,l}$ and $\sigma_{n_m}^2$ is the additive noise power at the m-th antenna. Models for both DSB and RSB methods may be derived using the same rationale used for the MMSE-IRC receiver but using in this case a Chi-squared distribution to model the covariance matrix estimation errors [8].

C. Channel Response Estimation Error

Assuming that perfectly orthogonal sequences are used as reference signals, the equivalent channel response estimation error depends only on the noise received on each antenna. The scalar $\hat{h}_{i,j,m}$ is the estimate of the equivalent channel coefficient $h_{i,j,m}$, which is the m-th element of the vector $\mathbf{h}_{i,j}$ corresponding to the m-th receive antenna. This estimate is given by

$$\hat{h}_{i,j,m} = h_{i,j,m} + e_{i,j,m} \qquad \text{(B.11)}$$

where $e_{i,j,m}$ is the estimation error. We model this error as a Complex Normal random variable with zero mean and $\sigma_{n_m}^2 / Q_{\mathrm{H}}$ variance [9], where $\sigma_{n_m}^2$ is the additive noise power at the m-th antenna and Q_{H} is the number of samples used for the channel response estimation. The number of samples Q_{H} depends on the reference symbol design as well as on the frequency correlation of the channel [10].

$$e_{i,j,m} \sim \mathcal{CN}\left(0, \frac{\sigma_{n_m}^2}{Q_{\mathrm{H}}}\right) \qquad \text{(B.12)}$$

D. Receiver Front-End Errors

In the 5G system, with the assumption of flexible UL/DL resource allocation, the received signal power may vary significantly due to multiple sources of interference turning on and off at every TTI. This process may affect some key receiver front-end components. Ideally, the Automatic Gain Control (AGC) mechanism estimates the total received signal power and chooses the amplifier gain that minimizes the errors caused by the Analog-to-Digital Converter (ADC) quantization and clipping effects [11]. If the AGC mechanism cannot track the variation of the total received signal power, these errors may become larger and impact the receiver performance. It also affects the estimation processes, leading to inaccurate received signal combining and poor interference rejection. We now update our received signal model by adding the effects of these imperfections.

Let us define $\sigma_{r_m}^2[t]$ as the total power of the input signal $r_m[t]$ at the m-th antenna and time t as

$$r_m[t] = \sum_{k=1}^{N_T} \sum_{l=1}^{N_S^k} h_{k,l,m}[t]s_{k,l}[t] + v_m[t] \tag{B.13}$$

where $v_m[t]$ represents the additive noise term with power σ_0^2 observed at the m-th antenna (before the receiver front-end components).

We divide our front-end model in three stages: amplification, quantization and clipping. At the amplification stage, we first model the noise figure of the amplifier by multiplying the additive noise power σ_0^2 by the average noise factor F. Then, we calculate the amplification gain based on the total received signal power per antenna. The gain is then given by

$$g[t] = \frac{A}{\sqrt{\epsilon \sigma_r^2[t - \tau]}} \tag{B.14}$$

where A is the ADC full range amplitude, ϵ is the back-off factor and τ is the delay of the estimation of the total received power σ_r^2 used by the AGC. Note that we drop the antenna index for the sake of simplicity. The back-off factor ϵ must be used to account for the ratio between the peak and the average values of the input signal. This value controls the probability of clipping in the case of ideal operation of the AGC and may be calculated for a desired probability by assuming the OFDM signal to be a band-limited Gaussian zero mean stationary process [11].

The quantization stage adds the ADC quantization noise. The quantization noise power σ_q^2 does not depend on the input signal power, but only on the ADC full range value A and the ADC word-length in bits b. By assuming the noise to be independently and uniformly distributed, the quantization noise is given by [12, 11]

$$\sigma_q^2 = \frac{A^2 2^{-2b}}{3} \tag{B.15}$$

The clipping stage adds the noise generated when the amplitude of the signal at the ADC input is higher than the ADC full range amplitude A. The clipping error power $\sigma_c^2[t]$ is calculated as a function of the received signal power at the input of the ADC and is given by [13]

$$\sigma_c^2[t] = (1 - e^{-\beta^2[t]} - \alpha^2[t])\sigma_r^2[t] \tag{B.16}$$

where $\beta[t]$ is the clipping ratio, defined as

$$\beta[t] = \sqrt{\frac{A^2}{\sigma_r^2[t]}} \tag{B.17}$$

and $\alpha[t]$ is the amplitude compression value, defined as

$$\alpha[t] = 1 - e^{-\beta^2[t]} + \frac{\sqrt{\pi}}{2}\beta[t]\,\text{erfc}(\beta[t]) \tag{B.18}$$

where $\text{erfc}(\cdot)$ denotes the complementary error function.

The output signal after the front-end can then be expressed as

$$r[t] = \sum_{k=1}^{N_T}\sum_{l=1}^{N_S^k} g[t]\alpha[t]h_{k,l}[t]s_{k,l}[t] + n[t] \tag{B.19}$$

where $n[t]$ is the additive noise term composed by the amplified input noise, the quantization noise and the clipping noise. This noise term is modeled as an independent complex normal random variable with zero mean and variance given by

$$\sigma_n^2[t] = (g^2[t]F)\sigma_0^2 + \sigma_q^2 + \sigma_c^2[t] \tag{B.20}$$

IV. Simulation Setup

In this section, we present the details about the simulation scenario used to study the impact of receiver imperfections on the performance of a multi-cell network with MMSE-IRC receivers. We also present the physical layer assumptions used in the simulations.

A. Simulation Scenario

The local area network scenario [14] used in the simulations consists of 40 indoor small cells. Figure C.2 presents the schematic of the scenario. Each cell is located in one of the offices of two buildings that are separated by a ten-meter wide street. Each building is composed by two rows of 10 square offices, each of them measuring 10 by 10 meters. In each cell, one AP and one UE are randomly positioned. Each UE connects to the AP in the same office, i.e. a CSG access mode is enforced.
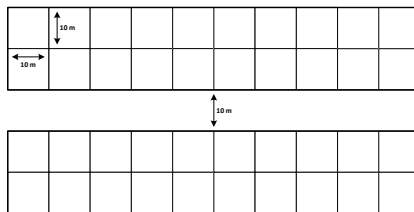

Fig. B.1: 3GPP Dual Stripe Simulation Scenario [14].

Table B.1: Simulation Scenario

Data Generation	Infinite Buffer UL/DL Flexible UL and DL resource allocation	
Access Mode	Closed Subscriber Group (CSG)	
Path Loss	3GPP Dual Stripe Model 45 dB Minimum Coupling Loss	
Wall Loss	Internal Walls	5 dB
	External Walls	10 dB
Shadowing Std. Deviation	Serving Cell	6 dB
	Other Cells	8 dB
Fast Fading	WINNER Phase II Model Indoor Office (A1) - 3 Km/h	
Antenna Configuration	Uniform Linear Array (ULA) 4 antenna elements (0.5λ spacing)	
System Bandwidth	198 MHz	

The data generation is modeled as an infinite buffer in both uplink and downlink. We model the flexible UL and DL resource allocation as a Markov Process with identical transition matrix and three possible outcomes: UL transmission, DL transmission or idle. The transmit direction decisions in each cell are independent and uncorrelated.

The large scale propagation effects (path loss and shadowing) are modeled using the 3GPP Dual Stripe model [14] whereas the small scale effects (fast fading and antenna characteristics) are modeled using the WINNER Phase II Indoor Office (A1) [15]. We assume that both APs and UEs are equipped with uniform linear array antennas with 4 elements each. The elements are placed at $\lambda/2$ distance of each other. Table C.1 presents further details regarding the scenario.

B. Physical Layer Assumptions

Ideal rank adaptation with no feedback or errors is assumed, i.e. the number of transmit data streams for each AP/UE is dynamically selected at each TTI depending on the instantaneous interference conditions. The LTE precoding matrix codebook for downlink closed-loop single user MIMO is used and a single rank is selected across the entire bandwidth [16]. We also assume ideal link adaptation with one codeword per spatial stream. The SINR of the

Table B.2: Physical Layer Parameters

Frame Format	Q_H	4 samples
	Q_{DSB}	165 samples
	Q_{RSB}	15 samples
Receiver Front-End	F	8 dB
	A	1 V
	ϵ	11.8 dB
	τ	0 or 1 TTI[1]
	b	6 or 10 bits

estimated symbol $\hat{s}_{i,j}$ is given by

$$\gamma_{i,j} = \frac{\mathbf{w}_{i,j}^H (\mathbf{h}_{i,j}\mathbf{h}_{i,j}^H)\mathbf{w}_{i,j}}{\mathbf{w}_{i,j}^H \left(\sum_{\substack{l=1 \\ l \neq j}}^{N_S^i} \mathbf{h}_{i,l}\mathbf{h}_{i,l}^H + \sum_{\substack{k=1 \\ k \neq i}}^{N_T} \sum_{l=1}^{N_S^k} \mathbf{h}_{k,l}\mathbf{h}_{k,l}^H + \mathbf{R}_n \right) \mathbf{w}_{i,j}}$$

We limit the minimum decodable SINR to -10 dB. Using the SINR and Shannon's AWGN channel capacity formulation, we calculate the spectral efficiency per spatial stream. The maximum spectral efficiency is limited to 8 bits/s/Hz, which is equivalent to uncoded 256-QAM modulation. We sum the spectral efficiency of all streams and multiply the result by the system bandwidth to obtain the total data rate.

Table B.2 presents the physical layer parameters related to the model. The number of samples used by channel response and covariance matrix estimation methods were calculated based on the frame format presented in [6]. The back-off parameter ϵ was calculated based on a Peak-to-Average Power Ratio (PAPR) equal to 11.8 dB, which results in a probability of clipping equal to 10^{-4}.

V. Performance Evaluation

A quasi-static system-level simulator was used to evaluate the performance of a network in which the described receivers with imperfections are used. Each simulation consists of 200 snapshots of 200 radio frames each. In each snapshot, the devices are randomly placed in the cells. The fast fading samples are updated at each TTI while the large scale parameters (path loss and shadowing) remain constant. We evaluate the performance using ECDFs of the

---

[1]There is no need to consider further delay values since there is no correlation between transmit decisions at consecutive TTIs.

average cell throughputs. In particular, we extract from the ECDFs the network's outage (5th percentile), peak (95th percentile) and average data rates, which are the key performance indicators used in the results analysis.

We first evaluate the impact of channel response and covariance matrix estimation errors on the performance of the receivers. Figure C.3 shows the average cell throughput ECDFs for different covarance matrix estimation methods. The ideal covariance matrix estimation case is also depicted. Both MRC and IRC receivers are considered, and the channel response estimation error is included. As expected from previous studies, the results show that the performance of the IRC receiver overcomes significantly that of the MRC receiver in this scenario. The results also show a clear difference between the DSB and RSB methods. While the RSB method presents results very close to the ideal case, the DSB method presents considerable performance loss.
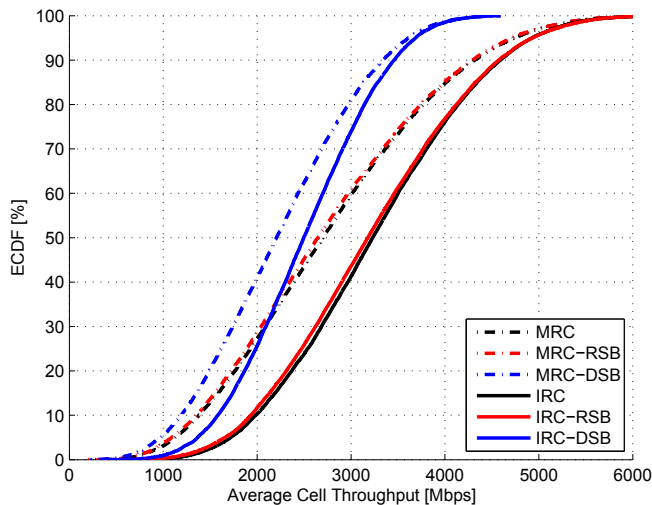
Fig. B.2: Average cell throughput ECDFs for different receivers and covariance matrix estimation methods.

The performance degradation for the different cases is also presented in Table C.2. The results show that the performance degradation impacts both receivers similarly when the RSB method is used, but the performance degradation of the IRC receiver is larger than that of the MRC receiver with the DSB method. This difference has an impact on the performance gain of IRC over MRC as it is shown in Table C.3. When the DSB method is used, the outage performance gain drops from 53% to 41% and the average performance gain drops from 17% to 12%, while the gains are approximately the same of the ideal case when the RSB method is used. The results show that the

Table B.3: Performance degradation due to covariance matrix estimation errors

Case	Receiver	Outage	Peak	Average
DSB	MRC	-14%	-24%	-20%
	IRC	-21%	-25%	-23%
RSB	MRC	-3%	-1%	-1%
	IRC	-3%	0%	-1%

Table B.4: Performance gain of IRC over MRC with different covariance matrix estimation methods

Case	Outage	Peak	Average
Ideal	53%	4%	17%
DSB	41%	2%	12%
RSB	52%	4%	17%

RSB method significantly outperforms the DSB method, even when channel response estimation errors and limited number of samples are considered. This is because the RSB method exploits the more accurate channel response estimate and the possibility of discriminating the contribution of the desired signals to the covariance matrix from the interference and noise contributions, leading to a better estimate of the covariance matrix. Note that this is enabled by the radio frame format discussed in Section II.

We now evaluate the impact of the receiver front-end imperfections on the overall network performance. Figure C.4 shows the average cell throughput ECDFs for the ideal front-end case and for the imperfect front-end cases for both MRC and IRC receivers. RSB covariance matrix estimation method is assumed, and channel response estimation error is included. Only the lower part of the ECDF is displayed in the figure in order to highlight the outage data rate. The results show that the performance of the receivers strongly depends on the AGC delay and the ADC resolution.

The performance degradation due to receiver front-end errors is also presented in Table B.5. Significant degradation is experienced in case of low ADC resolution (6 bits). The performance of both receivers is considerably worse than the ideal performance, reaching up to 21% average cell throughput reduction. This performance reduction is due to the impact that the quantization noise causes on the estimation accuracy, leading to poor received signal combining and poor interference rejection in the case of IRC. The results also show that, if we use a reasonably high resolution ADC (10 bits), the performance degradation is limited, reducing the key performance indicator by at most 6% in the worst case. Note that ADCs with 10 bits
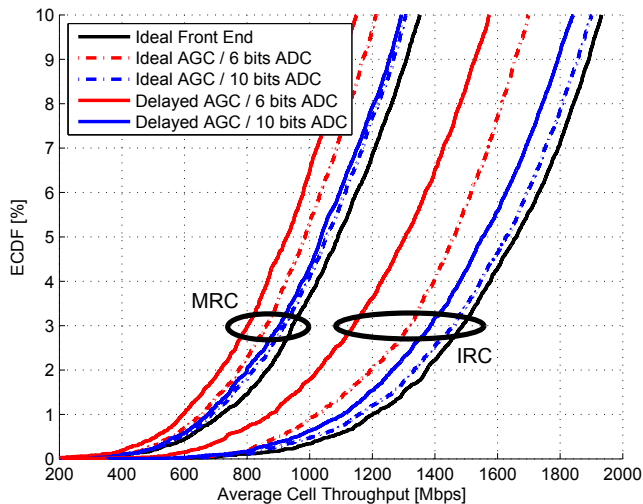
Fig. B.3: Average cell throughput ECDFs for different receivers and receiver front-end configurations.

resolution (or more) are commonly used in commercial LTE devices.

Analyzing the difference between the performance degradation with the ideal AGC ($\tau = 0$) and the delayed AGC ($\tau = 1$), we conclude that the rapidly varying interference sources impact the receiver performance significantly. Results show that the outage throughput degradation is higher when we compare the ideal AGC model to the delayed one. However, the use of higher resolution ADC (10 bits) reduces the overall impact of the AGC's inability to perfectly track the received signal power levels.

Table B.6 confirms that it is possible to obtain a realistic IRC receiver with performance very close to the ideal, even in a scenario with rapidly varying interference sources. An IRC receiver with delayed AGC and low resolution ADC (6 bits) would have much lower performance gain, especially in terms of outage throughput. However, using a higher resolution ADC (10 bits), the performance difference is almost negligible. Thus, we can conclude that it is possible to obtain the very high data rate gains of IRC by exploiting the mentioned radio frame format [6], as long as the RSB covariance matrix estimation method and a reasonably high resolution ADC (10 bits) are used.

VI. Conclusion

In this paper, we evaluated the impact of receiver imperfections on the performance of the MMSE-IRC receiver using system-level simulations. We pre-

Table B.5: Performance degradation due to receiver front-end errors

AGC	ADC	Receiver	Outage	Peak	Average
Ideal	6 bits	MRC	-10%	-16%	-14%
		IRC	-12%	-17%	-15%
	10 bits	MRC	-3%	+1%	-1%
		IRC	-2%	0%	-1%
Delayed	6 bits	MRC	-15%	-15%	-15%
		IRC	-21%	-17%	-17%
	10 bits	MRC	-5%	+1%	-1%
		IRC	-6%	0%	-2%

Table B.6: Performance gain of IRC over MRC with different receiver front-end configurations

AGC	ADC	Outage	Peak	Average
Ideal	Ideal	52%	4%	17%
Ideal	6 bits	48%	3%	16%
	10 bits	54%	3%	17%
Delayed	6 bits	41%	3%	15%
	10 bits	50%	3%	17%

sented a model that captures the effects of channel response and covariance matrix estimation errors as well as receiver front-end imperfections.

Performance results show that using a radio frame format designed to support the MMSE-IRC receiver, the adequate covariance matrix estimation method and a reasonably high resolution ADC, the MMSE-IRC receiver is able to reach performance levels close to the ideal. This realistic MMSE-IRC receiver presents low throughput degradation and keeps considerable performance gains over a realistic MMSE-MRC receiver.

Our future work will focus on radio resource management for 5G networks, such as rank and precoding matrix adaptation algorithms. Our aim is to investigate algorithms aimed at optimizing the operation of MMSE-IRC receivers with rapidly varying interference sources.

References

[1] Preben Mogensen, Kari Pajukoski, Bernhard Raaf, Esa Tiirola, Eeva Lähetkangas, Istvan Z. Kovács, Gilberto Berardinelli, Luis G. Uzeda Garcia, Liang Hu, and Andrea F. Cattoni. "B4G local area: High level requirements and system design". In: *Globecom Workshops (GC Wkshps), 2012 IEEE*. Dec. 2012, pp. 613–617. DOI: `10.1109/GLOCOMW.2012.6477644`.

[2] F.M.L. Tavares, G. Berardinelli, N.H. Mahmood, T.B. Sørensen, and P. Mogensen. "On the Potential of Interference Rejection Combining in B4G Networks". In: *Vehicular Technology Conference (VTC Fall), 2013 IEEE 78th*. Sept. 2013, pp. 1–5. DOI: `10.1109/VTCFall.2013.6692318`.

[3] M. Lampinen, F. Del Carpio, T. Kuosmanen, T. Koivisto, and M. Enescu. "System-Level Modeling and Evaluation of Interference Suppression Receivers in LTE System". In: *Vehicular Technology Conference (VTC Spring), 2012 IEEE 75th*. May 2012, pp. 1–5. DOI: `10.1109/VETECS.2012.6239964`.

[4] K. Pietikainen, F. Del Carpio, H. Maattanen, M. Lampinen, T. Koivisto, and M. Enescu. "System-Level Performance of Interference Suppression Receivers in LTE System". In: *Vehicular Technology Conference (VTC Spring), 2012 IEEE 75th*. May 2012, pp. 1–5. DOI: `10.1109/VETECS.2012.6239969`.

[5] Y. Ohwatari, N. Miki, T. Asai, T. Abe, and H. Taoka. "Performance of Advanced Receiver Employing Interference Rejection Combining to Suppress Inter-Cell Interference in LTE-Advanced Downlink". In: *2011 IEEE Vehicular Technology Conference (VTC Fall)*. Sept. 2011, pp. 1–7. DOI: `10.1109/VETECF.2011.6093196`.

[6]   P. Mogensen, K. Pajukoski, E. Tiirola, E. Lahetkangas, J. Vihriala, S. Vesterinen, M. Laitila, G. Berardinelli, G.W.O. Da Costa, L.G.U. Garcia, F.M.L. Tavares, and A.F. Cattoni. "5G small cell optimized radio design". In: *Globecom Workshops (GC Wkshps), 2013 IEEE*. Dec. 2013, pp. 111–116. DOI: 10.1109/GLOCOMW.2013.6824971.

[7]   Jinho Choi. *Optimal Combining and Detection: Statistical Signal Processing for Communications*. Cambridge: Cambridge University Press, 2010.

[8]   D. Morales-Jimenez, J.F. Paris, J.T. Entrambasaguas, and Kai-Kit Wong. "On the Diagonal Distribution of a Complex Wishart Matrix and its Application to the Analysis of MIMO Systems". In: *Communications, IEEE Transactions on* 59.12 (2011), pp. 3475–3484. ISSN: 0090-6778. DOI: 10.1109/TCOMM.2011.100611.100641.

[9]   3GPP R1-080506. *UE specific reference signal pattern*. Jan. 2008. URL: http://www.3gpp.org.

[10]   3GPP R1-062642. *Uplink Reference Signal Design in EUTRA*. Oct. 2006. URL: http://www.3gpp.org.

[11]   D. Dardari. "Joint clip and quantization effects characterization in OFDM receivers". In: *Circuits and Systems I: Regular Papers, IEEE Transactions on* 53.8 (2006), pp. 1741–1748. ISSN: 1549-8328. DOI: 10.1109/TCSI.2006.875170.

[12]   B. Widrow, I. Kollar, and Ming-Chang Liu. "Statistical theory of quantization". In: *Instrumentation and Measurement, IEEE Transactions on* 45.2 (1996), pp. 353–361. ISSN: 0018-9456. DOI: 10.1109/19.492748.

[13]   Chun-Tao Lin and Wen-Rong Wu. "Clipping ratio estimation for OFDM receivers". In: *Vehicular Technology Conference (VTC Spring), 2005 IEEE 61st*. 2005. DOI: 10.1109/VETECS.2005.1543414.

[14]   3GPP TR 36.814. *Evolved Universal Terrestrial Radio Access (E-UTRA); Further advancements for E-UTRA physical layer aspects*. v9.0.0. Mar. 2010. URL: http://www.3gpp.org.

[15]   P. Kyösti et al. *WINNER II Channel Models*. D1.1.2 v1.1. IST-WINNER, Sept. 2007. URL: https://www.ist-winner.org/WINNER2-Deliverables/D1.1.2v1.1.pdf.

[16]   3GPP TS 36.211. *Evolved Universal Terrestrial Radio Access (E-UTRA); Physical channels and modulation*. v11.1.0. Dec. 2012. URL: http://www.3gpp.org.

Paper C

Inter-cell interference management using Maximum Rank Planning in 5G small cell networks

Fernando M. L. Tavares, Gilberto Berardinelli, Nurul H. Mahmood, Troels B. Sørensen, and Preben Mogensen

Abstract

In this paper, we propose Maximum Rank Planning (MRP) as a novel inter-cell interference management technique for the ultra-dense uncoordinated deployment of small cells targeted by 5th Generation (5G) networks. Rather than operating in the frequency domain as the conventional Frequency Reuse Planning (FRP) technique, MRP acts by reducing the number of Multiple Input Multiple Output (MIMO) spatial multiplexing streams. This reduction leads to an increased probability that the Interference Rejection Combining (IRC) receiver will have sufficient degrees-of-freedom to reject the strongest interferers. System-level simulation results show that MRP outperforms FRP in both low and high traffic load conditions, with 44% and 49% outage throughput gains in each case, respectively.

I. Introduction

The ultra-dense uncoordinated deployment of local area small cells is envisioned as the main solution to reach the ambitious capacity requirements of future 5G networks [1]. However, this type of deployment can only provide the expected network capacity boost in case efficient inter-cell interference mitigation techniques are applied.

The conventional approach to deal with inter-cell interference is to use Frequency Reuse Planning (FRP) (static or dynamic) [2, 3, 4], i.e. allocating orthogonal frequency chunks to neighbor cells that experience significant mutual interference. Frequency reuse techniques can be used to improve the outage and average data rates, with the obvious drawback of limiting the peak network throughput since each cell is operating over only a portion of the available spectrum. FRP is particularly advantageous for mobile network operators that aim at guaranteeing minimum quality of service requirements for their subscribers.

The usage of advanced receivers is also a promising solution to deal with the inter-cell interference. In particular, IRC receivers exploit the degrees of freedom of multiple antenna transceivers for projecting the interfering signals onto an orthogonal subspace with respect to the desired ones [5]. Though advanced receivers such as IRC have been shown to significantly improve the network performance, they are typically able to suppress only a limited number of significant interferers; FRP may then still be needed to improve average and outage data rates. Nonetheless, conventional FRP is unaware of the interference suppression capabilities of the receivers, leading to inefficient radio resource management decisions.

In this paper, we present a novel Maximum Rank Planning (MRP) technique which is conceived as an alternative to FRP for networks equipped with IRC receivers. The principle of the novel technique is to act on the

spatial resources of the multiple antenna transceiver rather than on the spectrum resources. We present system-level simulation results that compare the performance of MRP and FRP in the context of the 5G small cell network concept envisioned in [1], though a generalization to other air interfaces is straightforward.

The paper is structured as follows. Section II recalls the usage of IRC receivers in 5G networks. We present the novel MRP technique in Section III and we describe the simulation setup in Section IV. In Section V, we present and discuss the simulation results. Section VI closes the paper with conclusions and future work.

II. Interference Rejection Combining in 5G

In [1] we have proposed a clean slate approach for a 5G concept optimized for ultra-dense deployment of small cells. Time Division Duplex (TDD) mode is recognized as the preferred operational mode given its flexibility and the possibility of exploiting unpaired bands. Fundamental technical features are MIMO antenna techniques, optimized frame structure, flexible uplink/downlink resource allocation and the aforementioned IRC receivers. It is well known that the degrees of freedom of MIMO transmission can be used to send multiple data streams or to increase the reliability of a number of streams lower than the antenna cardinality. Further, when IRC receivers are adopted, some of the degrees of freedom can be used for suppressing streams that compose the interfering signals, with penalty in terms of spatial multiplexing gain since the number of desired streams which can be transmitted has to be lowered.

The IRC receiver uses received samples or channel estimates to create an Interference-plus-noise Covariance Matrix (ICM) that is used to calculate the optimal combining matrix. To work efficiently, the IRC receiver requires accurate ICM estimation that can only be obtained if the interfering sources remain the same for the duration of the estimation period [6]. The frame structure proposed in [1] is particularly suited for an efficient usage of IRC. It assumes the transmission direction (UL or DL) to remain constant within a frame. By assuming neighbor cells to be time synchronized, such design allows the interference pattern to be constant within the frame. Further, the frame features a time symbol dedicated to the reference sequences used for channel estimation purposes. By assuming the use of orthogonal reference sequences, each AP or UE is able to estimate the channel of both desired and interfering nodes regardless of the transmission direction. This enables just-in-time estimation of the ICM and fast tuning of the IRC filter. Using this radio frame format, we have shown in previous studies that IRC can effectively reduce the inter-cell interference perceived by the receiver [7], even

when receiver imperfections and estimation errors are considered [8].

A rank adaptation algorithm is used to find for each cell the rank (number of spatial streams) that provides the best trade-off between spatial multiplexing gain and interference rejection capabilities according to the estimated interference scenario and channel fading conditions. Since the performance of the IRC receiver depends on the number of spatial streams that compose each interfering signal, the outcome of the rank adaptation algorithm may impact the performance in neighbor cells in case the decisions are taken at each cell independently. Each degree-of-freedom can be used to reject only one interfering spatial stream. Thus, depending on the decision of the rank adaptation algorithm of the interfering cell, the IRC receiver may be able to reject either completely or partially the interfering signal.

Generally, this dependency leads to low outage throughput performance whenever neighbor cells experience unbalanced reciprocal interference due to the specific topology. For instance, if cell A experiences significant interference from cell B, while cell B is not affected by the transmissions occurring in cell A, the rank adaptation in cell B may opt for the maximum number of transmission streams, but this would generate disruptive interference levels in cell A, which would react by drastically reducing its transmission rank. In some cases, the number of degrees-of-freedom may not be sufficient to reject the interfering signal completely, leading to very low throughput. The overall network throughput may then be penalized by such selfish behavior. The usage of a centralized entity that chooses the best rank for each cell or a decentralized victim-aware solution in which the transmission rank at each cell is chosen in a cooperative manner, such as [9], can avoid situations such as the above, but they require message exchange mechanisms between different cells which may not be feasible in real networks.

III. Maximum Rank Planning

Maximum Rank Planning (MRP) is an inter-cell interference management technique that consists in limiting the maximum rank that the rank adaptation algorithm at each transmitter may use. By reducing the rank of the strong interferers, MRP increases the probability that the interfered receivers will have enough degrees-of-freedom to reject them. Note that this technique is only recommended for networks in which all devices use receivers capable of rejecting interference and interference-aware rank adaptation algorithms are used to decide between spatial multiplexing and interference rejection.

The maximum rank limit may be configured individually for each transmitter and the configuration depends mostly on the expected inter-cell interference they generate to the neighbor cells. The limit can be static or dynamic (similar to dynamic FRP). In this paper, we show only the static case in which
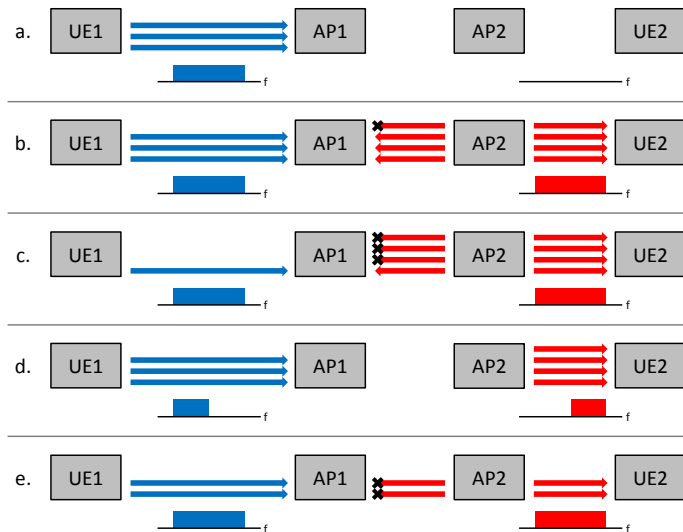
Fig. C.1: Example of Maximum Rank Planning (MRP) working principle.

all transmitters have the same maximum rank limit. Methods to select the limit individually for each transmitter and to adapt the selection according to the traffic dynamics are topics we plan to investigate in the future.

The schematic in Figure C.1 provides an example to demonstrate the working principle of MRP. The schematic shows in five different cases how two neighbor cells interact with each other. In this example, we assume that all devices use IRC receivers and all of them feature four transmit/receive antennas. We also assume that, given the position of the devices, the APs can generate strong mutual inter-cell interference, which impedes any reception in case there are not sufficient degrees of freedom to reject it, whereas UEs are not affected by inter-cell interference. The following notation is used in the example: T_s represents the maximum throughput per spatial stream over the entire system spectrum, and T_1 and T_2 represent the maximum overall throughput that Cell 1 (AP1 and UE1) and Cell 2 (AP2 and UE2) can reach in the different cases, respectively.

Figure C.1a) shows the case in which UE1 transmits to AP1 and the link between AP2 and UE2 is idle. We suppose in this case that the rank adaptation algorithm decided to use only 3 simultaneous spatial streams (rank 3) to transmit data to AP1 due to the current conditions of the channel, i.e. $T_1 = 3T_s$.

In Figure C.1b), AP2 starts to transmit to UE2 using 4 spatial streams (rank 4). Since both cells use the same portion of the spectrum, AP1 receives the inter-cell interference from AP2. The IRC receiver in AP1 has only one

free degree-of-freedom, so it is able to reject only one of the spatial streams coming from AP2 (the other spatial streams still cause interference). In this situation, the throughput in the link between UE1 and AP1 is severely reduced ($T_1 = 0$ and $T_2 = 4T_s$).

In Figure C.1c), the rank adaptation algorithm reduces the number of streams in the link between UE1 and AP1 to one (rank 1). Now the IRC receiver can reject 3 of the 4 spatial streams that transmitted by AP2. This new situation reduces the effect of the inter-cell interference, but the throughput is still very low ($T_1 = 0$ and $T_2 = 4T_s$). Since mobile network operators aim at guaranteeing a minimum quality of service requirement, a solution that improves the throughput in Cell 1 is required.

The typical solution for this problem is to use FRP. In Figure C.1d), the spectrum is divided in two orthogonal channels and a different channel is allocated for each cell. Now, the transmission in each cell does not interfere with the other, but the data rates are hard limited to half of what they could be if each cell were using the whole spectrum alone, i.e. $T_1 = 1.5T_s$ and $T_2 = 2T_s$.

Figure C.1e) depicts the case in which MRP is used. The network is configured such that both cells use the whole spectrum and their maximum rank limit is set to 2 spatial streams, forcing the rank adaptation algorithm to reduce the rank from 3 to 2 spatial streams in Cell 1 and from 4 to 2 spatial streams in Cell 2. Now the IRC receiver in AP1 can completely reject the inter-cell interference from AP2. The advantage of MRP when compared to FRP in this example is the higher throughput in Cell 1 ($T_1 = 2T_s$ and $T_2 = 2T_s$). With MRP, the throughput in Cell 1 is only reduced by one third (from 3 to 2 spatial streams), when compared to the situation in Figure C.1a), whereas it is reduced by half in the FRP case.

This example shows one possible situation in which the MRP technique outperforms FRP. Generally, MRP outperforms the FRP whenever rejecting small number of the strongest interfering streams improves significantly the SINR. In this case, MRP provides the advantage of quickly adjusting to the instantaneous interference conditions, rejecting the strongest interferers. This is particularly advantageous in the case of ultra-dense uncoordinated deployments (as targeted by our 5G concept) in which it is difficult to determine the strongest interferers beforehand. Conversely, FRP performs better than MRP when many interferers with relatively low power accumulate to cause disruptive interference. In this case, the IRC receiver will not have enough degrees of freedom to reject enough of interferers and significantly improve the performance.

It is difficult to determine analytically which of the two techniques will provide the best overall performance in each scenario. Their performance depends on the specific scenario topology, that varies due to the unpredictable position of each node and their probability of transmission. Thus, our pro-

posed technique will be evaluated with system level simulations.

IV. Simulation Setup

In this section, we present the simulation setup used to compare the performance of MRP and FRP. Figure C.2 shows a schematic that represents the indoor local area network scenario. The scenario is composed of 40 indoor small cells. Each cell is located in one of the offices of two buildings which are separated by a 10 meter wide street. Each building has 2 rows of 10 offices and each office measures 10 by 10 meters. One UE and one AP are located in each cell and their position inside the cell is randomly selected to emulate an uncoordinated deployment. Each UE can only connect to the AP in the same office i.e. the cell selection is limited by CSG.
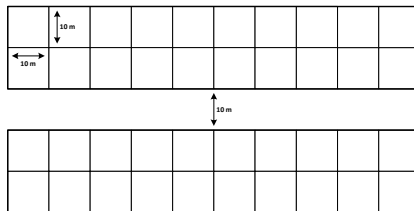

Fig. C.2: 3GPP Dual Stripe Simulation Scenario [10].

The large scale propagation effects (pathloss and shadowing) are modeled according to the 3GPP Dual Stripe Model [10]. The small scale effects (fast fading and antenna characteristics) follow the WINNER Phase II Indoor Office (A1) model [11]. In the simulations, all devices use Uniform Linear Array (ULA) antennas with 4 elements, which are spaced by $\lambda/2$ from each other. The same antenna array is used for both transmission and reception. We assume the system uses a 200 MHz band, which is the baseline assumption in our envisioned 5G concept [1].

We assume the cells to be time aligned; further each cell can freely decide at each Transmission Time Interval (TTI) the transmission direction (UL, DL or idle). This decision is modeled using a Markov Process. The transition probabilities are selected such that the probability of selecting the idle mode is controllable, but the probabilities of selecting either UL or DL modes are identical. The random processes in each cell are independent and uncorrelated.

A rank adaptation algorithm at the receiver side is used to select the number of spatial streams. The decision is based only on instantaneous channel and interference conditions. The decision is informed to the transmitter that

Table C.1: Simulation Scenario

Spectrum Allocation	200 MHz at 3.5 GHz	
Transmit Time Interval	0.25 ms	
Data Generation	Infinite Buffer UL/DL Flexible UL and DL resource allocation	
Access Mode	Closed Subscriber Group (CSG)	
Path Loss	3GPP Dual Stripe Model 45 dB Minimum Coupling Loss	
Wall Loss	Internal Walls	5 dB
	External Walls	10 dB
Shadowing Std. Deviation	Serving Cell	6 dB
	Other Cells	8 dB
Fast Fading	WINNER Phase II Model Indoor Office (A1) - 3 Km/h	
Antenna Configuration	Uniform Linear Array (ULA) 4 antenna elements (0.5λ spacing)	
Transmission Power	20 dBm	
Receiver Noise Figure	9 dB	
Error Vector Magnitude	5%	$\text{SINR}_{max} \approx 26\text{dB}$

Table C.2: Outage throughput performance comparison - Low network load (50%)

Case	Setup	MRC	IRC
Baseline	FR1/MR4	1218.0	1466.0
FRP	FR2/MR4	1226.0 (+1%)	1400.0 (-5%)
MRP	FR1/MR2	1044.0 (-14%)	1762.0 (+20%)

uses the selected number of streams in the next TTI. A precoding matrix is used to map the streams to the four transmit antennas (the LTE downlink closed-loop single user MIMO codebook [12] is adopted).

The instantaneous SINR is calculated at each TTI using an IRC receiver system-level simulation model [7]. The usage of IRC is also compared to the Maximum Ratio Combining (MRC) receiver, which represents the baseline inter-cell interference unaware receiver in this study. The models output one SINR value for each spatial stream. These values are adjusted using a EVM model to account for the receiver imperfections and limitations [13].

We assume ideal link adaptation with one codeword per spatial stream. We calculate the spectral efficiency for each stream using Shannon's capacity formula, considering that the minimum decodable SINR is -10 dB and that the maximum spectral efficiency per spatial stream is 8 bits/s/Hz (uncoded 256-QAM). The total throughput is obtained by multiplying the sum of the spectral efficiency of all spatial streams by the signal bandwidth.

V. Performance Evaluation

We evaluate the performance of MRP using a quasi-static system level simulator. Each simulation consists of 200 snapshots of 200 frames each. In each snapshot, the devices (AP and UE) are randomly placed in the cells. The fast fading samples are updated at each frame, but the large scale values (pathloss and shadowing) remain constant. We evaluate the performance using ECDFs of the average cell throughput. In particular, we consider the outage (5th percentile) throughput as the main key performance indicator (as mentioned in the introduction, we assume that mobile network operators aim at improving minimum quality of service requirements).

Two different network load situations are considered: a low load case (50% activity factor) and a high load case (100% activity factor), where the activity factor is the probability that a cell is not in idle mode. In each case, we provide ECDFs for both MRC and IRC receivers. We refer to the case with Frequency Reuse x and Maximum Rank y as FRx/MRy.

Figure C.3 shows the ECDF of the average cell throughput in the low network load case for different MRP and FRP combinations. The baseline case
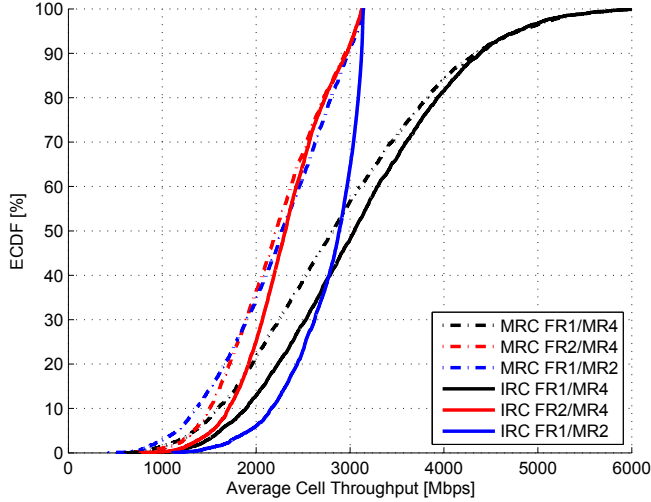
Fig. C.3: Average cell throughput ECDFs for different FRP/MPR combinations and low network load (50%).

in which all the cells use the entire spectrum and the maximum number of streams (FR1/MR4) is also included, along with the FRP/MRP combinations that are used in this case to improve the outage throughput in the network. We select the FRP/MRP combinations that reduce the peak throughput by half (by dividing the bandwidth in one case and limiting the number of streams in the other) as a reasonable trade-off. These combinations are the FR2/MR4 (FRP) and the FR1/MR2 (MRP).

We can notice in the figure that IRC clearly outperforms MRC in all the cases. FR2/MR4 case provides a slightly better outage throughput than FR1/MR4 in the case of MRC, whereas the overall performance with the FR1/MR2 setup is worse than FR1/MR4, because the MRC receiver is not capable of rejecting any interference. However, when the IRC receiver is used, the FR2/MR4 case does not provide any benefit whereas the FR1/MR2 case provides significant outage gains over the baseline FR1/MR4. The results clearly show that MRP outperforms FRP when IRC receiver are used in this scenario. This is due to the uncoordinated characteristic of the deployment that favors a technique that can adapt to the unpredictable position of the strongest interferers.

Table C.2 presents the outage throughput values for the low network load case. The table shows the outage throughput gains for different FRP/MRP combinations over the baseline FR1/MR4. The numbers clearly show that the best strategy for the MRC receiver is the FRP (FR2/MR4) with 1% gain over
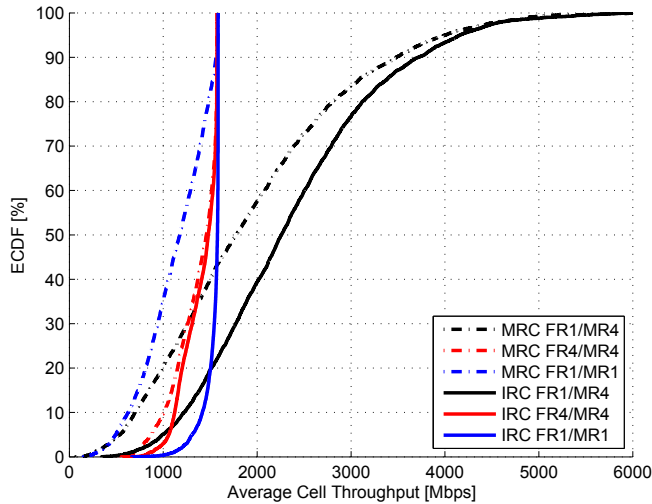
Fig. C.4: Average cell throughput ECDFs for different FRP/MPR combinations and high network load (100%).

Table C.3: Outage throughput performance comparison - High network load (100%)

Case	MRC	IRC
FR1/MR4	487.0	907.0
FR4/MR4	798.0 (+64%)	967.0 (+7%)
FR1/MR1	448.0 (-9%)	1191.0 (+31%)

the MRC baseline whereas the best strategy for IRC is the MRP (FR1/MR2) with 20% gain over the IRC baseline. Further significant insights can be obtained by comparing the performance of the MRC and the IRC receivers when the corresponding best strategy for each receiver is used. When the IRC is used with FRP, the outage gain over the MRC with FRP is only 14% in this scenario. In case the IRC is used in combination with the MRP strategy, the gain is increased to 44%.

A similar situation occurs in the high network load case. The ECDF curves in Figure C.4 show that the inter-cell interference problem is more severe in this case. Thus, it is necessary to use the FR/MR combinations that reduce the peak throughput to one fourth of its maximum value to significantly improve the outage performance. Once more, we observe that the IRC receiver outperforms the MRC receiver. It is also clear that the strategy that provides the best outage performance is the FRP in the MRC receiver case and the MRP in the IRC receiver case.

The outage performance gains for the high network load case are presented in Table C.3. Again, the outage performance in the MRC receiver case is only improved when the FRP is used. FRP provides 64% gain whereas the MRP reduces the gain by 9%. Conversely, the outage performance in the IRC receiver case is improved when the MRP is used, with 31% over the baseline, whereas the FRP only improves the outage performance by 7%. We can also compare the benefit of using the MRP by comparing the gain of the IRC receiver over the MRC receiver. The outage performance in the IRC receiver with FRP case is 21% better than the MRC with FRP case while it is 49% better in case the MMSE-IRC with MRP is used instead.

VI. Conclusion

In this paper, we presented the Maximum Rank Planning technique as a novel inter-cell interference management technique for 5G local area networks. This technique operates on the MIMO spatial domain by relying on the capability of the advanced receiver to reject inter-cell interference. By limiting the maximum rank used by each transmitter, it increases the probability that the receivers will be able to effectively reject the inter-cell interference, thus improving the outage data rates. We evaluated the performance of MRP by using system-level simulations and compared it to the performance of conventional FRP in the same network. Performance results show that MRP outperforms FRP when IRC receivers are used, providing 44% and 49% outage throughput gains in low and high traffic load conditions, respectively.

Our future work will focus on methods to dynamically configure the maximum rank that may be used by each transmitter in the network. Our aim is to investigate algorithms that can adjust the maximum rank according to the network topology as well as take into account long-term traffic variations.

References

[1] Preben Mogensen, Kari Pajukoski, Esa Tiirola, Jaakko Vihriälä, Eeva Lähetkangas, Gilberto Berardinelli, Fernando Menezes Leitão Tavares, Nurul Huda Mahmood, Mads Lauridsen, Davide Catania, and Andrea Fabio Cattoni. "Centimeter-wave concept for 5G ultra-dense small cells". In: *Vehicular Technology Conference (VTC Spring), 2014 IEEE 79th*. May 2014.

[2] I. Katzela and M. Naghshineh. "Channel assignment schemes for cellular mobile telecommunication systems: a comprehensive survey". In: *Communications Surveys Tutorials, IEEE* 3.2 (2000), pp. 10–31.

[3] Yuanye Wang et al. "Fixed Frequency Reuse for LTE-Advanced Systems in Local Area Scenarios". In: *Vehicular Technology Conference, 2009. VTC Spring 2009. IEEE 69th*. Apr. 2009, pp. 1–5.

[4] J. Ellenbeck, C. Hartmann, and L. Berlemann. "Decentralized inter-cell interference coordination by autonomous spectral reuse decisions". In: *Wireless Conference, 2008. EW 2008. 14th European*. June 2008, pp. 1–7.

[5] Jinho Choi. *Optimal Combining and Detection: Statistical Signal Processing for Communications*. Cambridge: Cambridge University Press, 2010.

[6] P. Mogensen, K. Pajukoski, E. Tiirola, E. Lahetkangas, J. Vihriala, S. Vesterinen, M. Laitila, G. Berardinelli, G.W.O. Da Costa, L.G.U. Garcia, F.M.L. Tavares, and A.F. Cattoni. "5G small cell optimized radio design". In: *Globecom Workshops (GC Wkshps), 2013 IEEE*. Dec. 2013, pp. 111–116. DOI: 10.1109/GLOCOMW.2013.6824971.

[7] F.M.L. Tavares, G. Berardinelli, N.H. Mahmood, T.B. Sørensen, and P. Mogensen. "On the Potential of Interference Rejection Combining in B4G Networks". In: *Vehicular Technology Conference (VTC Fall), 2013 IEEE 78th*. Sept. 2013, pp. 1–5. DOI: 10.1109/VTCFall.2013.6692318.

[8] Fernando M.L. Tavares, Gilberto Berardinelli, Nurul H. Mahmood, Troels B. Sørensen, and Preben Mogensen. "On the Impact of Receiver Imperfections on the MMSE-IRC Receiver Performance in 5G Networks". In: *Vehicular Technology Conference (VTC Spring), 2014 IEEE 79th*. May 2014, pp. 1–6. DOI: 10.1109/VTCSpring.2014.7023014.

[9] B. Clerckx et al. "A Practical Cooperative Multicell MIMO-OFDMA Network Based on Rank Coordination". In: *Wireless Communications, IEEE Transactions on* 12.4 (Apr. 2013), pp. 1481–1491.

[10] 3GPP TR 36.814. *Evolved Universal Terrestrial Radio Access (E-UTRA); Further advancements for E-UTRA physical layer aspects*. v9.0.0. Mar. 2010. URL: http://www.3gpp.org.

[11] P. Kyösti et al. *WINNER II Channel Models*. D1.1.2 v1.1. IST-WINNER, Sept. 2007. URL: https://www.ist-winner.org/WINNER2-Deliverables/D1.1.2v1.1.pdf.

[12] 3GPP TS 36.211. *Evolved Universal Terrestrial Radio Access (E-UTRA); Physical channels and modulation*. v11.1.0. Dec. 2012. URL: http://www.3gpp.org.

[13] Harri Holma and Antii Toskala. *LTE for UMTS: Evolution to LTE-Advanced*. Wiley, 2011.

Paper D

Managing inter-cell interference with advanced receivers and rank adaptation in 5G small cells

Fernando M. L. Tavares, Gilberto Berardinelli, Davide Catania, Troels B. Sørensen, and Preben Mogensen

Abstract

The use of receivers with interference suppression capabilities is expected to be a significant performance booster in 5th Generation (5G) ultra-dense small cell networks. In this respect, they could represent an alternative to traditional frequency reuse techniques, facilitating the inter-cell interference management. In this paper, we evaluate whether it is possible to rely on such advanced receivers as the main tool to deal with the inter-cell interference problem. We present a system-level performance evaluation in three different dense indoor small cell scenarios using a receiver model that includes both interference rejection combining (IRC) and successive interference cancellation (SIC) principles, as well as different rank adaptation strategies. Our results confirm that interference suppression receivers with a supportive system design can indeed represent a valid alternative to frequency reuse. They achieve similar outage data rate performance in comparison to reuse strategies (resource orthogonalization), but higher average and peak throughput.

I. Introduction

The deployment of ultra-dense small cell networks is foreseen as a cost-effective solution for coping with wireless network congestion caused by the ever increasing demand for mobile broadband services, but the existing RAT standards are not well suited for this type of deployment. For this reason, a novel 5G RAT concept optimized for small cell networks operating at carrier frequencies bellow 6 GHz has been proposed in [1].

The main performance limiting factor in such ultra-dense deployments is the presence of strong inter-cell interference. While traditional approaches for dealing with inter-cell interference are based on the usage of static or dynamic frequency reuse techniques, advanced receivers with interference suppression capabilities also have the potential to boost the performance of dense small cells and could be used as an alternative to the traditional approaches. Such an alternative is important for this type of networks, because static frequency reuse planning may be inherently impracticable in the case of uncoordinated deployments and dynamic frequency reuse has significant system costs in terms of signalling overhead. Besides, the dynamic techniques may not be able to promptly adapt to the quickly varying interference patterns which are expected in dense small cell networks [1].

In a previous work [2], we have identified that the linear IRC receiver consistently outperforms its inter-cell interference unaware counterpart, the Maximum Ratio Combining (MRC) receiver, when the supportive system design proposed in [1] is used. The frame design that is part of this concept provides the mechanisms to guarantee high-performance inter-cell interference suppression, even when estimation errors and receiver front-end imper-

fections are considered in the evaluation [3].

Nevertheless, the use of interference suppression receivers as an alternative to frequency reuse techniques has not been evaluated yet. In this paper, we evaluate with system-level simulations whether replacing traditional frequency reuse techniques is actually possible by comparing them with the network performance of interference suppression receivers in three representative dense indoor small cell scenarios. This evaluation is performed using an updated receiver model that includes the use of a Successive Interference Cancellation (SIC) decoding stage [4] to reduce the negative effects of inter-stream interference and considering the latest results regarding the use of smart victim-aware rank adaptation algorithms [5, 6] as additional protection mechanism to manage the inter-cell interference levels in dense small cell networks.

The paper is structured as follows. Section II presents the system model used in the simulations. The details related to the simulation setup are described in Section III. We present and analyse the simulation results in Section IV and we close the paper with conclusions and future work in Section V.

II. System Model

In this section, we present the model used in our system-level simulations. We will first review some important details about the 5G RAT concept proposed in [1], and then present the mathematical model used to evaluate the performance of the receivers. Finally, we will present the principles of the rank adaptation algorithms used in the evaluation.

A. 5G Frame Format Concept

The goal of this subsection is to present the relevant assumptions which ease the usage of advanced receivers in our proposed 5G concept [1]. In particular, the aim in [1] was to integrate in a single concept the support for the technical features that are expected to have fundamental roles in dense small cell networks. Some of these features include: (i) TDD, given its flexibility and the possibility of exploiting unpaired bands, (ii) very short frame length, to fulfil the latency requirement, (iii) flexible UL/DL resource allocation (also known as Dynamic TDD), to provide flexibility to adjust to the instantaneous traffic demands, and (iv) Single User MIMO (SU-MIMO) and IRC receiver, as mentioned before. The need to consider all these features in a single concept led us to design the frame format depicted in Figure D.1.

We assume a system based on OFDM in which all network nodes transmit time-aligned frames. The proposed frame is 0.25 ms long (short enough to
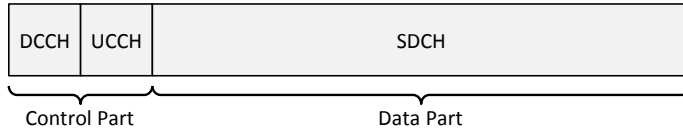
Fig. D.1: Frame format.

support 1 ms latency) and is divided in two parts: a control part, which includes UL and DL Control Channels (UCCH and DCCH), and a data part, which includes the Shared Data Channel (SDCH), which is shared by nodes transmitting in both directions. This shared data part is designed to provide the flexibility required to support the Dynamic TDD feature. Each cell may independently decide at each frame whether to use the data part for UL or DL data transmission.

However, such flexibility may compromise the performance of the IRC receiver. The IRC receiver uses an estimate of the received signal covariance matrix to calculate the optimal combining vectors. To properly reject the interference, such estimate should accurately represents the instantaneous interference conditions during the frame, and this can only be used to tune the IRC receiver as long as the interference sources do not change. Thus, we decided to embed in the frame format the support for high-performance interference rejection by: (i) limiting the use of the shared data part for only one direction per frame, (ii) enforcing the use of identical formats for both UL and DL transmissions, and (iii) including orthogonal reference signals at the beginning of the data part (similar to the Demodulation Reference Signal (DMRS) in LTE [7]). The aforementioned design criteria allows just-in-time estimation of the received covariance matrix which can be used to tune the IRC filter at each frame, according to the specific interference sources in that frame.

The possibility of using SIC receivers to deal with inter-cell interference was also considered during the design of the concept. To successfully detect a signal, a SIC receiver needs information about the transmission format, such as Modulation and Coding Scheme (MCS) and Transport Block Size (TBS) in the case of Long Term Evolution (LTE) networks [7]. This type of information is normally conveyed to the receiver using control channels, which are however intended for communication among nodes in the same cell. Providing the same information to neighbour cells would require very complex and costly inter-cell control channels or computationally expensive receivers capable of blind detection of transmission parameters [8, 9].

As opposed to inter-cell interference cancellation, it is straightforward to design a system that uses SIC to cancel inter-stream, because the information for detecting the desired streams must be available at the receiver even if SIC

is not used. Although it does not deal directly with the inter-cell interference problem, the use of inter-stream interference cancellation can potentially improve the network performance by improving the efficiency of SU-MIMO, increasing the peak and average cell throughputs.

This frame format concept is the base on top of which we derive our receiver model described in the next section.

B. Receiver Model

In this subsection, we present the receiver model used in our system-level simulations. The schematic of the receiver on which the model is based is depicted in Figure D.2. The schematic includes both the linear and the non-linear receivers. The non-linear receiver includes also the dashed part, which represents the blocks used for interference cancellation.
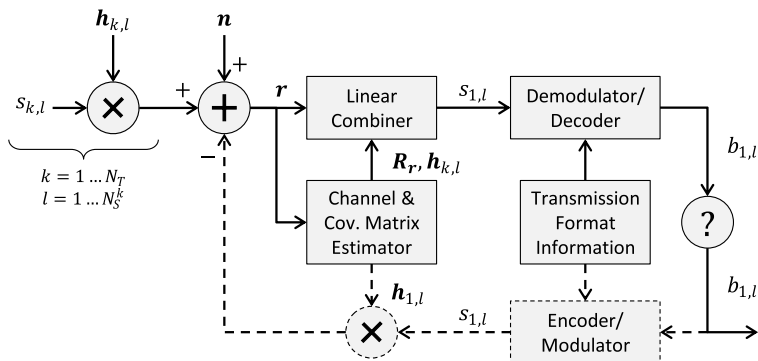

Fig. D.2: Receiver Schematic: (i) linear receiver (full lines); (ii) non-linear receiver (full and dashed lines).

We assume a network composed of nodes with N_{tx} transmitting and N_{rx} receiving antennas. At each frame, N_T nodes transmit. Each transmitting node k transmits $N_S^k \leq min(N_{\text{rx}}, N_{\text{tx}})$ streams. The received signal $\mathbf{r}$ $[N_{\text{rx}} \times 1]$ is given by

$$\mathbf{r} = \sum_{k=1}^{N_T} \sum_{l=1}^{N_S^k} \mathbf{h}_{k,l} s_{k,l} + \mathbf{n} \tag{D.1}$$

where the scalar $s_{k,l}$ represents the symbol transmitted in the l-th layer by the k-th transmiter, $\mathbf{h}_{k,l}$ $[N_{\text{rx}} \times 1]$ is the vector of the equivalent channel coefficients that models the path of the symbol stream of the l-th layer from the k-th transmitter to the receiver and the vector $\mathbf{n}$ $[N_{\text{rx}} \times 1]$ represents the additive noise. Note that this equation holds for a generic subcarrier in a generic OFDM symbol, whose indexes are omitted for the sake of simplicity.

We assume that the transmitted symbols $s_{k,l}$ have zero mean and unit power, and that there is no correlation between the multiple symbols sent by all the transmitters. We also assume that the channel response is constant for the duration of a frame (block fading), and that the equivalent channel vectors $\mathbf{h}_{k,l}$ include the effect of the transmit power amplification, large scale and small scale propagation effects, and the $[N_{tx} \times N_S^k]$ precoding matrix at the transmitter.

Let us assume that $k = 1$ always refers to the transmitter that transmits the desired signal. The first step is to linearly combine $\mathbf{r}$ to obtain an estimate of the N_S^1 desired signals $s_{1,l}$ ($l = 1 \ldots N_S^1$). The estimates can be obtained as follows

$$\hat{s}_{1,l} = \mathbf{w}_{1,l}^H \mathbf{r} \tag{D.2}$$

where $\mathbf{w}_{1,l}$ are the linear combining vectors, which according to the MMSE criterion are given by

$$\mathbf{w}_{1,l} = \hat{\mathbf{R}}_r^{-1} \hat{\mathbf{h}}_{1,l} \tag{D.3}$$

where $\hat{\mathbf{R}}_r$ is the estimate of the covariance matrix $\mathbf{R}_r$ of the received signal $\mathbf{r}$, and $\hat{\mathbf{h}}_{1,l}$ is the estimate of $\mathbf{h}_{1,l}$.

We assume that the covariance matrix $\mathbf{R}_r$ is estimated using the orthogonal reference symbols transmitted at the beginning of the data part. Thus, in the case of the IRC receiver, i.e. the receiver that uses the inter-cell interference-aware MMSE linear combiner (MMSE-IRC), the estimate $\hat{\mathbf{R}}_r$ can be calculated as

$$\hat{\mathbf{R}}_r = \sum_{k=1}^{N_T} \sum_{l=1}^{N_S^k} \hat{\mathbf{h}}_{k,l} \hat{\mathbf{h}}_{k,l}^H + \hat{\mathbf{R}}_n \tag{D.4}$$

where $\hat{\mathbf{R}}_n$ is the estimate of the additive noise covariance matrix $\mathbf{R}_n$. The $\mathbf{R}_n$ matrix is diagonal and each one of the diagonal terms σ_m^2 represents the power of the additive noise at the m-th antenna. In this case, $\sigma_m^2 = \sigma_n^2$, where σ_n^2 is the noise power.

For comparison, we also model the Maximal Ratio Combining (MRC) receiver, i.e. the receiver that uses the inter-cell interference-unaware MMSE linear combiner (MMSE-MRC). This receiver treats inter-cell interference as noise, i.e. it assumes that there is no correlation between the inter-cell interference signals received by the different antennas. In this case, the estimate $\hat{\mathbf{R}}_r$ is given by

$$\hat{\mathbf{R}}_r = \sum_{l=1}^{N_S^1} \hat{\mathbf{h}}_{1,l} \hat{\mathbf{h}}_{1,l}^H + \hat{\mathbf{R}}_n \tag{D.5}$$

and the diagonal elements of $\hat{\mathbf{R}}_n$ are given by

$$\sigma_m^2 = \sum_{k=2}^{N_T} \sum_{l=1}^{N_S^k} |h_{k,l,m}|^2 + \sigma_{n_m}^2 \tag{D.6}$$

After linear combination, the signal estimates $\hat{s}_{1,l}$ are demodulated and decoded, resulting in the estimated stream of bits $\hat{b}_{1,l}$. These bits are then verified to detect if the reception was correct by using e.g. Cyclic Redundancy Check (CRC) verification. If correct, $\hat{b}_{1,l} = b_{1,l}$. In the case of the linear receiver, this process will be repeated for all the N_S^1 streams and the receiving process will end.

Conversely, in the case of the non-linear receiver, an iterative process takes place. The receiver attempts to increase the probability of decoding each stream by successively removing the interfering contribution of each correctly decoded signal from the received signal. This is done by (i) encoding and modulating the detected bits $b_{1,l}$ to obtain $s_{1,l}$, (ii) multiplying it by the vector of equivalent channel coefficient estimates $\hat{\mathbf{h}}_{1,l}$, and (iii) subtracting the obtained vector from the received signal vector $\mathbf{r}$. This process improves the SINR of the signals that are still to decode, potentially increasing the link capacity.

In our model, each cell decides independently at each frame the rate selected for the transmission in each spatial stream (independent codeword per stream). We assume that this link adaptation process is ideal, i.e. the transmitter always uses the highest rate that has 100% decoding probability. Hence, we can assume that $\hat{b}_{1,l}$ is always correct.[1]

We extend the receiver model by adding the possibility of removing the reconstructed decoded signals from the received signal $\mathbf{r}$. In this case, for every iteration the received signal used in the input of the receiver is updated. Then, the vector $\mathbf{r}$ is given by

$$\mathbf{r} = \sum_{k=1}^{N_T} \sum_{l=1}^{N_S^k} \mathbf{h}_{k,l} s_{k,l} + \mathbf{n} - \sum_{l \in \mathcal{D}} \hat{\mathbf{h}}_{1,l} s_{1,l} \tag{D.7}$$

where $\mathcal{D}$ denotes the set of indexes of the signals that have already been decoded. The covariance matrix used to obtain the combining vector is then updated as follows

$$\hat{\mathbf{R}}_r = \sum_{k=1}^{N_T} \sum_{l=1}^{N_S^k} \hat{\mathbf{h}}_{k,l} \hat{\mathbf{h}}_{k,l}^H + \hat{\mathbf{R}}_n - \sum_{l \in \mathcal{D}} \hat{\mathbf{h}}_{1,l} \hat{\mathbf{h}}_{1,l}^H \tag{D.8}$$

Using this model, we can then calculate the SINR $\gamma_{1,l}$ of the estimated signal $s_{1,l}$, which is given by

$$\gamma_{1,l} = \frac{\mathbf{w}_{1,l}^H (\mathbf{h}_{1,l} \mathbf{h}_{1,l}^H) \mathbf{w}_{1,l}}{\mathbf{w}_{1,l}^H (\mathbf{R}_r - \mathbf{h}_{1,l} \mathbf{h}_{1,l}^H) \mathbf{w}_{1,l}} \tag{D.9}$$

---

[1]Note that this assumption would not be reasonable in an inter-cell interference cancellation model, because each cell would have to select rates that guarantee 100% decoding probability also at the receivers in the neighbour cells. Therefore, this model can only be applied to inter-stream interference cancellation, as we do in this paper.

The total throughput will be the sum of the individual stream throughputs. As a performance bound, we calculate the throughputs as the achievable rates (Shannon capacity) at the SINRs in (D.9).

Although the model considers the possibility of imperfect channel and received signal covariance matrix estimation, in this paper, we assume perfect estimation, i.e. $\hat{\mathbf{h}}_{k,l} = \mathbf{h}_{k,l}$ and $\hat{\mathbf{R}}_r = \mathbf{R}_r$.

C. Rank adaptation

The rank adaptation mechanism is responsible for balancing in each link the trade-off between spatial multiplexing gain and interference suppression capabilities by properly selecting the number of streams to be transmitted. Since the total number of received interfering streams impacts the performance of the IRC receiver (as a rule of thumb, the IRC receiver is capable of rejecting up to $N_{\mathrm{rx}} - 1$ streams), the rank adaptation decision in one cell also affects the performance of neighbour cells. Therefore, the use of victim-aware rank adaptation algorithms, i.e. algorithms that consider this potential negative effect, may help improve the performance of the network. In this paper, the following rank adaptation approaches are used in the performance evaluation:

Selfish Rank Adaptation (SRA)

If selfish rank adaptation is used, each node k selects the transmission rank (N_S^k) as the one which is expected to maximize its Shannon capacity $C_{N_S^k}$ given its estimated SINR conditions. By using a selfish rank adaptation, each node aims then at boosting its throughput regardless to the impact it may generate to neighbour cells.

Victim-aware Rank Adaptation (VRA)

If victim-aware rank adaptation is used, each node selects the transmission rank with some regard to the interference it may generate to the neighbour cells. In this work, we refer to the rank adaptation technique proposed in [6], which has been shown to guarantee a good outage performance, while providing the benefit of higher average throughputs in both low and high inter-cell interference conditions. The principle of this algorithm is to introduce a taxation mechanism which discourages the selection of higher ranks in case of high generated interference. Node k selects the transmission rank N_S^k which is expected to maximize the following metric Π_k:

$$\Pi_k = C_{N_S^k} - \underbrace{f_W(N_S^k)C(I)}_{\text{Taxation for rank } N_S^k} \tag{D.10}$$

where $C(I)$ is the capacity of the interfering channels, and f_W is a monotonically increasing weighting function of rank N_S^k which quantifies the level of discouragement. Further details are in [6]. Ideally, the term $C(I)$ should be computed according to the outgoing interference, i.e. the interference which is generated to the neighbour cells. However, obtaining such information is not feasible in practice since it would require impracticable amounts of control information exchange among neighbour cells. As done in [6], $C(I)$ is then sub-optimally computed as a function of the incoming interference rather than outgoing interference, since such information can be easily retrieved given our described frame structure.

III. Simulation Setup

Three different scenarios are used in the performance evaluation. Figure D.3(a) depicts the network topology for Scenario A. This topology simulates an Indoor Hotspot network, similar to an airport check-in hall or a large conference hall, for example. The total area of the hall is divided in "virtual" square areas (there are no internal walls) and one AP is installed in the centre of each of them, summing up 40 APs. In this scenario, the user may connect to any of the available APs, i.e. the network operates in Open Subscriber Group (OSG) access mode. One UE is randomly placed in each square area and each UE selects which AP to connect based on the highest received power. In case an AP does not serve any UE, it is switched off for the rest of the simulation drop; if an AP serves more than one UE, a fair round-robin frequency-frequency domain scheduling is assumed.

Scenarios B and C use the same Indoor Office network topology [10], but different access modes. Figure D.3(b) depicts the network topology, which consists of 40 cells deployed in 2 office buildings (one cell per office). Each building is divided in 2 rows of 10 offices. Each office measures ten-by-ten meters. The two buildings are separated by a ten-meter wide street. In each cell, there is one AP and one UE. In Scenario B, the OSG access mode is assume (the same as Scenario A), but in Scenario C, a CSG access mode is enforced and an UEs can only connect to the AP in the same office.

In all scenarios, both APs and UEs are equipped with uniform linear antenna arrays, composed of 4 elements equally spaced by half wavelength. The system operates at 3.5 GHz carrier frequency and occupies 200 MHz of spectrum. Table D.1 presents further details on the simulation scenarios.

We model the effect of flexible UL/DL resource allocation on the interference pattern using a three-state model. In this model, each cell independently selects either to transmit in UL, in DL or not to transmit at all (mute). A three-state Markov process is used to control the state transition probabilities. The processes regarding different cells are uncorrelated. In this study, we use the
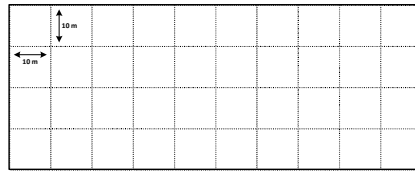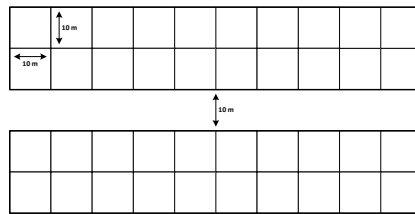
(a) Indoor Hotspot

(b) Indoor Office [10]

Fig. D.3: Network topologies

Table D.1: Simulation Scenario Details

Indoor Hotspot (Scenario A)		
Path Loss	WINNER II Indoor Hotspot (B3) Model [11] 70 dB Minimum Coupling Loss	
Shadowing Std. Deviation	Line of Sight	3 dB
	Non Line of Sight	4 dB
Fast Fading	WINNER II CDL Model [11] Indoor Hotspot (B3) - 3 Km/h	
Indoor Office (Scenario B and C)		
Path Loss	3GPP Dual Stripe Model [10] 45 dB Minimum Coupling Loss	
Wall Loss	Internal Walls	5 dB
	External Walls	10 dB
Shadowing Std. Deviation	Serving Cell	6 dB
	Other Cells	8 dB
Fast Fading	WINNER Phase II Model [11] Indoor Office (A1) - 3 Km/h	

term activity factor to refer to the probability that the cell is not idle. When not idle, the probability of transmitting in each direction is always identical (50% UL and 50% DL). This parameter is used to control the network load and will be used in the performance evaluation.

The physical layer model assumes one codeword per spatial layer (which implies one Modulation and Coding Scheme (MCS) per layer) and the SINR is calculated per layer using (D.9). The values are then adjusted using an EVM model (EVM = 5%). The link adaptation model used is ideal: the rate of each codeword perfectly matches with the instantaneous capacity of the channel at reception time. However, the rate is upper limited by a maximum spectral efficiency constraint of 8 bps/Hz, which is equivalent to uncoded 256-QAM modulation, and lower bounded by a minimum decodable SINR of -6 dB, below which codewords are discarded.

The model also assumes ideal rank adaptation, i.e. each cell independently selects the number of streams at each frame based on instantaneous interference conditions, according to the selfish or victim-aware strategies defined above. The LTE Release 8 precoding matrix codebook for closed-loop SU-MIMO [7] is used for mapping the number of streams to the number of transmit antennas.

The network performance is evaluated using a quasi-static system-level simulator. Each simulation consists of 200 snapshots of 200 frames each. In each snapshot, one AP and one UE are randomly positioned in each cell. The fast fading is updated at each frame (block fading model), but the pathloss and the shadowing remain constant for the duration of the snapshot.

IV. Performance Evaluation

In order to test the hypothesis that interference suppression receivers can be used to manage inter-cell interference as an alternative to frequency reuse planning, both strategies are compared in the three scenarios presented above. The network performance are quantified by calculating the average cell throughput for each cell[2], collecting these results to create empirical Cumulative Distribution Functions (CDFs) and calculating the key performance indicators that are used in our performance analysis: outage (5th percentile), average and peak (95th percentile) network throughputs.

The use of interference suppression receivers is considered a valid alternative to traditional frequency reuse techniques (confirming the hypothesis) if the outage throughput observed using the former is equal or larger than the baseline outage throughput with traditional frequency reuse. In that re-

---

[2]Since each cell may randomly select the link direction at each frame, the average cell throughput is calculated as the average of the instantaneous throughput per frame, including both UL and DL frames and excluding idle frames.

spect, we define for comparison a *baseline configuration*, which includes the interference-unaware MRC receiver, a selfish rank adaptation (SRA), and the frequency reuse scheme that guarantees the best outage throughput observed among the reuse 1 (FR1), reuse 2 (FR2) and reuse 4 (FR4) options.

All the configurations using interference suppression receivers (IRC and IRC-SIC) adopt instead universal frequency reuse (FR1), and their rank adaptation method may be either selfish (SRA) or victim-aware (VRA).

A. Scenario A - Indoor Hotspot (OSG)

In Scenario A, the baseline configuration assumes FR1, since it can be shown to provide better outage performance than FR2 and FR4 when the network is fully loaded (100%); the benefits of higher SINR obtained using frequency reuse planning do not compensate the smaller bandwidth used per cell in this large indoor hall.

The hypothesis is tested in this scenario by comparing the baseline to the performance of configurations that use IRC and SIC receivers, frequency reuse 1 (FR1) and selfish rank adaptation (SRA). This comparison is depicted in Figure D.4, where the average cell throughput CDFs for the different receiver types are shown. It is clear from the curves that IRC and SIC configurations outperform the baseline configuration; as presented in Table D.2, all network performance indicators are improved, indicating that the use of interference suppression receivers in Scenario A is not only an alternative, but also a bonus for the network.

Table D.2: Scenario A - Key performance indicators [in Mbps] and performance gains over the baseline configuration (100% network load)

Configuration	Outage	Average	Peak
MRC/FR1/SRA	218.1	487.7	823.7
IRC/FR1/SRA	291.4 (+33.6%)	595.8 (+22.2%)	959.9 (+16.5%)
SIC/FR1/SRA	302.6 (+38.7%)	594.2 (+21.8%)	971.8 (+18.0%)

The results also show that there is almost no difference between the performance of IRC and SIC. This situation occurs because the very high inter-cell interference levels observed in this scenario force the rank adaptation algorithm to select rank 1 almost all the time. In such situation, the benefit of SIC disappears because there are no inter-stream interfering signals to be cancelled. It also indicates that the use of victim-aware rank adaptation would not improve the performance of the network, since all transmitters are already using the lowest rank.
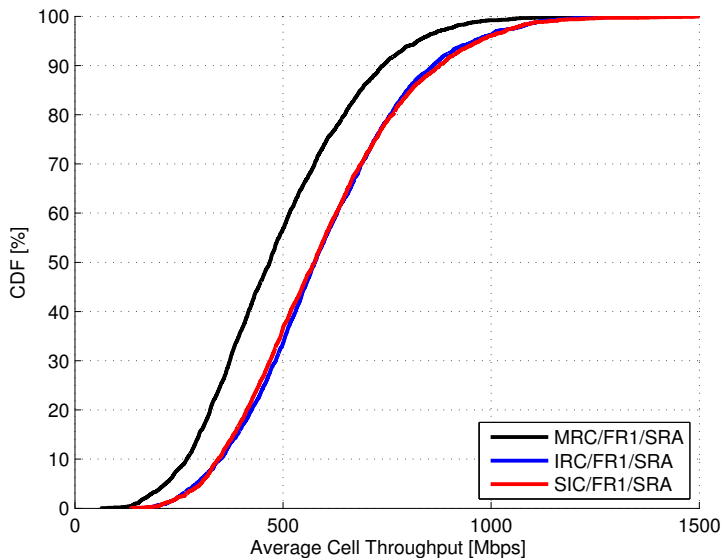
Fig. D.4: Average cell throughput CDFs - Scenario A (100% network load)

B. Scenario B - Indoor Office (OSG)

In Scenario B, the walls provide some protection against inter-cell interference. Nevertheless, the uncoordinated deployment of cells still creates situations in which receivers are interfered by strong inter-cell signals. The use of OSG access mode alleviates the problem, but it is still useful to apply a conservative frequency reuse plan when the network is fully loaded. In this case, for the baseline configuration the frequency reuse plan that provides the highest outage throughput can be shown to be FR4.

Figure D.5 shows the average cell throughput CDFs for the different configurations, still assuming a fully loaded network. Again, the configurations with IRC and SIC and selfish rank adaptation are shown to outperform the baseline (victim-aware rank adaptation is also not need in this scenario). This is also observed in the numbers presented in Table D.3.

Table D.3: Scenario B - Key performance indicators [in Mbps] and performance gains over the baseline configuration (100% network load)

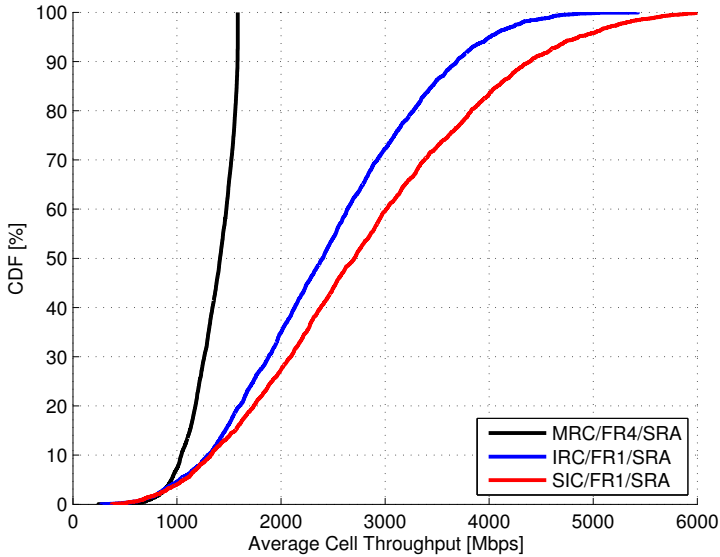| Configuration	Outage	Average	Peak
MRC/FR4/SRA	964.2	1357.7	1584.0
IRC/FR1/SRA	1023.3 (+8.1%)	2439.8 (+79.7%)	4009.7 (+153.1%)
SIC/FR1/SRA	1068.0 (+12.9%)	2795.7 (+105.9%)	4862.7 (+207.0%)

178

Fig. D.5: Average cell throughput CDFs - Scenario B (100% network load)

The outage throughput is very similar in the three cases (with only small throughput gain), but the average and peak throughputs are considerably improved; the average and peak throughputs are up to 106% and 207% higher when the interference suppression receivers are used. It is therefore possible to claim that the use of interference suppression receivers is also a valid interference mitigation strategy in scenario B, with a large improvement over average and peak throughputs as additional benefits.

C. Scenario C - Indoor Office (CSG)

The inter-cell interference levels in Scenario C are higher than in Scenario B due to the CSG access mode. The use of frequency reuse planning provides the required protection to guarantee reasonable outage levels: FR4 is then selected here for the baseline configuration.

As opposed to the other scenarios, the use of interference suppression receivers is here not enough to reach the same outage throughput of the baseline configuration if the network is fully loaded. Figure D.6 and Table D.4 show a worse outage performance of both IRC and SIC configurations, even though their average and peak throughputs are much higher. In this scenario, interference suppression receivers can provide outage throughputs higher or equal to MRC with FR4 only if the network load is 50% or less.

The outage throughputs for the configurations with advanced receivers may be improved using the victim-aware rank adaptation algorithm. Two
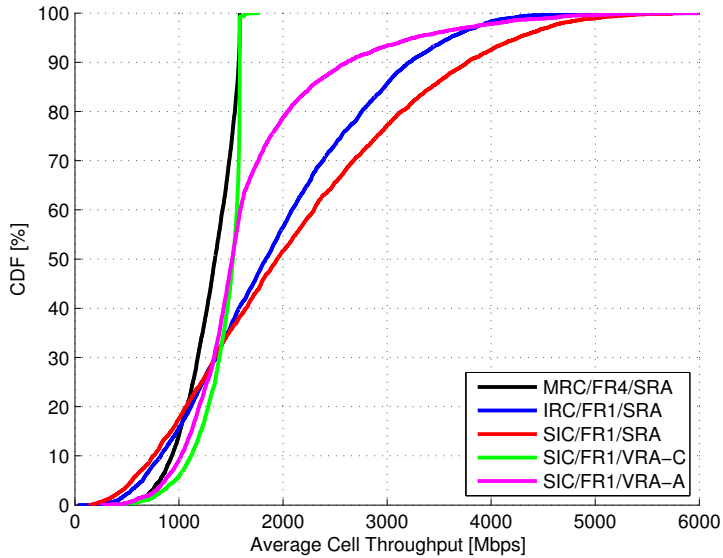
Fig. D.6: Average cell throughput CDFs - Scenario C (100% network load)

Table D.4: Scenario C - Key performance indicators [in Mbps] and performance gains over the baseline configuration (100% network load)

Configuration	Outage	Average	Peak
MRC/FR4/SRA	818.6	1294.7	1583.3
IRC/FR1/SRA	652.4 (-20.3%)	1942.7 (+50.1%)	3612.3 (+128.2%)
SIC/FR1/SRA	549.0 (-32.9%)	2123.6 (+64.0%)	4265.6 (+169.4%)
SIC/FR1/VRA-C	973.9 (+19.0%)	1434.4 (+10.8%)	1584.0 (+0.0%)
SIC/FR1/VRA-A	874.3 (+6.8%)	1743.7 (+34.7%)	3397.1 (+114.6%)

options are used for the victim-aware rank adaptation, namely *conservative* (VRA-C) and *aggressive* (VRA-A), corresponding to high and low taxation for higher ranks, respectively, with reference to Equation D.10. It is clear from results in Figure D.6 that both configurations can provide outage through-puts comparable with the baseline configuration.[3] The difference lies in the average and peak throughputs, as it is shown in Table D.4. The conservative configuration limits such indicators to similar values of the baseline configuration, whereas they perform better in the case of aggressive rank adaptation.

The difference between the two strategies is more evident when the network is operating at low load (25% network load). Here, the conservative configuration shows poor performance, because it imposes a large limitation when the load is low, as it is shown in Figure D.7 and Table D.5. Conversely, the aggressive configuration provides a good trade-off between protection in high load conditions (reasonable outage performance) and performance in low load conditions.
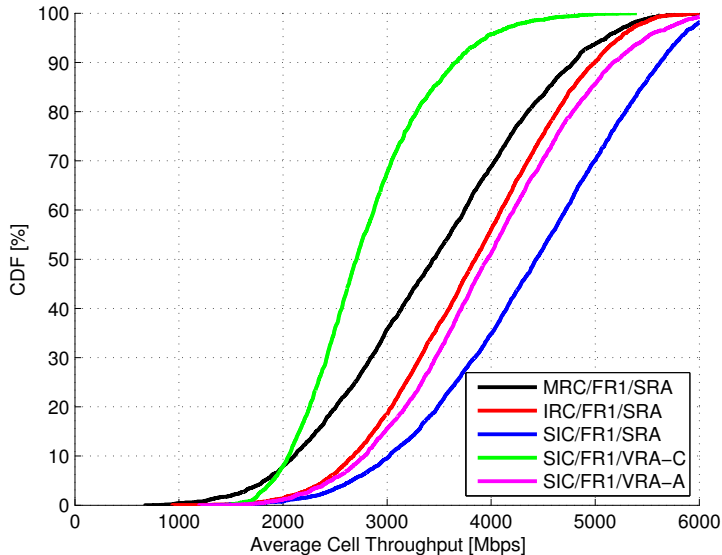

Fig. D.7: Average cell throughput CDFs - Scenario C (25% network load)

Therefore, it is possible to confirm that interference suppression receivers are also a valid alternative for Scenario C, where the use of a victim-aware algorithm is required to reach the required outage throughput.

---

[3]Note that a configuration combining victim-aware rank adaptation and the MRC receiver is not recommended since the number of interfering streams does not impact the MRC receiver performance. Therefore, this possibility is not included in this performance evaluation.

Table D.5: Scenario C - Key performance indicators [in Mbps] and performance gains over the baseline configuration (25% network load)

Configuration	Outage	Average	Peak
MRC/FR1/SRA	1823.0	3439.5	5105.1
IRC/FR1/SRA	2396.7 (+31.5%)	3830.5 (+11.4%)	5249.7 (+2.7%)
SIC/FR1/SRA	2660.3 (+45.9%)	4367.2 (+27.0%)	5818.1 (+14.0%)
SIC/FR1/VRA-C	1990.1 (+4.2%)	2790.2 (-18.9%)	3951.4 (-22.6%)
SIC/FR1/VRA-A	2463.1 (+35.1%)	3973.4 (+15.5%)	5488.2 (+7.5%)

V. Conclusion and Future Works

In this paper, we tested the usage of computationally feasible advanced receivers, namely IRC and IRC-SIC, as an alternative solution to traditional frequency reuse techniques for managing inter-cell interference in an ultradense small cell scenario. We discussed how the proposed 5G RAT concept provides the support required for high performance interference suppression and how victim-aware rank adaptation strategies may be used to reach the desired outage throughput performance.

The results obtained in an indoor hall and an indoor office scenario (OSG access mode) show that it is possible to obtain the same or higher outage throughput performance than frequency reuse using the interference suppression receivers and a selfish rank adaptation, with the extra advantage of higher average and peak throughput. In the indoor office scenario operating in CSG access mode, similar performance results are obtained with the usage of a victim-aware rank adaptation, confirming that the use interference suppression receivers is indeed an valid alternative.

Our future work will focus on the extended evaluation of interference suppression receivers in 5G dense small cell networks considering the effects of estimation errors and receiver front-end imperfections and the evaluation of different victim-aware rank adaptation strategies.

References

[1] Preben Mogensen, Kari Pajukoski, Esa Tiirola, Jaakko Vihriälä, Eeva Lähetkangas, Gilberto Berardinelli, Fernando Menezes Leitão Tavares, Nurul Huda Mahmood, Mads Lauridsen, Davide Catania, and Andrea Fabio Cattoni. "Centimeter-wave concept for 5G ultra-dense small cells". In: *Vehicular Technology Conference (VTC Spring), 2014 IEEE 79th*. May 2014.

[2] F.M.L. Tavares, G. Berardinelli, N.H. Mahmood, T.B. Sørensen, and P. Mogensen. "On the Potential of Interference Rejection Combining in B4G Networks". In: *Vehicular Technology Conference (VTC Fall), 2013 IEEE 78th.* Sept. 2013, pp. 1–5. DOI: 10.1109/VTCFall.2013.6692318.

[3] Fernando M.L. Tavares, Gilberto Berardinelli, Nurul H. Mahmood, Troels B. Sørensen, and Preben Mogensen. "On the Impact of Receiver Imperfections on the MMSE-IRC Receiver Performance in 5G Networks". In: *Vehicular Technology Conference (VTC Spring), 2014 IEEE 79th.* May 2014, pp. 1–6. DOI: 10.1109/VTCSpring.2014.7023014.

[4] Sergio Verdu. *Multiuser Detection.* 1st. New York, NY, USA: Cambridge University Press, 1998. ISBN: 0521593735.

[5] N.H. Mahmood, G. Berardinelli, F.M.L. Tavares, and P. Mogensen. "A distributed interference-aware rank adaptation algorithm for local area MIMO systems with MMSE receivers". In: *Wireless Communications Systems (ISWCS), 2014 11th International Symposium on.* Aug. 2014, pp. 697–701. DOI: 10.1109/ISWCS.2014.6933443.

[6] Davide Catania, Andrea Fabio Cattoni, Nurul Huda Mahmood, Gilberto Berardinelli, Frank Frederiksen, and Preben Mogensen. "A Distributed Taxation Based Rank Adaptation Scheme for 5G Small Cells". Accepted to the 2015 IEEE 81st Vehicular Technology Conference (VTC Spring), May 2015.

[7] 3GPP TS 36.211. *Evolved Universal Terrestrial Radio Access (E-UTRA); Physical channels and modulation.* v11.1.0. Dec. 2012. URL: http://www.3gpp.org.

[8] 3GPP TR 36.866. *Study on Network-Assisted Interference Cancellation and Suppression (NAIC) for LTE.* v12.0.1. Mar. 2014. URL: http://www.3gpp.org.

[9] W. Nam, D. Bai, J. Lee, and I Kang. "Advanced interference management for 5G cellular networks". In: *Communications Magazine, IEEE* 52.5 (May 2014), pp. 52–60.

[10] 3GPP TR 36.814. *Evolved Universal Terrestrial Radio Access (E-UTRA); Further advancements for E-UTRA physical layer aspects.* v9.0.0. Mar. 2010. URL: http://www.3gpp.org.

[11] P. Kyösti et al. *WINNER II Channel Models.* D1.1.2 v1.1. IST-WINNER, Sept. 2007. URL: https://www.ist-winner.org/WINNER2-Deliverables/D1.1.2v1.1.pdf.